# HYPERSEEING

The Publication of the International Society of the Arts, Mathematics, and Architecture

SUMMER 2020
www.isama.org

## *The Proceedings of the SMI 2020 Fabrication & Sculpting Event (FASE)*

*Special Issue on Shape Modeling International 2020*

**2-4 June 2020
Strasbourg
France**

# HYPERSEEING
# Special Issue on SMI 2020

## Shape Modeling International 2020
## Fabrication and Sculpting Event

*Nineteenth Interdisciplinary Conference of the International Society of the Arts, Mathematics, and Architecture*

**Strasbourg, France**
**June 2-4, 2020**

### SMI Conference Chairs

Loïc Barthe (University of Toulouse, France)
Frédéric Cordier (University of Haute-Alsace, France)
Hui Huang (Shenzhen University, China)

### FASE Paper Chairs

Oleg Fryazinov (Bournemouth University)
Melina Skouras (Inria, Grenoble)
Shinjiro Sueda (Texas A&M University)

**Steering Committee:** Ergun Akleman, Loic Barthe, Karina Rodriguez Echavarria, Negar Kalantar, Guiseppe Patane, Konrad Polthier, Vinayak Krishnamurthy, Carlo Sequin, Courtney Starrett, Wei Yan

## FASE Program Committee

Valery Adzhiev
Bournemouth University

Ergun Akleman
Texas A&M University

Loic Barthe
IRIT - Université de Toulouse

Michael Birsak
King Abdullah University of Science and Technology

Adrien Bousseau
INRIA

Vladimir Bulatov
Shapeways, Inc

Daniela Cabiddu
CNR IMATI

Nathan Carr
Adobe Systems Inc.

Raphaëlle Chaine
LIRIS Université Lyon 1

Weikai Chen
The University of Hong Kong

Francesco De Comite
University of Sciences and Technology Lille

Olga Diamanti
TU Berlin

Ye Duan
University of Missouri at Columbia

Gershon Elber
Technion- Israel Institute of Technology

Bianca Falcidieno
Consiglio Nazionale delle Ricerche (CNR)

Greg N. Frederickson
Purdue University

Oleg Fryazinov
Bournemouth University

Abel Gomes
University of Beira Interior

Robert Krawczyk
Illinois Institute of Technology

Xin Li
Louisiana State University

James Mallos
Sculptor

Marcel Morales
Univ. Grenoble Alpes

Alexander Pasko
Bournemouth University, UK

Giuseppe Patanè
CNR-IMATI

Helmut Pottmann
Vienna University of Technology

Karina Rodriguez
University of Brighton

Henry Segerman
Oklahoma State University

Carlo H. Séquin
University of California, Berkeley

Melina Skouras
INRIA

Shinjiro Sueda
Texas A&M University

Kenshi Takayama
National Institute of Informatics

Remco Veltkamp
Utrecht University

Charlie Wang
Delft University of Technology

Jean-Philippe Vandeborre
IMT Lille Douai

**FASE Supported by**

Texas A&M University
University of Strasbourg

# CONTENTS

**Proceedings of Fabrication and Sculpting Event**

# Preface

### History Fabrication and Sculpting Event (FASE)

*We dedicated this issue to the Memory of Nat Friedman, the founder of ISAMA and Hyperseeing. He passed away of COVID-19 complications on 2 May in Gloversville at the age of 82.*

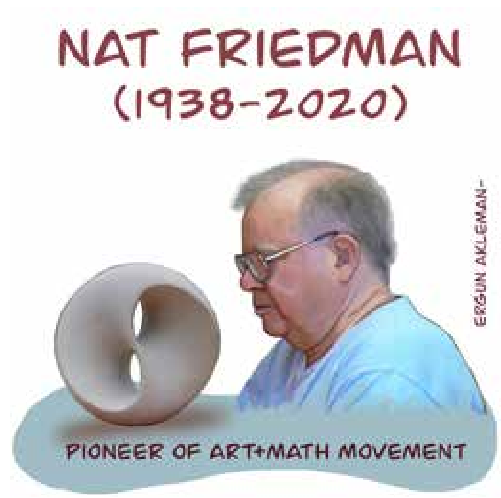


The Fabrication and Sculpting Event started as an experiment in expanding the scope of shape modeling international (SMI) conference in 2012. We also had another FASE event in SMI'2013. There were very positive responses to the FASE papers and presentations in both 2012 and 2013. Although we skipped FASE in SMI'2014, based on the success of earlier events, we continued the FASE event from 2015 to 2020 as a part of SMI conference.

In 2013, Nat Friedman, the chair of the International Society of the Arts, Mathematics, and Architecture (ISAMA), asked me if we could organize the event as an annual ISAMA conference. I presented the idea to the SMI steering committee. The Committee unanimously agreed with the suggestion. As a result, this event can now be considered also as the Nineteenth Interdisciplinary Conference of ISAMA.

The ISAMA conference has a rich history. The first Art and Mathematics Conference (AM 92) was organized by Nat Friedman at SUNY-Albany in June, 1992. This conference was followed by annual conferences AM93-AM97 at Albany and AM 98 at the University of California, Berkeley, co-organized with Carlo Sequin. ISAMA was founded by Nat Friedman in 1998 along with the ISAMA publication Hyperseeing co-founded with me in 2006. In addition, the Art/Math movement has taken off with the formation of many additional conferences and organizations. In particular, we mention the very successful Bridges conference organized by Reza Sarhangi in 1998 and the excellent Bridges Proceedings. The significance of the art/math movement is now recognized internationally and in particular by the extensive art/math exhibit at the annual Joint Mathematics Meeting of the American Mathematical Society and the Mathematical Association of America organized by Robert Fathauer.

The main difference with other math/art conferences is that FASE focuses solely on 3D shapes. We invite submissions mainly from practitioners such as sculptors and architects to describe their methods. We expect that such papers and the following discussions can provide new problems, issues and questions for theoretical shape modeling research.

Ergun Akleman

Editor, Hyperseeing

# Preface

## Fabrication and Sculpting Event 2020

There are at least two aspects to shape modeling: theoretical and practical. The mathematical and theoretical aspects of shape modeling have traditionally been supported by the SMI conference. With the Fabrication and Sculpting Event (FASE) our goal is to include more hands-on, application-oriented ways by designers and sculptors who construct sophisticated real-world objects.

FASE has its own program committee, and the accepted papers are published in Hyperseeing. With FASE, we hope to attract practitioners who might usually be less inclined to write papers containing formal algorithms or mathematical proofs, but who nevertheless have important things to say that are of interest to the shape modeling community and who also might provide visually stimulating material.

For this year's Fabrication and Sculpting Event, we solicited papers that pose new questions and motivate further research in designing, fabrication and sculpting. Topics should be useful, for example, in the following areas: Fabrication of digital models, Advanced manufacturing techniques such as additive manufacturing, laser cutting or CNC milling, Interactive or procedural design of manufacturable shapes, Interconnections of complex modeling and fabrication processes, visually stimulating fabrication techniques or printed structures.

Thus, the scope of FASE is the intersection of shape modeling and fabrication methods/algorithms, and papers may focus on both the digital/theoretical and the physical domain or just one of these domains – as long as the connection to the other domain is clear. It is not a requirement that the techniques presented in the paper involve computation as such, but they need to have a clear algorithmic or mathematical element.

We received nine submissions this year and four of them were accepted as eight-page or longer full papers, and another four were accepted as four-page extended abstracts. The extended abstracts will be presented as posters at the conference. The four accepted papers span a wide range of topics and views on the fabrication process of various artistically interesting artifacts. We wish to thank the authors and the reviewers for their participation in the SMI/ISAMA 2020 Fabrication and Sculpting Event. We hope that new ideas and partnerships will emerge from the FASE papers that can offer a glimpse into a much larger territory and the event can enrich interdisciplinary research in Shape Modeling. We hope that the attendees of SMI 2020 will enjoy this event of the conference.

Oleg Fryazinov, Melina Skouras, and Shinjiro Sueda

FASE Papers chairs

# A Tribute to Nat Friedman

**15 March 1938 (Chicago, Illinois) - 2 May 2020 (Gloversville, New York)**

**Milena Chilla-Markhoff**

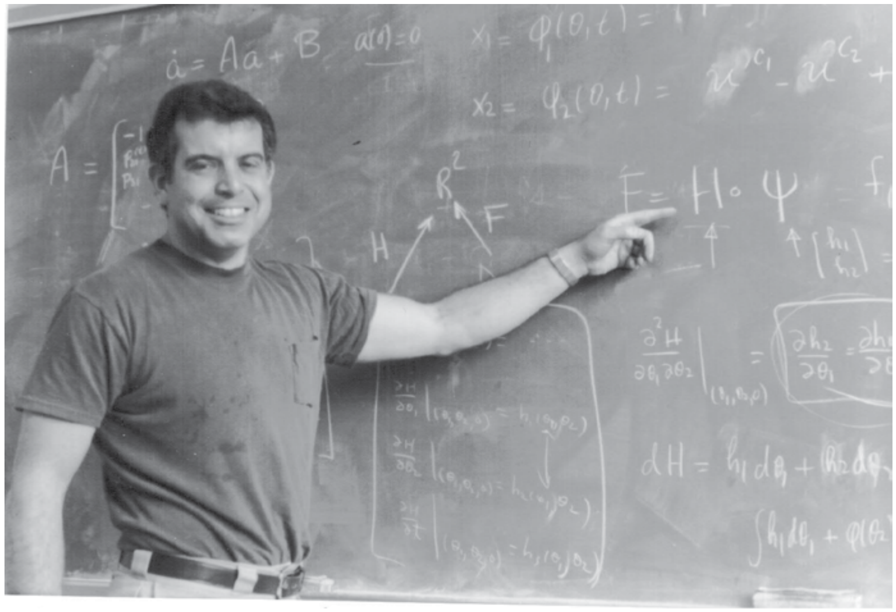

Nat Friedman received his B.A. and M.A. in Mathematics from U Michigan and his PhD in Mathematics from Brown University in 1964. He was Professor of Mathematics at SUNY Albany 1968-2000. He made an enormous impact in the early years of ergodic theory and measurable dynamics. Nat took his first sculpture course in 1971 with my father, Alex Markhoff, and began carving works in wood and stone, later also working with ceramics and metals. Concurrently, he began collecting works by artists that appealed to his interest in mathematics, surface structures, and “seeing relationships.” In 1992, while teaching at SUNY Albany, Nat Friedman founded the international and interdisciplinary Art and Mathematics Conference. The conference convened annually at SUNY Albany for six years and in 1998 Nat founded ISAMA (The International Society for the Arts, Mathematics, and Architecture) which held annual conferences at academic institutions in the USA and Europe and published HYPERSEEING regularly since 2006. Nat was always excited to hear about [art math community]. He so treasured the art/math connections that he fostered both locally and later globally through ISAMA.This photo is one of the pictures we have looked at together in October 2019 and it made him smile.

**Steve Luecking**
**Emeritus Professor, Applied Computer Science & Digital Media**
**DePaul University**

I first met Nat at a math-art conference in Granada, Spain. I was unfamiliar with the math-art scene and had been corresponding with him prior to the conference. I came prepared to complement him on one of his sculpture, which, it turned out, was a piece by Helaman Ferguson. He accepted my faux pas graciously and we became fast friends. I was lucky to live in Chicago where Nat was raised and was able to see him when he visited his mother. I have never met anyone with his love of learning and gift for discovery. On one visit he joined me in a workshop I held for elementary school math teachers. It involved crafting polyhedral from rubber modules, which among other concepts demonstrated the notion of duals. In the space of a few breaths, Nat was gleefully lost in experimenting on the sculptural possibilities of rubber geometry. On two occasions, we co-hosted ISAMA conferences at DePaul University. Nat saw to it that the conferences were informal and great fun. He was a joy to work with and I shall miss that joy.

**George Hart**
**President of Bridges Organization**
**Research Professor, Stony Brook University**

Nat Friedman was the initial impetus for many of us to take on an academic art/math direction. I have wonderful memories of attending several of his Art and Math conferences at SUNY Albany in the 1990's and then some of the ISAMA and other conferences that followed. The Bridges community grew from the seed Nat planted. The Hyperseeing Magazine is a wonderful resource and archive. Nat wrote a page about the Art and Math meetings he organized, which can be seen here: http://www.isama.org/ To this I'll add the following notes which Nat emailed me in 2003 when I asked him about the early history of his Art and Math Meetings in Albany. He told me the 1992 meeting was basically a small gathering of friends but that he was excited that the community really began to grow in 1993:

*"Back in 91, I phoned Helaman [Ferguson] and suggested we contact other mathematician-stone carvers and have a meeting. At that time sculpture was my therapy from math research. Turned out there were no other math-stone carvers we knew of. So I decided to organize a general AM conference in 92. Then AM 93 was great---there were 25 sculptors there, 40 main talks in 5 days, and 175 people attended.*"

On a personal note, I will add that Nat and I arranged to meet and spend a fun touristic week together in Belgium in September, 2000 before the Colloquium on Math and Arts that was held in Maubeuge, France. We did a lot of sightseeing together in Brussels, Bruges, and Antwerp before heading to Mons. I vividly remember Nat's great fondness for the mussels in Brussels and similarly his great gusto for bringing people together to share their mathematical art.

My most colorful memory of Nat illustrates both his passionate action-approach to life and what was no doubt a side-benefit skill from his ballroom-dancing physicality. Something inappropriate was said in small crowd at the back of a room and Nat effortlessly did a one-two that sent the offender sprawling. (I will not name the perpetrator and just assure you that Nat was in the right to feel that honor had to be defended.) I have been to a good many math conferences in my life, but that was the only one I have ever heard of in which two mathematicians came to fisticuffs at the rear of the auditorium!

**Carlo Sequin**
**Professor of Computer Science**
**University of California, Berkeley**

Many of us art-math-lovers owe a lot to Nat. He brought us into the fold, and through his ArtMath workshops in Albany created the community that flourished because of ISAMA and Bridges! Among the (somewhat fuzzy) memories I have of the crucial 1997 ArtMath gathering in Albany relates to Nat doing experiments with prints made from broken stone slabs.

**Keizo Ushio**
**Japanese Sculptor**

I [would like to offer] my condolences to [all art math community] with this sad news. It has been 20 years since I [first met] Nat Friedman, and he has given me great courage. He analyzed my sculpture, found its value, and introduced it to the world. He is a great benefactor. He wrote papers about my sculptures. He is also a collector of my sculpture. This time I would like to [provide] you photos of my encounter with him from my album. Please sleep peacefully with best regards.




**Doug Dunham**
**Chair SIGMAA-ART**
**Professor Emeritus,**
**Computer Science**
**University of Minnesota, Duluth**

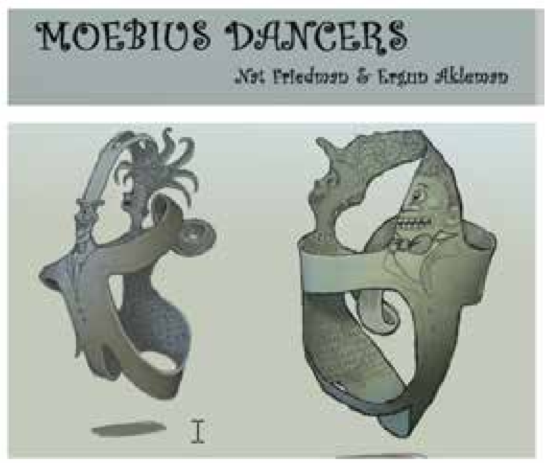


I am sad to report that one of our founding members, Nat Friedman, passed away earlier this month from COVID-19. Nat was the first Chair of SIGMAA-ARTS, serving from its inception in fall, 2006 until summer, 2012. I will miss Nat's art and his enthusiastic leadership in the mathematics and art community.

Nat also had a great interest in dance. In particular, there was a Bridges conference in Granada and an excursion to a flamenco dance hall late one night. It did not take much to get Nat to get up with the other dancers to show his stuff.

It was also a privilege to visit Nat at his home. I have never seen so many art-math objects in one place. I purchased one of Nat's ceramics, which unfortunately has broken (see picture).

**Elizabeth (Beth) Whiteley**
**Sculptor**

We all knew him as a sculptor, a mathematician, a visionary/executor for an international Math-Art community, an impresario, and a person who just liked to ballroom dance. In 2006, Nat was our houseguest for a few days. We traipsed to every museum in Washington to look at sculpture and to discuss, in depth, the pieces he favored. Nat's aesthetic judgement was equal to his math/geometric observations, which was rare ability I appreciate deeply. I am attaching a photo of him during that happy visit when he was in my studio. You can see that he had drawn a teaching point about knots on the paper and was tying a knot. I recall suggesting that he use two colors of rope and he constructed an eight crossings knot, which I photographed as well. I pray that he is at peace.

It is also ironic that Doug Dunham will be piecing the shards from Nat's sculpture together. I am attaching a photo of a sculpture I own, that Nat made in the 1990's, for which I exchanged one of my paintings. He told me the piece is made of discards from a place near Albany that made gravestones. Moreover, he titled it "Putting the Pieces Back Together Again." I believe that it had deep personal meaning for him.

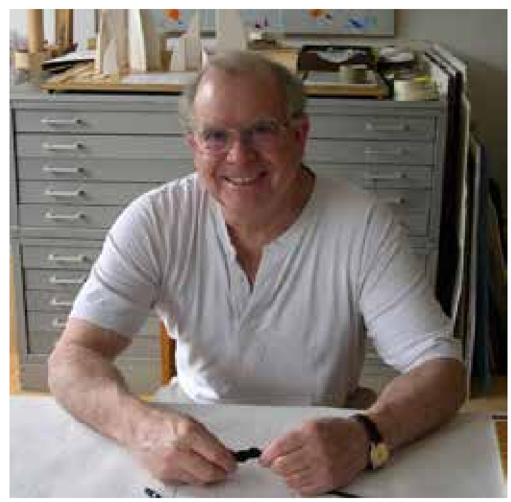

Nat Friedman's construction of Eight Crossing Knot using two color rope

**David A Reimann**
**Professor, Mathematics & Computer Science**
**Albion College**

Nat's passion for math, architecture, and the arts was very inspirational to me. I was fortunate to get to know him through the ISAMA conferences he organized in Chicago. Those were great meetings with excellent talks from interesting people.

## Recollections of Nathaniel Friedman

**Alex Feingold**
**Professor, Department of Mathematics**
**Binghamton University (SUNY)**

I was invited by a colleague to give a talk in the Department of Mathematics of the University at Albany, SUNY, in Spring 2009. While visiting, I met Nat Friedman and discovered that we had a common interest in mathematical art. When I heard about the ISAMA (International Society of the Arts, Mathematics and Architecture) conference being planned for June, I wrote to Nat asking about a one-day participation. He kindly responded with an offer to give me a one-day $50 fee, discounted from the $200 full fee. I was particularly interested in hearing the talk by Kenneth Snelson scheduled for June 23.

I made the 2-hour drive from Binghamton to Albany on June 23, and was very pleased to hear many interesting talks about mathematical art. I got the chance to meet and speak with Kenneth Snelson, bought a copy of his book, and got his autograph. I also spoke with Nat at the end of the day, and got invited to see the art collection at his house.

When we entered his house, there was a narrow path to walk in among the artwork. It seemed that every possible surface was full of art that he had either bought from other artists or had made himself. I could not imagine how he actually lived in the house, which was more like an art warehouse than a home! He explained that one way he had discovered to make knot sculptures was using a ceramic material which could be shaped and then hardened by baking. I bought one of his ceramic trefoil knots, whose picture I am attaching to this note. You can clearly see his initials, NF, signed on the surface. The cross-section is a narrow rectangle, but he had not twisted it to make a one-sided Moebius surface as I did later when I made my own cast bronze Moebius trefoil knot sculpture.

Nat was happy that I bought one of his sculptures, so he made me another one on the spot, a Moebius strip made from a 6" wide strip of aluminum sheet metal. It took him only a few minutes to cut the strip from a roll of sheet metal, bend it into shape, and rivet it together in two places. I have attached two pictures, showing it from two sides.

Nat Friedman Sculptures – Alex Feingold Collection

I was quite jealous of his art collection, which included a beautiful piece by Bathsheba Grossman. I wish I had kept in closer touch with Nat over the years. I know that he was an organizer for many conferences such as the SMI (Shape Modeling International) and the FASE (Fabrication & Sculpting Event), whose proceedings he edited with Ergun Akleman into the HYPERSEEING magazine for many years. Sometimes I tried to be helpful as a referee for submitted articles, but I know the hard work was done by the editors.

**Art Math Gatherings**
**Gary Greenfield**
**Emeritus Professor of Mathematics & Computer Science**
**University of Richmond**

This is Art and Math (AM) group photo from Albany in June 24-26, 1995. This was the third gathering of Art Math group. The first Art Math gathering was in 1992. Art Math gatherings organized by Nat Friedman continued until 1998 in Albany and morphed into ISAMA and the locations started to vary. Reza Sarhangi (1952-2016), the founder and president of the Bridges Organization, is also in this picture, next to Nat Friedman. Bridges conference started three years later in 1998.

Famous mathematician John H. Conway, who also died from complications of COVID-19 on April 11, 2020 at age 82, is also in this picture. Nat Friedman and Reza Serhangi are in the front row. Elizabeth Whiteley and John Conway can be spotted at upper middle left. Gary Greenfield in second row sort of peeking out from behind a woman in a black dress, who could be Eva Knoll. The reason almost none of the people look familiar is because more than half were local area high school teachers who were getting professional development credit for attending morning plenaries and afternoon workshops.

**Dick Termes**
**Sculptor**

Nat certainly got me involved in the art /math movement in Albany and by doing this I met all kinds of wonderful math/art people so I will very much miss Nat. He did a great job with his life.

**Robert Fathauer**
**Sculptor & Artist**

My first math/art conference was Nat's get-together in Albany in 1995. In 2004, Nat, Reza, and I organized the first art exhibition at the Joint Mathematics Meetings. There's been one every year since, and it's become an important feature of the meeting. Starting around 2008 I got into hiking and exploring slot canyons in northern Arizona and southern Utah. Nat loved some of the photos I took, and we ended up collaborating on a couple of articles for Hyperseeing that were basically a collection of these photos with some commentary from Nat.

Nat had friends in Tucson and starting spending several weeks in Arizona every winter sometime in the 2010's, if not earlier. He took to spending quite a bit of that time in Sedona, where he loved the rock formations. In 2014 we met up in Phoenix, and I drove us to Antelope Canyon, in the northern part of the state. It was Nat's first visit there, and it would be hard to overstate how much he loved that place. To him it was one giant walk-through stone sculpture. We went again in 2015 and on up into southern Utah to check out some slot canyons there. It was during these trips that I really go to know Nat, as we spent many hours together in the car. I enjoyed the long discussions we had about art and sculpture. I was sorry he had to discontinue those trips when his health started deteriorating and will miss him.

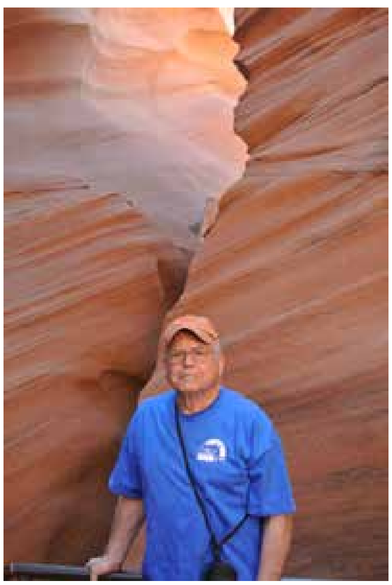

In Lower Antelope Canyon (2015).

Descending stairs into the lower end of the canyon

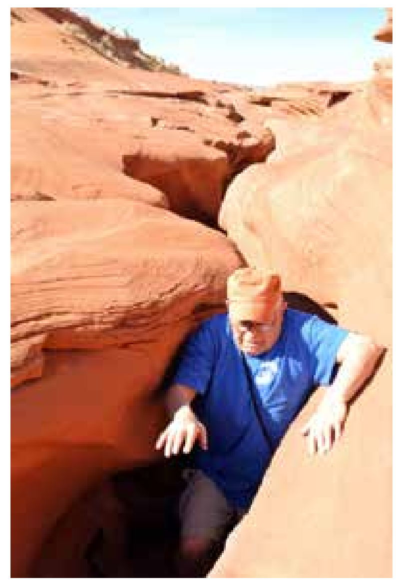

Emerging at the top end.

**Robert Longhurst,**
**Sculptor, Chestertown, NY**

I first met Nat when he invited me to participate in an art/math conference at SUNY Albany in the early 90s. I was not quite sure what it was all about but am glad that I agreed. Nat lived and breathed art/math. As time went by Nat and I kept in touch and he frequently visited the Chestertown studio as he always wanted to see what I was working on and it was enjoyable for me to hear what he had been working on as well. We made numerous trips to Vermont to scrounge marble cut offs which I could cut down, polish and make into sculpture bases and he would mostly just collect interesting shaped pieces which piled up in his back yard in Albany. Aside from the topics of art and math my most memorable thoughts of Nat are just that of a good friend and getting together for lunch or dinner to catch up.

**Ergun Akleman**
**Professor, Departments of Visualization &**
**Computer Science and Engineering**
**Texas A&M University**

I knew Nat Friedman for a while; however, I met with him relatively late, just 14 years ago. We had a workshop in August 2006 in Bridges, London on developable surfaces based on methods of Sculptor Ilhan Koman. Nat was one of the participants. He enjoyed the workshop and wanted to meet with me. I found workshop photos that demonstrate how intensely he worked with paper models. The first photo also shows both of us in the same frame during workshop.


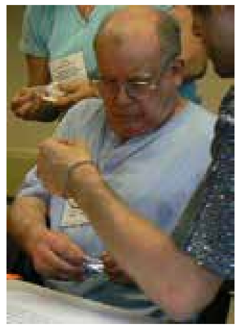

After the workshop, Nat wanted to meet with me to discuss. He asked me to help him to start Hyperseeing. I do not know how he knew that I had experience with publication. Once we returned from London, he send me his initial newsletter idea. After a few iterations, we started to publish Hyperseeing in September 2006. We had book reviews, articles, and cartoons (see the cartoon from September 2006 issue in Doug Dunham's tribute). I worked on to turn it into a magazine format. He liked the new design a lot. We moved the new format in November 2006 and continue.

He suggested having ISAMA conference in College Station in May 2007. He came a few days before the conference to help me organizing the conference. It was my first conference organization and I was a little worried. He told me that *"A conference is a like a wedding. Everybody knows what to do when you put everything in place."* I observed that he was right. We had a successful conference with no problem.

He came to College Station for one more time to present in the first FASE conference as a part of Shape Modeling International 2012. It was hard for him to continue to organize the ISAMA conferences. After SMI'2012, he suggested to continue ISAMA conference as an Event in Shape Modeling International (SMI). I proposed it to SMI steering committee and everybody agrees.

The last Hyperseeing issue he involved as an editor was summer 2014. He also wrote several articles about upcoming sculptors. Unfortunately, his health deteriorated quickly after that point. Not to be able to work and dance anymore made him very sad. Without his energy and support, it was hard for me to have additional issues every year. Hyperseeing, as a result, practically became "Proceedings of SMI Fabrication and Sculpting Event".

Nat was always very proud of Hyperseeing. He always said that he did not invent Hyperseeing, but he coined the word "Hyperseeing." It is really a great word to explain the complexity of sculpting. I hope we can turn Hyperseeing into a quarterly journal again in the future as his legacy.

# FULL PAPERS

# Symmetrical Vortex Knots

Carlo H. Séquin

CS Division, University of California, Berkeley;
sequin@cs.berkeley.edu

## Abstract

My goal is to create sculptural models of mathematical knots that exhibit a high degree of symmetry. I start with an arbitrary torus knot and turn it into a circular braid with the same symmetry by selectively reversing some of the displayed crossings in a knot projection along the rotational symmetry axis. In the simplest case, I make the knot completely alternating. The resulting braid can then be draped around a cylinder to result in a classical Turk's Head Knot. Alternatively, the braid can be fit around a sphere to yield a ball-shaped knot. Different choices for the sequence of over- and under-crossings result in different mathematical knots. The approach can be generalized by choosing an appropriate short braid segment and stitching together a number of identical copies of it. The resulting knots all have the common property that the knot filament travels around the rotational axis in a monotonic manner; I call such knots "Vortex Knots." Small scale models, about five inches in diameter, have been made by additive manufacturing on a Fused Deposition Modeling (FDM) machine. To make a truly artful knot sculpture, a more interesting cross-section, e.g., a crescent shape, is swept along the knot curve, and the plastic maquette is turned into a small bronze sculpture, perhaps embellished with a colorful patina.

## Possible Knot Symmetries

The type of symmetry that mathematical prime knots can exhibit is rather limited [3]. Except for the trivial *Unknot*, they cannot display simple mirror symmetry [6]. Their symmetries are limited to just three families of rotational symmetry groups:

- "$\mathbf{C}_n$" (Schönfliess notation [10]) or "***nn***" (Conway's Orbifold notation [9]) exhibits one *n*-fold rotational symmetry axis (Figure 1a); here the axis is perpendicular to the plane of the paper.
- "$\mathbf{D}_n$" or "***nnn***" has the same type of rotation axis, but also has *n* 2-fold rotation axes perpendicular to the primary *n*-fold axis (Figure 1b). In the simplest case, $\mathbf{D_2}$, there is just a single 2-fold rotation axis (Figure 1c); here it lies in the plane of the paper.
- "$\mathbf{S}_{2n}$" or "***n*X**" also has a primary *n*-fold rotation axis, and in addition exhibits glide symmetry, involving a reflection along the primary axis combined with a rotation through an angle of 360°/*n* around that axis (Figure 1d).

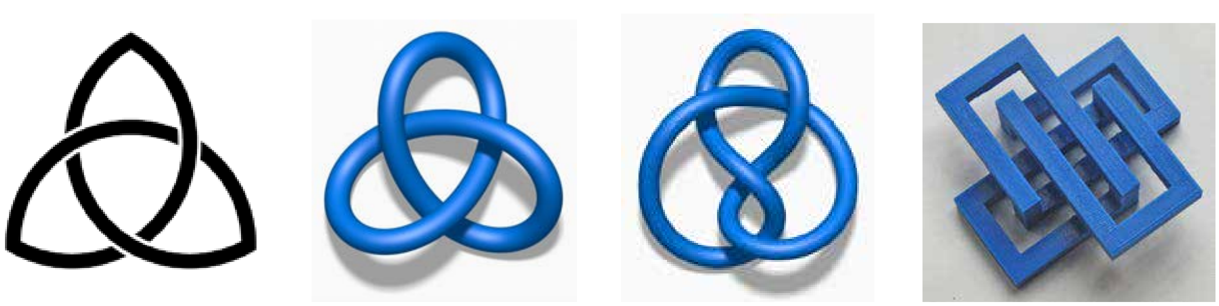

(a) (b) (c) (d)

**Figure 1:** *Trefoil-knot (Knot $3_1$): (a) 2D diagram with $C_3$ symmetry; (b) 3D model with $D_3$ symmetry. Figure-8 knot (Knot $4_1$): (c) 3D model with $C_2$ symmetry; (d) 3D model with $S_4$ symmetry.*

Most prime knots of low complexity can be re-shaped to display more geometrical symmetry than is implied by the depictions in the Rolfsen Knot Tables [5]. All but one knot (Knot $8_{17}$) [4] that have eight or less crossings, can exhibit one of the above rotational symmetries. However, there seems to be no robust algorithm that automatically finds the maximal symmetry of a given particular knot. In order to find a possible symmetrical configuration of a given knot, one must use some ad-hoc trial-and-error approach. One might start with a projection of the given knot and apply various *Reidemeister-moves* [6] to shift some trace segments in the knot projection across one another without changing the topology of the knot. However, it is not clear what sequence of moves should be applied to tease out a projection that displays a higher degree of symmetry. Alternatively, one might form the knot of interest from a loop of wire or with some pipe-cleaners or chenille stems. Yet again, there is no recipe for the sequence of deformations that might bring about a more symmetrical configuration.

In view of this, a more effective way of creating mathematical knots of high symmetry is to use a procedural approach to define a path that moves through Euclidean 3-space, $R^3$, following a symmetrical pattern. In the following I outline a few techniques for generating such symmetrical paths. I might not know the label of the generated knot in the knot table, but the result is still useful to produce a knot sculpture with high symmetry. A tool like *SnapPy* [2] can help identify the generated knot, if its crossing number is not too high.

## From Torus Knots to Vortex Knots

The most obvious and quick way to obtain a prime knot with $s$-fold rotational symmetry is to construct a TorusKnot($s,t$), where the knot filament shoots through the central hole of a donut $s$ times, while completing $t$ turns around the hole (Figure 2a). These knots exhibit $D_s$ symmetry. But, as the values of $s$ and $t$ get larger, the result does not look so much like a complex "Gordian" knot, but more like the cooling pipes in a power plant.

However, this can be remedied by turning the torus knot into a more intricate circular braid. First, the torus knot is squashed into a 2D circular template by setting all $z$-values to zero (Figure 2b). Now there is a choice how one might alter the original sequence $(\text{oooo uuuu})^3$ of the over- and under-passes at all crossing points (Figure 2c). In order to maintain a symmetrical configuration, one must respect the original $s$-fold symmetry of the initial torus knot, or, at the very least, choose the crossing pattern to follow an integral subset, *s/I*, of that symmetry group. A first choice that immediately presents itself is to turn the flat 2D template into a strictly alternating knot (Figure 2d), resulting in a Turk's Head Knot [11]. The original TorusKnot(3,5) (Figure 2c) corresponds to Knot $10_{124}$ in the knot table, while the alternating knot (Figure 2d) is Knot 12a1019.

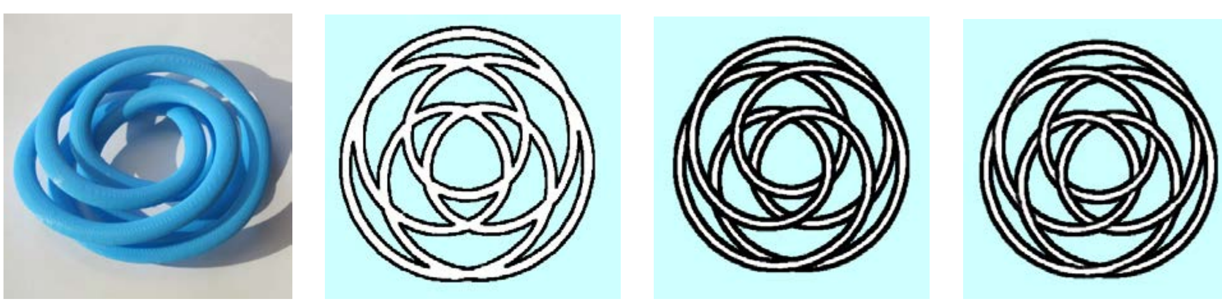

(a) (b) (c) (d)

**Figure 2:** *(a) TorusKnot(3,5); (b) flattened template; (c) braid representing the original knot; (d) an alternating over- under-crossing pattern, resulting in a Turk's Head Knot.*

Of course, the sequence of over- and under-passes can be made more intricate. For the above example, starting with a TorusKnot(3,5), there are a total of six different ways of choosing the over-/under-sequence so that one obtains different knots while maintaining full $D_3$ symmetry. The remaining four possibilities are shown in Figure 3. Figure 3a uses the pattern (ooou ouuu)$^3$; this yields Knot $11_{387}$. The pattern (oouu oouu)$^3$ (Figure 3b) results in Knot 12n708. Similarly, pattern (oouo uouu)$^3$ (Figure 3c) results in Knot 12n839, and (ouuo uoou)$^3$ (Figure 3d) produces Knot 12n837.

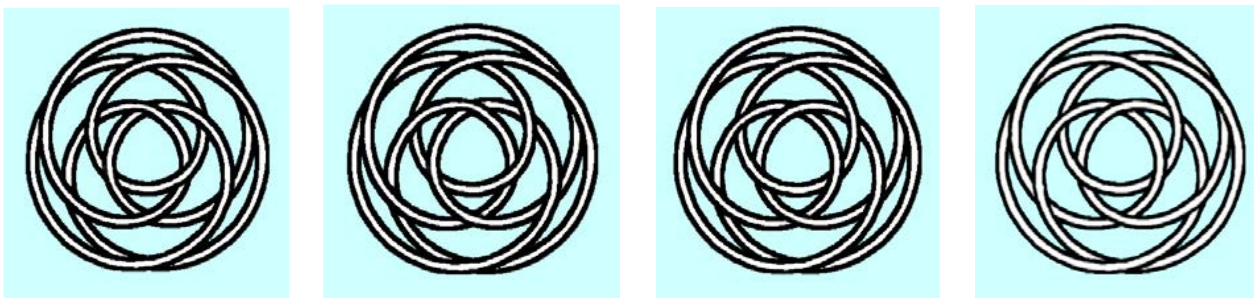

(a) (b) (c) (d)

**Figure 3:** *Circular braids: (a) (ooou ouuu)$^3$; (b) (oouu oouu)$^3$; (c) (oouo uouu)$^3$; (d) (ouuo uoou)$^3$.*

These circular braids still look rather flat. To obtain attractive 3D sculptures, I need to give these knots more "3-dimensionality." Figure 4 shows a few ways how this can be done. Here I started with TorusKnot(2,5) and changed the crossing pattern to the sequence (oouu oouu)$^2$ for subsequent over- and under-passes (Figure 4a); this produces Knot $6_3$ in the knot tables. This flat, circular braid is now rotated through itself like a smoke ring. A 90° rotation results in a cylindrical braid (Figure 4b). I can drape this braid around a sphere or around an ellipsoid, rather than around a cylinder, to obtain a more ball-shaped sculpture (Figure 4c). Different colors in the upper half and the lower half of this sculpture, make it easier to see that the two halves can be transformed into one another through a 90° rotation around the *z*-axis with a simultaneous mirroring along the *z*-axis; this is the hallmark of $S_4$ symmetry.

This particular symmetry can be made even more visible, if the top- and bottom-pair of inter-linked lobes are pulled apart so that they form stretched, open chain links. These links can be seen as some kind of double-covering on two of the six edges of the tetrahedral frame. The top-pair and the bottom-pair are twisted in opposite directions, reflecting the mirroring operation inherent in the $S_4$ glide symmetry. During all these deformations, the knot topology remains unchanged; it happens to correspond to Knot $6_3$ in the knot table. These transformations also preserve the property of a vortex knot that the filament spirals around the rotation axis in a monotone way.

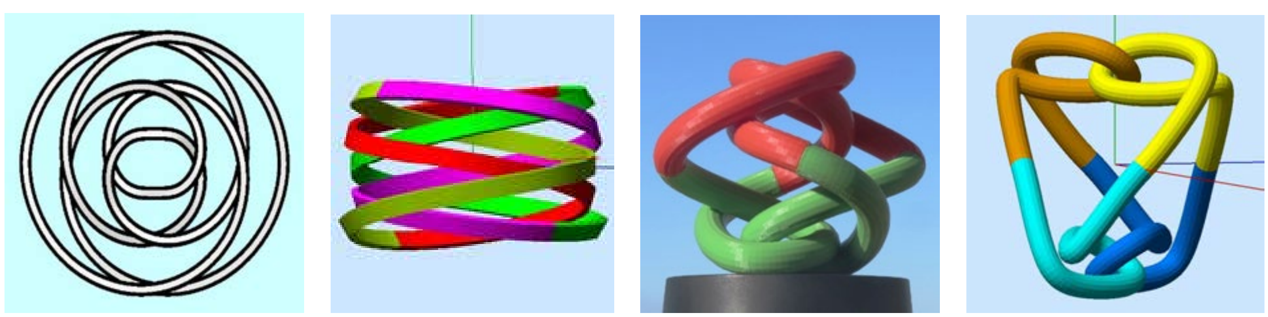

(a) (b) (c) (d)

**Figure 4:** *Knot $6_3$ shown: (a) as a flat 5-strand circular braid, (b) as a cylindrical braid, (c) as a ball-knot, (d) in a tetrahedral configuration with linked top- and bottom-edges.*

Figures 5 and 6 show additional examples of alternating Turk's Head Knots, THK(*s,t*), that were turned into more spherical BallKnots(*s,t*). The symmetry parameter *s* defines the number of *bights* or "bays" in the Turk's Head Knot, and the parameter *t* corresponds to the number of *leads* or "parts" in that knot. Depending on whether *t* is even or odd, the overall *s*-fold rotational symmetry will be of type $D_s$ or $S_{2s}$, respectively. In either case, the filament takes *t* turns around the z-axis.

(a) (b) (c)

**Figure 5:** *BallKnots(s,t) based on Turk's Head Knots, THK(s,t), and their symmetries:*
*(a) THK(4,3): $S_8$; (b) THK(3,4): $D_3$; (c) THK(4,5): $S_8$.*

(a) (b) (c)

**Figure 6:** *BallKnots(s,t) based on Turk's Head Knots, THK(s,t), and their symmetries:*
*(a) THK(5,6): $D_5$; (b) THK(6,5): $S_{12}$; (c) THK(6,7): $S_{12}$.*

In Figure 7, I am using the pattern (oouu oouu)$^s$ with 2-, 3-, and 4-fold rotational symmetry, and the knot strand is always circling the *z*-axis five times. The results are presented in the form of BallKnots(s,5). In Figures 7a and 7c, the differently colored parts are all identical and show the *s*-fold rotational symmetry. In Figure 7b, the knot has been split into upper and lower lobes, which are mirror images of one another.

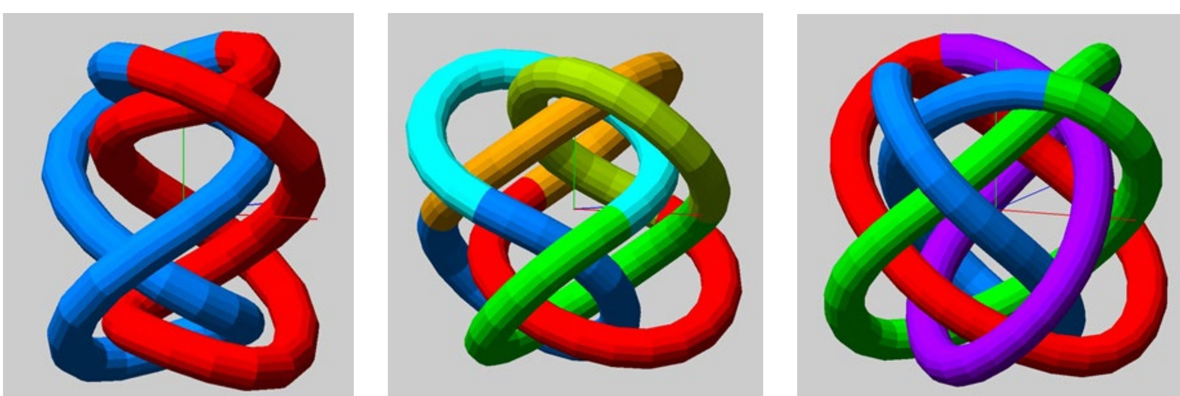

(a) (b) (c)

**Figure 7:** *BallKnots, BK(s,t), using crossover-pattern (oouu oouu)$^s$ and their symmetries:*
*(a) BK(2,5): $S_4$, (b) BK(3,5): $S_6$, (c) BK(4,5): $S_8$.*

## Generalized Vortex Knots

All the results so far, derived from some torus knots, have the property that the knot strand undulates s times in a regular manner back and forth from one edge of the braid to the other one. I will refer to the resulting knots as *regular* VortexKnots(*s,t*). Now I generalize the braid behavior so that in some regions the undulations of the strand have smaller amplitudes. One way to accomplish this is to start with a proper braid segment, e.g., the *minimum braid representation* of a Knot $6_3$ (Figure 8a). This braid by itself does not exhibit a repetitive, periodic structure that would then automatically lead to a configuration with rotational symmetry when the braid is closed end-to-end to form a circular loop (Figure 8b). To remedy this situation, I concatenate *s* copies of such a braid into a longer braid, which then will yield a construction with *s*-fold rotational symmetry. However, one must be careful; not every value of *s* will lead to a single knot; some values will produce a link. For the 3-strand braid of Knot $6_3$ (Figure 8a), two concatenated copies (Figure 8c) will result in a proper generalized vortex knot (Figures 8d, 8e); but concatenating three copies would result in complex link of three loops.

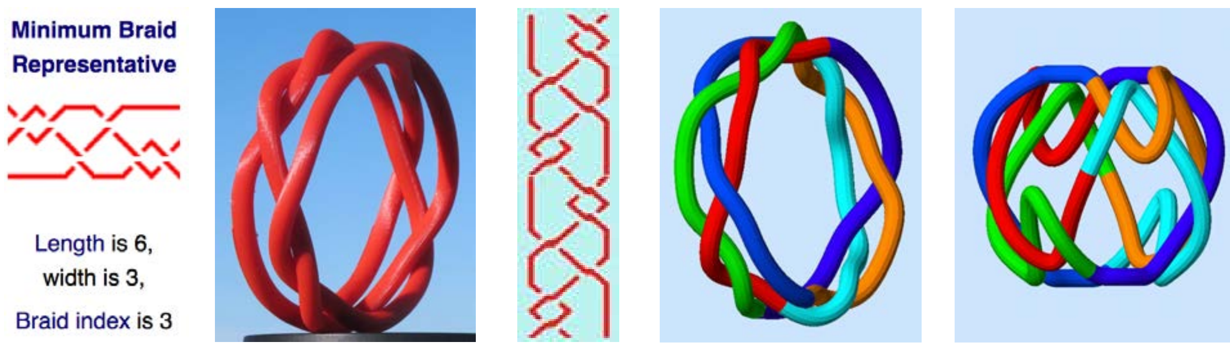


(a) (b) (c) (d) (e)

**Figure 8:** *(a) The braid representation of Knot $6_3$, (b) Knot $6_3$ as a cylindrical braid sculpture. (c) Two concatenated braids, (d) closed into a cylindrical braid, (e) formed into a ball-knot.*

For another example, I start with the 5-strand minimum braid representation of Knot $10_{43}$ (Figure 9a). Concatenating three of these braid segments into a cylindrical loop (Figure 9b) results in a generalized vortex sculpture with $C_3$ symmetry (Figure 9c). If I use only two copies of the braid segment, I obtain a sculpture with $C_2$ symmetry (Figure 9d).

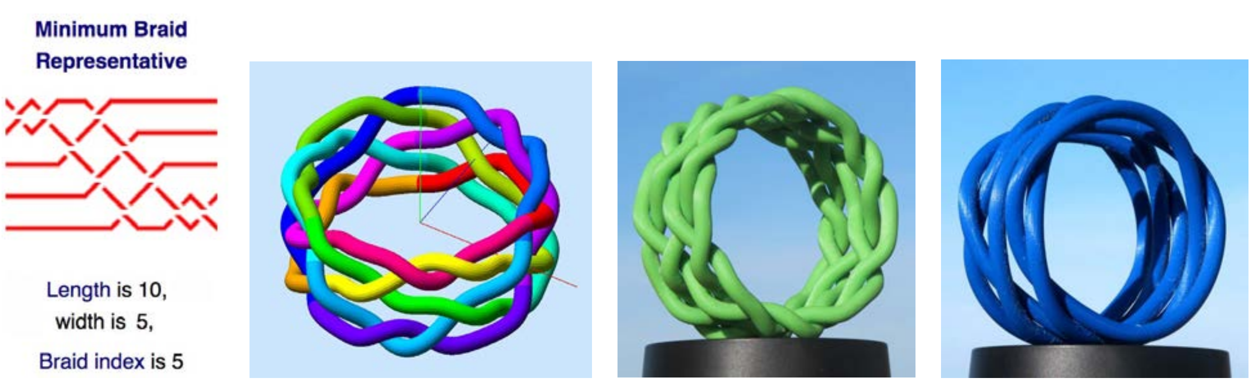


(a) (b) (c) (d)

**Figure 9:** *(a) The braid representation of Knot $10_{43}$. (b) Three concatenated braids in a loop; (c) resulting sculpture with $C_3$ symmetry, (d) $C_2$ sculpture formed with 2 braid segments.*

## Beyond Vortex Knots: "Braids" that Loop Back

Proper braids (Figures 10a, 10b) must not have any backward turns as shown in Figure 10c. That latter braid, when closed into a loop, would no longer yield a proper vortex knot in which the knot filament travels in a monotone manner around the primary rotation axis. Figure 10d shows an example of a nice knot with 2-fold rotational symmetry; but this is no longer a vortex knot.

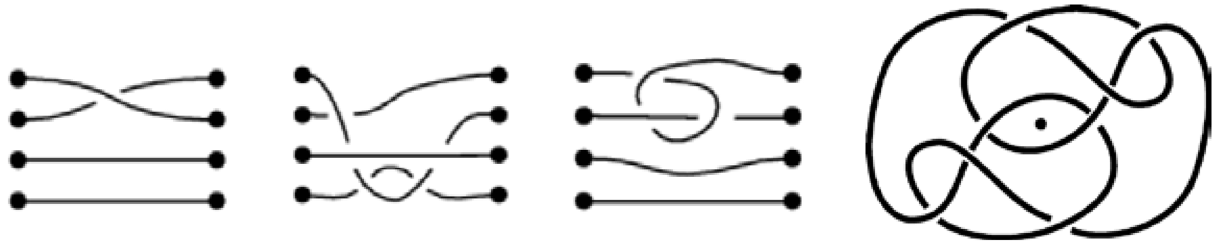

(a) (b) (c) (d)

**Figure 10:** *(a, b) Two proper representations of the same braid. (c) Not a true braid. (d) a symmetrical knot that is <u>not</u> a proper vortex knot.*

Figure 11a gives another example of a knot projection with $C_3$ symmetry that is not a vortex-knot; but it still makes a rather attractive 3D model, when this "bad" braid is wrapped around a cylinder (Figure 11b).

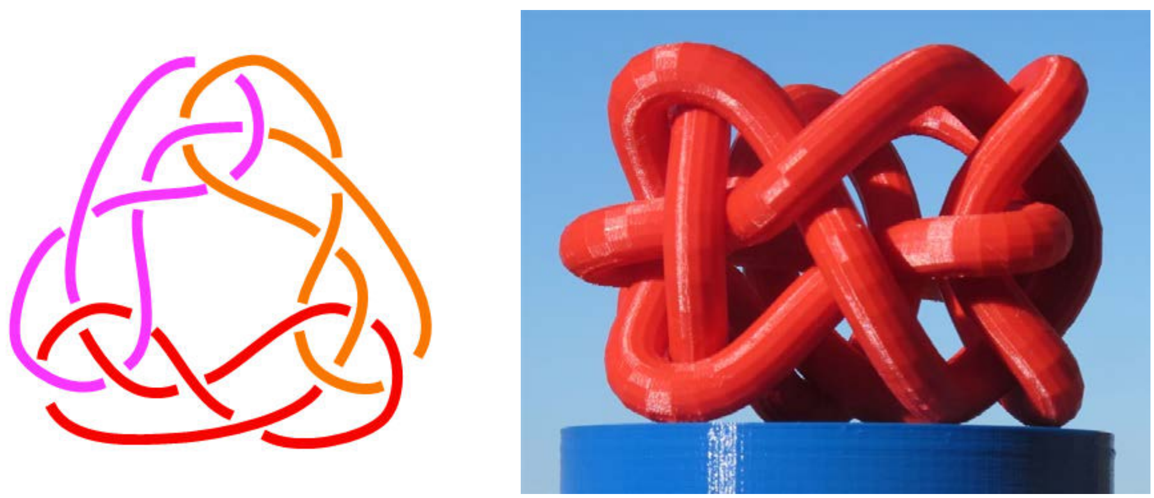

(a) (b)

**Figure 11:** *(a) Another $C_3$-symmetrical knot; (b) its realization as a cylindrical braid.*

## CAD Modeling

The various 3D models shown above have been constructed with Berkeley SLIDE [7], but any other CAD system would work just as well. The key step is to create an iterated process that creates the desired knot curve in 3D, which can then be used as the sweep path for a "fleshed-out" physical knot model. In most of the above models, I have defined a sequence of control points for a cubic B-spline. Typically, I use four times as many control points as there are crossings in the knot projection. I place two control points at every crossing, and the separation between them allows me to control the clearance between the crossing knot strands. In addition, there is an additional control point between subsequent crossings, which I use to create fairly smooth transitions between the crossings. This is good enough for the simple plastic models used to demonstrate the knot symmetries. For any final artistic sculpture models, I would use some additional control points, or I would employ a quartic B-spline rather than a cubic one.

## Summary and Discussion

Symmetrical prime knots all have a dominant ***n***-fold rotational symmetry axis, because their overall symmetry must fall into one of the three families $\mathbf{C}_n$, $\mathbf{D}_n$, or $\mathbf{S}_{2n}$ (Schönfliess notation [10]) or "***nn***", "***nnn***", or "***n*X**" (Conway's Orbifold notation [9]). A knot with ***n***-fold rotational symmetry of type $\mathbf{C}_n$, thus can be constructed by grouping ***n*** copies of an appropriate tangle of trace segments symmetrically around a common rotation center (Figure 12a). The symmetry of the resulting construction can be further enhanced, and the number of group elements doubled, by adding copies of each tangle that are flipped through an angle of 180° around an axis that intersects the dominant rotation axis at right angle; this yields $\mathbf{D}_n$ symmetry (Figure 12b). Alternatively, the number of tangles can be doubled by interspersing into the first $\mathbf{C}_n$-set of tangles another set of ***n*** tangles that are mirrored along the dominant rotation axis (Figure 12c).

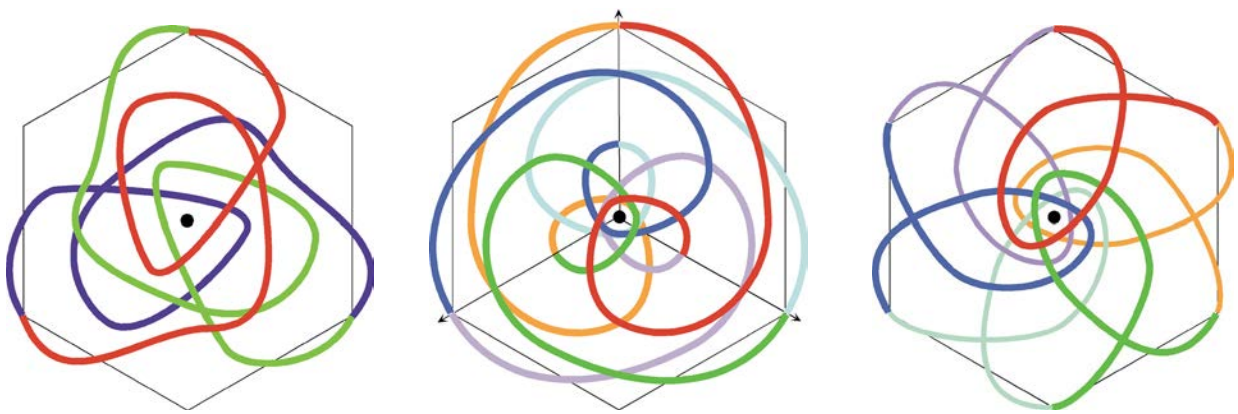

(a) (b) (c)

**Figure 12:** *Knot constructions with **n**-fold rotational symmetry (**n**=3):*
*(a) $\mathbf{C}_n$ symmetry; (b) $\mathbf{D}_n$ symmetry; (c) $\mathbf{S}_{2n}$ symmetry.*

Among all such constructions, Vortex knots, in the form of almost-planar circular braids, in which the knot filament spirals around the main symmetry axis in a monotone way, are particularly efficient in providing a desired level of symmetry with a minimal amount of bending energy (the integral of squared curvature along the whole knot trace); they contain no "unnecessary" tight turns. Most "efficient" in this respect are the simple, regular TorusKnots(*s,t*), which exhibit crossover-patterns of the type (ooo…o uuu…u)$^s$. But for large values of *s* and *t*, they start to look like industrial cooling pipes.

To make them look more like interesting, intricate knots, the crossover-sequence must be changed into a more varied pattern. The alternating pattern (ouououou…ou)$^s$ will result in a Turk's Head Knot [11], and there are also many other possible patterns. Once the mathematical knot type has been determined in this manner, the knot geometry can be refined by mapping the initial flat circular braid around a cylinder or around an ellipsoid, and the thin knot trace can be replaced with a sweep of a more interesting geometrical profile (Figure 13).

## Vortex Knots in Bronze

Some of the described vortex knot constructions lead to well-known knots from the knot table. For instance Torus-knot(2,3) turned into an alternating braid will result in the Figure-8 Knot (Knot $4_1$), exhibiting $S_4$ symmetry. Similarly, Torus-knot(3,4) turned into an alternating braid will result in the Chinese Button Knot (Knot $9_{40}$), exhibiting $D_3$ symmetry. Figure 13 presents artistic bronze sculptures based on these two simple knots, which I have done many years ago. They were modeled by sweeping a crescent-shaped cross-section along the given knot curve. The basic geometry was fabricated on a Fused Deposition Modeling (FDM) machine; this is a 3D-printer that extrudes semi-liquid plastic with the consistency comparable to toothpaste. These ABS-plastic models were then converted into bronze in a classical investment-casting process by Steve Reinmuth in his Bronze Studio in Eugene, OR. It turns out that ABS as well as PLA plastic models sublimate cleanly in the kiln in which the plaster shell is fired. Steve Reinmuth also created the colorful patinas with a combination of heat (from a flame torch) and chemistry (from a spray bottle).

(a) (b)

**Figure 13:** *Bronze sculptures: (a) Knot $4_1$ (Figure-8 Knot); (b) Knot $9_{40}$ (Chinese Button Knot).*

## References


[1] C. C. Adams. *The Knot Book*. Originally published by W.H. Freeman and Company... reprinted with corrections in 2004 by the American Mathematical Society.

[2] M. Culler, N. M. Dunfield, M. Goerner, and J. R. Weeks. "SnapPy." 2020. https://www.math.uic.edu/t3m/SnapPy/

[3] B. Grünbaum and G. C. Shephard. "Symmetry Groups of Knots." Mathematics Magazine, vol. 58, no. 3, 1985, pp. 161–165. http://www.jstor.org/stable/2689914

[4] The Knot Atlas. "$8_{17}$." 2005. http://katlas.org/wiki/8_17

[5] The Rolfsen Knot Table. 2005. http://katlas.org/wiki/The_Rolfsen_Knot_Table

[6] C. H. Séquin. "Physical Illustrations of Knot Deformations and Surface Eversions." *ICERM*, Brown U., Sept. 18, 2019. http://people.eecs.berkeley.edu/~sequin/TALKS/2019/2019_ICERM-Talk.ppt

[7] J. Smith. "SLIDE design environment." (2003). http://www.cs.berkeley.edu/~ug/slide/

[8] E. W. Weisstein. "Reidemeister Moves." MathWorld – A Wolfram Web Resource. 2020. http://mathworld.wolfram.com/ReidemeisterMoves.html

[9] Wikipedia. "Orbifold Notation." 2020. https://en.wikipedia.org/wiki/Orbifold_notation

[10] Wikipedia. "Schönfliess Notation." 2020. https://en.wikipedia.org/wiki/Schoenflies_notation

[11] Wikipedia. "Turk's head knot." 2020. https://en.wikipedia.org/wiki/Turk%27s_head_knot

# Portal: Design and Fabrication of Incidence-Driven Screens

S. Vahab Hosseini[1], Usman R. Alim[2], Ali Mahdavi Amiri[3]
Lora Oehlberg [4], and Joshua M. Taron [5]

[1]Computational Media Design, University of Calgary; hosseini.vahab@gmail.com
[2]Dept. of Computer Science, University of Calgary; ualim@ucalgary.ca
[3]Dept. of Computer Science, Simon Fraser University; amahdavi@sfu.ca
[4]Dept. of Computer Science, University of Calgary; lora.oehlberg@ucalgary.ca
[5]School of Architecture, University of Calgary; jmtaron@ucalgary.ca

## Abstract

We introduce "Portal", an optically-illusive screen panel with a grid of mirrors serving as its pixels. The RGB values of each mirror are obtained from its environment using the law of reflection. Specifically, we employ two images: one target image for the mirror panel, and another which serves as a palette to lend mirrors its RGB values. Our methodology uniquely orients each mirror in the grid to reflect a particular region of the palette image to a specified viewpoint. The holistic image from the mirror grid composes the target image. Within the process, we need to satisfy a set of rules to secure the maximum approximation of the result with the intended images.

We also propose a methodology to fabricate Portal using laser cuttings. As a proof of concept, we created a Portal equipped with 540 mirrors. Based on the physical and digital simulation results, we speculate possible applications of Portal in a range of disciplines, including computer graphics, art, and architecture.

**Figure 1:** *Portal is a structure composed of cellular mirrors that creates an image by reflecting colors from another image that acts as a palette. Here, the Mona Lisa (left, in each panel) is our palette image that is used to produce other artworks.*

## Introduction

*"Remember that the Mirror shows many things, and not all have yet come to pass."*

*J.R.R. Tolkein*

Our perception of the world is fundamentally influenced by our viewpoint. Prior work in graphics has explored the subjectivity of viewpoints through effects that emerge based on a unique *privileged point*. There are many examples of leveraging privileged points to create meaningful images by using shadow; even in shadow puppetry (Figure 2a), a performer's hand arrangements against a source of light create recognizable shadows on a background. Along the same idea, several artists have produced sculptures that cast meaningful shadows that are uniquely different from the sculpture or installation itself (Figures 2b and 2c). In computer graphics, this concept has been elaborated upon further, to automatically design and fabricate an object that generates multiple shadows along different directions [31] (Figure 2d).

**(a)** **(b)** **(c)** **(d)**

**Figure 2:** *Shadow puppetry (a), Wire sculpture by Matthieu Robert-Ortis (b), Dirty White Trash by Tim Noble and Sue Webster (c), and ShadowArt [31] (d).*

In these shadow examples, the privileged point is the source of light; however, it can also be the point where hidden images are revealed to a viewer. We can use other perceptual techniques – like reflection – to produce images that are not apparent from the source object itself. In literature, characters encounter magic mirrors that show them distant objects or scenes from futures that do not yet exist (e.g., Galadriel's mirror from *The Lord of the Rings*, Figure 3).

**Figure 3:** *Mirror of Galadriel, by Alan Lee, 1992.*

Inspired by these components – privileged point and reflection – we designed and fabricated "Portal", a structure composed of a grid of mirrors. These mirrors, viewed from a specific viewpoint, collectively reflect and reconstruct a meaningful *target* image that does not exist in the environment. To reproduce this image, the mirrors are meticulously oriented towards a *palette* image which is the source of color for each mirror pixel (see Figure 1).

The main visual attribute of Portal is a screen panel composed of cellular mirrors arranged along a grid. The color of each mirror is obtained from the palette considering the law of reflection. Our proposed methodology preserves the features of the target image as much as possible. This is plausible by searching within the palette to find certain areas with specific colors and assigning those colors to each cellular mirror in the Portal. Since finding the exact desired color might be a futile attempt, our method alternatively finds the areas of the palette with minimal color discrepancies, and links them to the corresponding color on the target image. This search and assignment takes place under a privileged point towards Portal, meaning that Portal generates the target image when it is seen from a specific viewpoint.

Since Portal is a precise optical device, any degree of deviation from the privileged point, results in the imperfection of the generated image. Accordingly, to improve Portal's functionality, we have provided solutions to pick colors from regions that are more uniform and less susceptible towards slight viewpoint perturbation.

In this paper, we offer two contributions: first, we present the Portal technique as an optically-illusive structure that generates an image that does not exist in the environment. Second, we propose a fabrication strategy, using accessible machinery and materials, to produce real-world Portal structures. We also discuss the challenges and solutions we faced throughout the process.

The paper is organized as follows. We first discuss related work. Next, we describe the methodology and introduce notations. There is also a section, devoted to detailed fabrication strategies, followed by a section to discuss results and limitations. Finally, in the last section, we conclude with proposed future research.

## Related Work

Although our problem statement is novel, there exist related works, tackling similar problems in computer graphics as well as art and architecture. As the construction of our structure is based on the light and reflection phenomena, we first discuss related works that try to manipulate light (shadows and reflections) to produce optically-illusive effects. Next, we review a category of anamorphic, and privileged-point-oriented works in which one object can resemble multiple visual and physical paradoxical characteristics under distortion, transformation, or reflection, when viewed from different privileged points (multi-character objects). Eventually, we highlight a number of recent advances in computational fabrication to suggest the possibilities that these techniques offer (computational fabrication).

### *Light and Shadow*

An interesting line of research has been spent on the study of lights and shadows to reproduce a given image. For instance, fabricating surfaces with controlled appearance has been the subject of several previous works [27, 24, 29, 37, 4, 32, 33]. In these works, the material property is modified at micro scale in order to replicate a specific image or pattern on a surface under light. In this line of work, SHADOWPIX [5] is the most related research to our application, where one single fabricated object produces several images under different light directions.

Although related, the main idea of these works is different from ours as we are making a screen composed of cellular mirrors to generate an image from another given image by means of reflection. In addition to our work, the idea of cellular or micro mirrors has been also used in some other applications with completely different purposes. For instance, Hoskinson et al. [17] have used micro mirrors to improve the contrast and brightness of conventional projectors by reallocating the light of dark parts to the bright parts that need improvements in contrast.

As mentioned earlier, reflection and shadows are tightly related. A number of research works have investigated the potential of shadows in generating fascinating structures. For instance, Mitra and Pauly [31] have introduced ShadowArt in which an object is generated, capable of having meaningful shadows under lights from different orientations. To make such a structure, they find the intersection of a number of given images under various privileged points (e.g. directional lights) in a 3D visual hull to construct a 3D structure with shadows the same as the given images. The idea of manipulating shadows to reconstruct a given image is also used in [41] in which perforated lampshades are constructed so that their shadow produces a given image. To build such lampshades, a set of cylindrical micro structures are arranged on the lampshade to control how much light passes through. Although our work shares some commonality with [41], as well as ShadowArt [31] and SHADOWPIX [5], we propose different approaches towards fabrication and application.

A number of relevant precedents to this research can be found in the arts, where artists harness light and the law of reflection to create meaningful forms and shapes. For example, there is an art installation at The Israel Museum, by artist Daniel Rozin, called Broken-Mirror, where a series of mirror fragments are thoughtfully oriented to reconstruct an image scattered across a wall [10]. In addition, Floating Point is the name of an urban-scale installation, designed by Esteban Serrano, in which three computer-controlled mirrors track sun path to form an elliptical pattern onto an adjacent building [15].

Moreover, there is a series of projects conducted by Art+Com studio where a team of artists and scientists collaborate to generate forms by means of reflections and light; two noteworthy projects are Anamorphic Mirror [2] and Á la Recherche [3]. The former is a wall-sized arrangement of mirrors, each of which in a particular direction, to construct a form when viewed from a certain point in space. The latter is a giant rotating sculpture covered with mirrors that compose a message using reflected light.

### *Multi-character Objects*

This is a category of optically-illusive works in which the visual entity of an object contradicts its physicality. In other words, any object, other than its physical characteristic, manifested by the actual geometry, owns a variable visual characteristic, based on the viewpoint from which it is represented. The potential discrepancy between these characteristics incorporates an optical illusion. The core concept behind most of the works under this category is the principle of anamorphic projection. More specifically, one or more privileged points in space are defined through which a specific effect is perceived. The emergence of anamorphic projection has been thoroughly discussed in [34, 39, 40]. Nonetheless, there is a wide range of recent precedents in various disciplines, in which a visual effect is dependant on the audience's point of view. In addition to ShadowArt [31], and SHADOWPIX [5], we can refer to [35] in which an object inherits multiple meaningful visual attributes through multiple viewpoints. Moreover, there are research regarding an application of *collineation* [16], as well as a ray-casting technique [11] to generate anamorphic effects.

Anamorphosism has also been a remarkable subject in architecture. For instance, optically illusive architecture [19] is an architecture-oriented research toward manipulating perception of depth by suppressing three-dimensionality in a built environment. In addition, in [21] an anamorphic brick wall is designed that resembles a given image from a defined viewpoint. An in-depth technique to generate and digitally fabricate anamorphic effects on more complex surfaces is provided by [12]. Another approach in this field is an application of mirror-assisted anamorphic projection to reconstruct a set of 2D data distributed within an architectural space [18].

Artistically approaching the topic of anamorphic projection, we acknowledge "Wire Sculpture" by Matthieu Robert-Ortis, "Dirty White Trash" by Tim Noble and Sue Webster (Figures 2b and 2c), and also mirror-assisted optically-illusive works of Kokichi Sugihara [25], and Markus Raetz [30], to name a few.

### *Computational Fabrication*

Computational fabrication is now prevalent in a wide variety of applications. For instance, in [28, 13] reversible shapes are reproduced as a jigsaw puzzle pieces so that one shape can be transformed into another.

Also, Chen et al. offer a fabrication method to fasten a set of patch elements together, to form a given surface [8]. Computational fabrication is, however, not limited to additive fabrication methods. For example, [6] presents laser-cut results of their proposed technique to synthesize vector patterns with visual appearance. In [7] an application has been defined that reconstructs a given mesh with wooden pieces, using a laser cutter.

Likewise, [36, 20] utilize 2D laser cuttings for physical visualizations.

## Methodology

The inputs to our problem are a privileged point $P$, and two images: palette image $I$ and target image $\acute{I}$. The goal of our work is to design a structure, which is an incidence-driven screen — or Portal — composed of a grid of cellular mirrors. Every single mirror $m_i$ is assigned a unique orientation to reflect a specific region or block $b_i$ of image $I$. Reflections of all cellular mirrors compose image $\tilde{I}$, when viewed from $P$. It is desired that image $\tilde{I}$ be as close as possible to target image $\acute{I}$.

Since constructing a structure with the same level of detail as a given image requires many tiny cells, we sample images with coarser cells to provide an approximation for target image $\acute{I}$. This also facilitates the subsequent fabrication process. Sampling takes place by averaging the pixel values covered by a cell on an image.

First, target image $\acute{I}$ is divided into a number of cells called $c_i$ (see Figure 4). Each cell $c_i$ corresponds to a cellular mirror $m_i$ in Portal. It is desired that the colors that $m_i$ attains, be close to the color of cell $c_i$ in the target image. By default, $c_i$ are chosen to be hexagonal in Portal. However, the core of our algorithm is independent of cell type and other cellular shapes can also be incorporated. Later in this section, we discuss the choice of cells based on the shape of the target image.

**(a)** **(b)** **(c)**

**Figure 4:** *Image $I$ (a) is divided into a number of blocks $b_i$. Image $\tilde{I}$ (b) is produced by Portal. Each cell of image $\tilde{I}$ corresponds to a mirror on Portal. Target image $\acute{I}$ (c) is sampled coarsely by cells $c_i$. The color of each mirror $m_i$ in Portal should be as close as possible to $c_i$.*

The palette image $I$ is also divided into a number of blocks called $b_i$ to facilitate the search over its color space (Figure 4). For each block, we save the average of pixel values of that block and its neighborhood. Then, to assign the right color to mirror $m_i$, our algorithm searches and selects a number of blocks on the palette (i.e. images $I$) whose colors are closest to cell $c_i$ on $\acute{I}$. Among these blocks, the algorithm later chooses the one with more color consistency with $c_i$ (i.e., lower variance). It is worth noting that our algorithm uses Euclidean colour difference metric, treating RGB values as coordinates in the space. However, perception-oriented metrics that are based on human's sight sensitivity could also be employed [9].

For $b_i$, we choose quadrilateral grids, since we do not modify image $I$ and quadrilateral blocks simplify our calculations. However, other cells such as hexagonal cells are also applicable.

### *Law of reflection*

To formulate and solve our problem, we take advantage of the well-known laws of reflection. The laws of reflection govern the reflection of light-rays off smooth conducting surfaces, such as a mirror. Essentially, there are two primary statements in the laws of reflection:

- The incident ray, the reflected ray, and the normal of the mirror lie in the same plane $\rho$.
- The angle of the incidence ray, $\theta$, with respect to the normal $n$ is the same as $\gamma$, the angle that the reflection ray constructs with the normal $n$ (i.e. $\theta = \gamma$)

The laws of reflection are the core of many rendering techniques, most notably ray tracing [38, 1]. In this work, using the laws of reflection, a ray is cast from point of view $P$ and the plane $\rho_i$ of each cellular mirror $c_i$ is oriented in such a way that the desired color from image $I$ is sampled. We assume that the mirrors are fully reflective and environmental shading effects are negligible.

### *Structure*

To sample image $I$ and reconstruct image $\acute{I}$, Portal is built by a set of cellular mirrors $m_i$ whose centers are placed on the centers of previously-generated blocks of image $\acute{I}$ (Figure 5). Since the number of cells corresponds to the number of blocks into which the images are divided, higher number of cells results in better approximation of image $\acute{I}$ but makes the fabrication process more difficult and expensive (Figure 6).

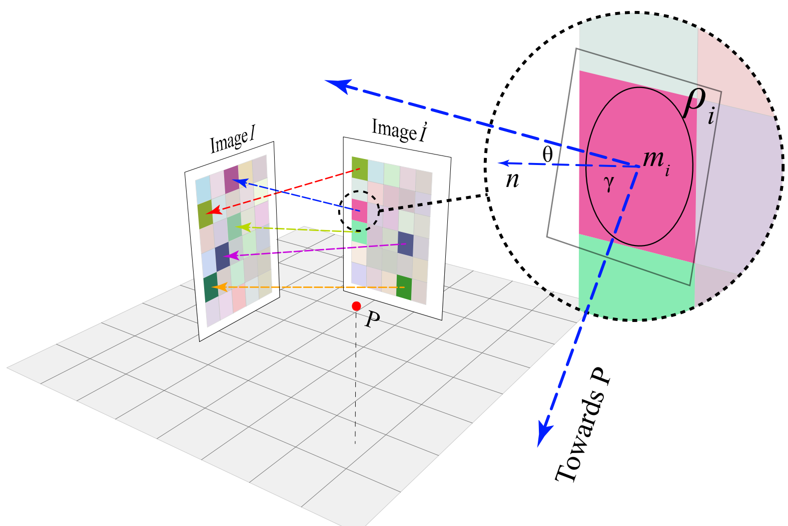


**Figure 5:** *For every block, hosting $c_i$, within image $\acute{I}$, the algorithm finds a matching block within image $I$. Next, $m_i$ is oriented to reflect that specific block of image $I$ to point of view $P$.*

Hexagonal grids have lower quantization error in comparison with quadrilateral and triangular grids [23]. However, since our methodology is not dependant on the form of the grid, we can choose the grid form with respect to features of image $\acute{I}$. For example, in specific paintings with sharp edges and straight lines, such as compositions of Dutch painter Piet Mondrian, representation through a quadrilateral grid is more accurate as opposed to a hexagonal grid (Figure 7).

### *Point of View*

The privileged point $P$ can be selected anywhere as long as both images are visible within human's cone of vision, and there is no occlusion from one image to another. Therefore, we define it to be on the bisector plane of the two planes hosting image $I$ and image $\acute{I}$. Another concern here is to ease the fabrication process. Accordingly, we set $P$ to be equidistant to both images such that when an individual is looking through the privileged point, both images remain within their arm's reach.

(a) (b) (c)

**Figure 6:** *Vincent van Gogh self-portrait, 1887 (a). Higher resolution is plausible through higher number of blocks and consequently higher number of mirror cells. Images generated by our method with 4800 blocks (b), and 540 blocks (c).*

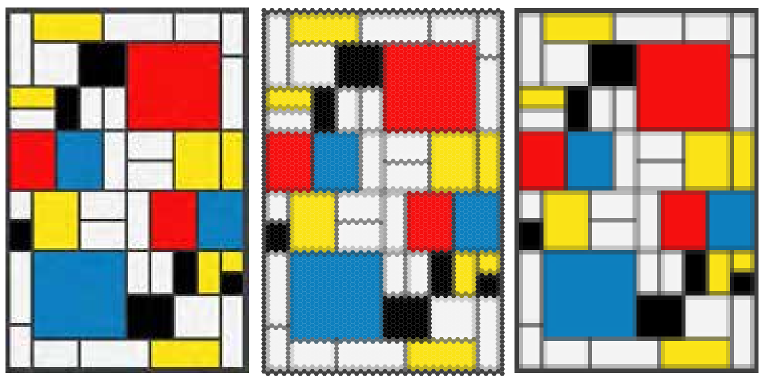

(a) (b) (c)

**Figure 7:** *Composition, by Piet Mondrian (a). A hexagonal grid (b) may fail to flawlessly represent straight lines as opposed to a quadrilateral grid (c).*

***Mirror Orientations***

To find the best orientation for each mirror, we need to consider several factors. First, any degree of deviation from the privileged point would cause imperfection of the result (i.e., color of $m_i$). To tackle this issue, we optimize the match-finding portion of the methodology to maintain the readability of Portal, once viewed within a privileged space surrounding the privileged point $P$. Toward this end, for every block $b_j$ of image $I$, the algorithm saves the average color ($\tau_j$) of the block and its adjacent blocks. Figure 8 illustrates how this step affects image $I$ by fading borders of colors and blending them together. This is equivalent to applying an averaging convolution filter to the image.

Next, these blocks, with their $\tau_j$ values, undergo match-finding process with those cells of the image $\acute{I}$ to assign the right block to mirror $m_i$. It is desired that a chosen block $b_j$ (with average color $\tau_j$) for mirror $m_i$ will have small color difference with $c_i$. Meaning that we are looking for blocks $b_j$ minimizing the following quantity: $E_{color} = |\tau_j - c_i|$. For each mirror $m_i$, a set of candidate blocks $B$ are chosen. In practice, we choose ten blocks with the lowest $E_{color}$ values.

After filtering many blocks by only considering their average color, we can now choose the appropriate block among blocks in $B$. Note that averaging the colors of a block may cause deficiency to the readability of

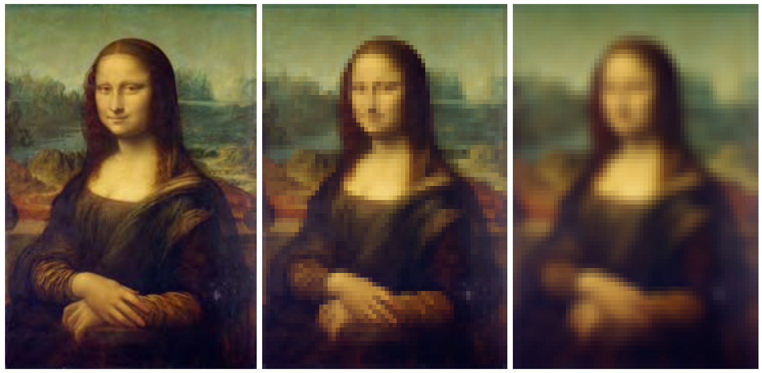

**(a)** **(b)** **(c)**

**Figure 8:** *Mona Lisa, by Leonardo da Vinci 1500s (a). Image I is generated with 4800 blocks, each of which is assigned average RGB value of its own pixels (b), and average RGB value of a neighborhood, embracing the block and its adjacent blocks (c).*

Portal. For instance, in an extreme scenario, the average color of a block with a checker pattern is grey. However, every single pixel has extreme distance with the average. To replicate the correct and consistent colors in Portal, it is desired that each pixel $p_k$ of the block $b_j \in B$ is close to its average. Deviation of each pixel from its average can be captured in an energy term called $E_{smooth}$ which is equivalent to variance of the pixel colors in each block. $E_{smooth}$ for $b_j$ is defined as follows: $E_{smooth} = \frac{\sum_k (p_k - \tau_j)^2}{N}$, where N is the total number of pixels in block $b_j$ and its neighborhood, and $p_k$ are the individual pixels that are in block $b_j$ and its neighborhood. Among blocks in $B$, we choose the block with smallest $E_{smooth}$.

In addition to these color-based energies, we could orient the cells to follow a smooth variation in the normal to avoid gaps between cells. This means that it is desired that the normal of a cell $c_i$ be as close as possible to the normal of its adjacent cells. In our experiments, even without this consideration, our methodology provides a level of smoothness in the normals of the cells (further details provided in section "Results"). As a result, we did not consider this additional term for our algorithm.

Now that we know the block, each mirror needs to reflect, we can find the right orientation for each cellular mirror. Towards this end, we consider two vectors extending from the center-point of each cell $c_i$ on the screen panel. One, hitting the center-point of the corresponding block on the palette, and the other one, targeting the privileged point. Having placed a mirror at the center-point of the cell $c_i$, and reorienting it in a way that its normal becomes the bisector of the two vectors, the mirror will reflect the corresponding block on the palette (Figure 5). Algorithm 1 summarizes the above discussion. In this algorithm we set M equal to 4800 blocks ($80 \times 60$) to yield the results shown in Figure 1.

## Fabrication

As mentioned earlier, the quality of the result of this work significantly relies on the utmost precision of the process. Accordingly, we use a subtractive fabrication method, and specifically 2D laser-cuttings, whereas it provides sharper edges and more accurate surfaces as opposed to additive fabrication methods (such as 3D printing), alongside being faster, cheaper, and more accessible [14, 26, 22]. Toward this end, we designed a notch-stem mechanism to be laser-cut out of flat sheet medium-density fibreboard (MDF). This snug-fit mechanism consists of a base, embracing notches, upon which stems are mounted. On top of the stems, mirrors are glued and fixed in their positions (Figure 9).

To secure the specific position and orientation of the mirrors, every notch must be uniquely oriented,

**Algorithm 1** Palette image $I$, Target image $\acute{I}$, and privileged point $P$ are given. This algorithm finds orientations (i.e., normals) $n_i$ for each cell $m_i$.

Sample Image $\acute{I}$ by $M$ hexagonal cells, $c_i$;
Segment Image $I$ into $M$ number of blocks $b_k$;
Assign the average color of $b_k$ and its four neighbors to $\tau_k$;
**for** each cell $c_i$ **do**
    Place ten blocks with lowest $E_{color}$ values in set $B$;
    Choose block $b_j$ from $B$ with smallest $E_{smooth}$;
    Assign $b_j$ to $m_i$;
    $v$ is the vector connecting the center of $m_i$ to $b_j$;
    $w$ is the vector connecting the center of $m_i$ to $P$;
    $n_i$ is the bisector of $v$ and $w$;
**return** all $n_i$'s.

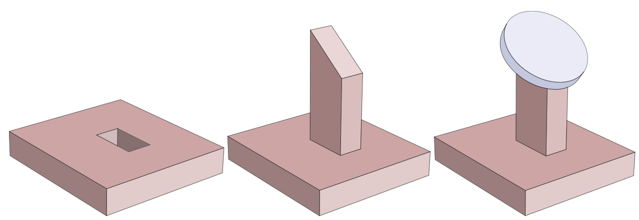

**Figure 9:** *The notch-stem mechanism. Mirrors are the only parts that need to be glued in their positions.*

and the top of each stem must be cut in a particular angle. To host notches, we define plane $\pi$, parallel to image $\acute{I}$ and behind it. Direction of each notch derives from $\vec{n}_i$ which is its corresponding mirror's normal. Next, having $\vec{n}_i$, projected on plane $\pi$ (i.e. $\vec{n_i'}$), we extend a curve, on both sides, along $\vec{n_i'}$, and project it back towards the corresponding mirror. The intersection of each projection and mirror, returns diameter $d$ of the mirror. The surface, confined with $d$ and its projection on $\pi$ (i.e. $\acute{d}$), forms a uniquely-tapered stem to hold the mirror. Regarding the dimensions, the projected diameter $\acute{d}$ refers to the length of each mirror's stem and notch.

Moreover, the material sheet thickness defines the width of the notches as well as the stems' thickness. In this fabrication process, we used MDF sheets with 5 millimeters of thickness. Figure 10 illustrates this entire process.

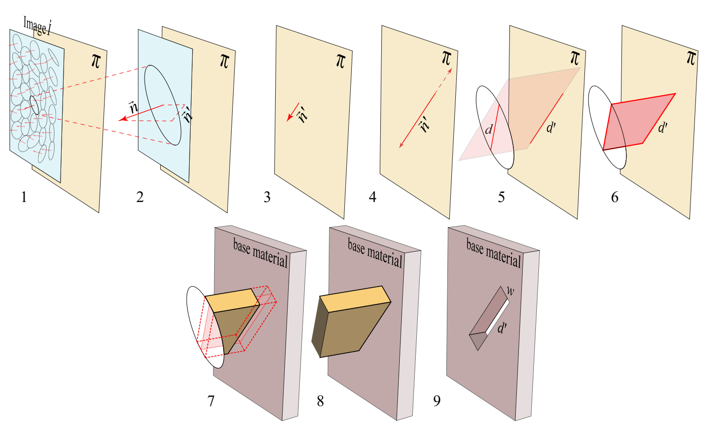


**Figure 10:** *Stems and notches are derivatives of the mirrors' normals.*

As stated above, we defined plane $\pi$ behind image $\acute{I}$. The distance between $\pi$ and the image $\acute{I}$, affects the height of the stems. Stems are designed to be perpendicular to their base. On the other hand, loose notch-stem connections may cause inclination of the stems, and therefore, imprecision of the mirrors' positions. We take two steps to avoid this issue as much as possible.

First, we run an experiment to achieve an efficient snug-fit joinery. In this regard, we inward-offset a notch outline in steps of 0.005mm, within the range of 0.000mm to 0.040mm, and then, in steps of 0.001mm, within the range of 0.020mm and 0.025mm. Next, we run an experiment to set the distance of the plane $\pi$ to the image $\acute{I}$. Short distances make fabrication process harder due to the lack of hand-grip of the stems. Long distances, on the other hand, would put the precision at stake whereas any possible inclination of the stems would drastically change the mirrors' positions. Based on our experiment we set the distance at 15 mm.

As a proof of concept, we design and fabricate two small prototypes (Figure 11). We replace a grid of labelled holes instead of image $I$, and provide a checklist to correspond mirrors and holes. It is crucially important to label the joinery, even in these small prototypes with 25 unique stems and notches. To avoid lengthy labels, we divide the cells/mirrors to rows (r) and columns (c).

The labeling is also used to detect the right orientation of stems and notches, whereas any stem can be placed in its notch in two directions. Accordingly, we laser-engrave labels to the right side of the notches, as well as the front side of the stems. Another sign to indicate the orientation of the notches is the laser-engraved line representing projected normal $\vec{n_i}'$ on plane $\pi$ (Figure 11).

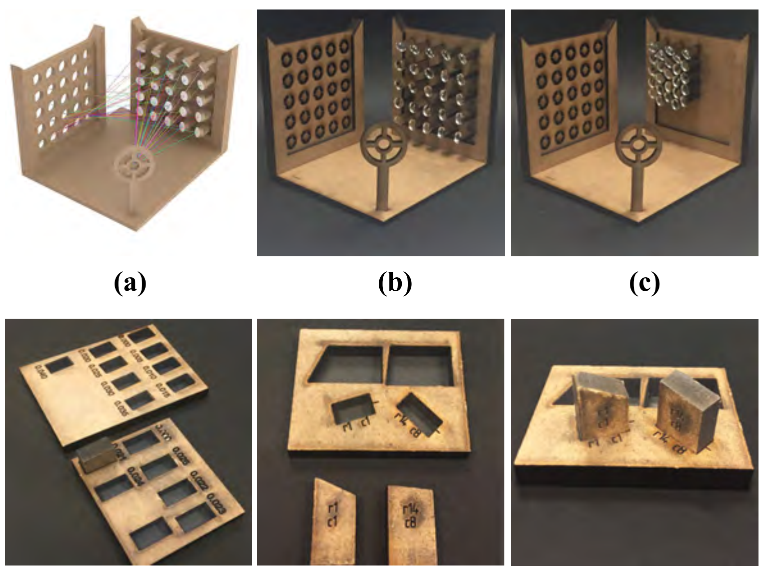

(a) (b) (c)

(d) (e) (f)

**Figure 11:** *A digital model with a quadrilateral grid (a). Its physical model (b). The second prototype with hexagonal grid (c). Based on our experiment, the ideal notch inward-offset for snug-fit joinery out of 5mm-thick MDF sheet is 0.021mm (d). Labelling on front side of the stems, and right side of the notches, as well as a line representing $\vec{n}_i'$ (e) and (f).*

## Results

As established before, Portal harnesses the law of reflection to generate images through its grid of mirrors. We employed the iconic Mona Lisa painting, as the palette for Portal, to generate a number of classic paintings using 4800 mirrors scattered in grids (Figure 1). Type of the grids comply with features within the represented image. As shown in Figure 1, all Portals are equipped with hexagonal grids, except the one with quadrilateral grid representing the compositions of Dutch painter Piet Mondrian.

To improve the images generated by Portal, we performed a number of experiments. For example, we explored the possibility of introducing a privileged space surrounding our privileged point, aiming that our Portal does not fall apart, once viewed with slight deviation from the privileged point (Figure 12).

**(a)** **(b)** **(c)** **(d)**

**Figure 12:** *An image generated with slight deviation from the privileged point before optimization (a), after optimization (b), and the image generated from the privileged point (c). The target image, Homage To Picasso II, by John Nolan, 2007 (d).*

In addition, we discussed the concept of orientation smoothness, that refers to the difference between the normal of cell $c_i$ and the normal of its neighbors. Accordingly, we provide a visual mapping from angles to colours that illustrates how much each mirror has to rotate from its default position (i.e. mirrors' normals being perpendicular to image $\acute{I}$) to reflect a specific portion of image $I$. As it is seen in Figure 13, the transition of colors within the spectra is smooth, in accordance with the color transition smoothness of the images. This resonates the consistency of mirrors' orientations within the Portal. Nonetheless, our algorithm excludes this parameter, and therefore we cannot confidently extrapolate the orientation smoothness, from a few tests of this work.

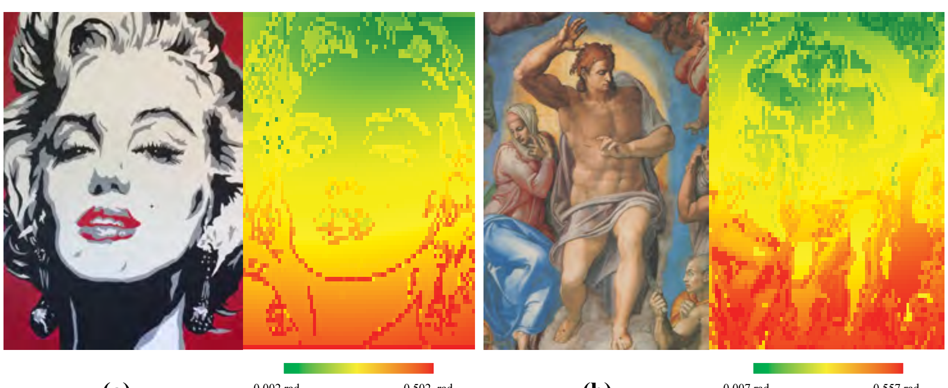


**(a)** **(b)**

**Figure 13:** *A visualization of mirrors' reorientation compared to their default positions. Source images: Hand-painted portrait of Marilyn Monroe, by Danny Raisor-Micheletti (a). The Last Judgment, by Michelangelo, 1541 (b).*

Moreover, our histogram analysis of the images, generated by Portal, shows that these images inherit certain characteristics from their parental image $I$ and image $\acute{I}$. As shown on Figure 14, these constructed images have the color range, identical to the palette image $I$, while they receive shape attributes, represented by spikes in histograms, of the image $\acute{I}$.

Our work also casts light on various fabrication methods and, as a proof of concept, proposed a walk-through to fabricate a prototype using 2D laser cuttings out of MDF with 5 millimeters of thickness (Figure 15). In this prototype, we have designed a hexagonal grid of 540 mirrors, to maintain the aspect ratio of both image $I$ and image $\acute{I}$. The entire model fits within a cube of 60 by 60 by 45 centimeters. Unlike the cutting time, that was barely three hours, the installation became a bit tedious (approximately ninety man-hours). This was due to the unforeseen impact of glue thickness on mirrors' positions. Accordingly, we had to take extra measurements to calibrate all mirrors and making sure they are all precisely oriented.

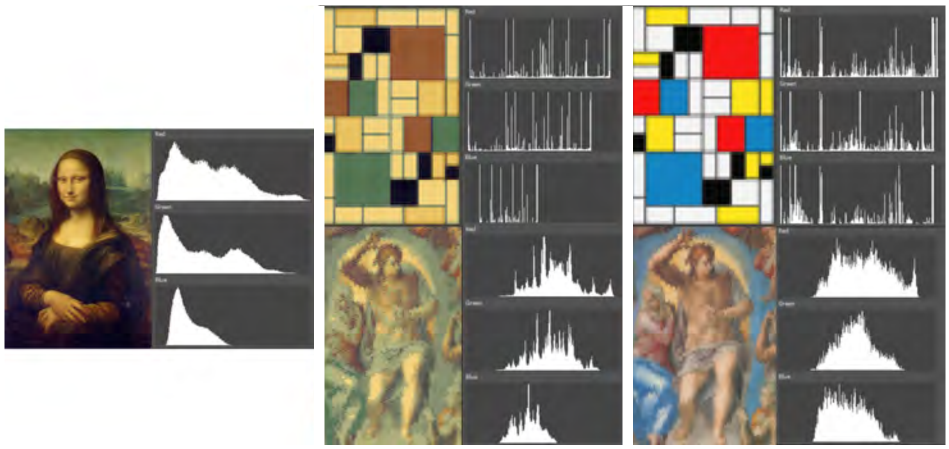

**(a)** **(b)** **(c)**

**Figure 14:** *Histogram analysis. An input image serving a palette (a), constructed images by Portal (b). Images that Portal aims to reconstruct (c).*

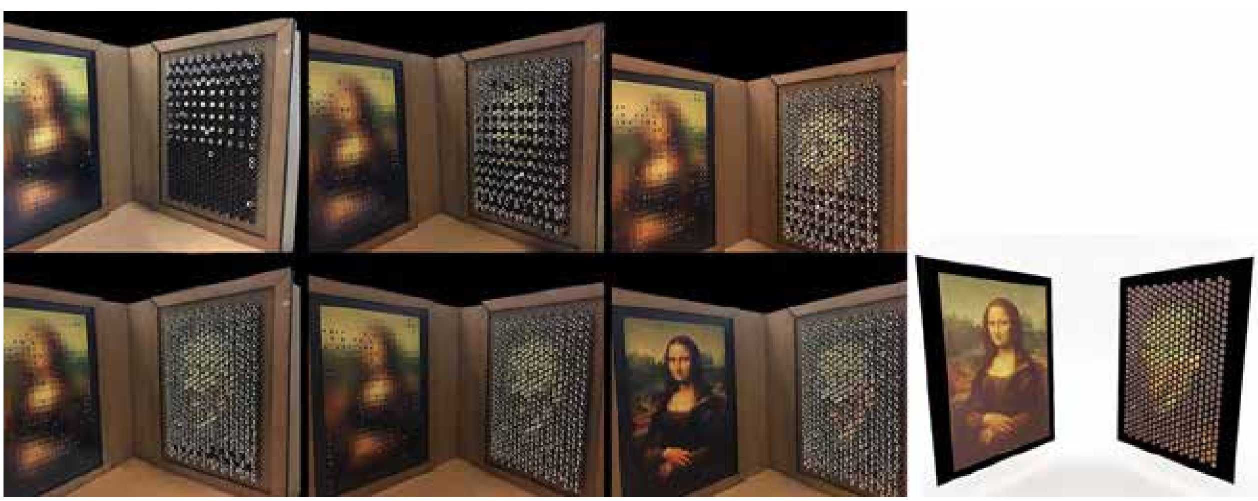

**(a)** **(b)**

**Figure 15:** *Portal equipped with a hexagonal grid of 540 mirrors, represents Vincent van Gogh's self portrait using Mona Lisa as its palette. The process of physical fabrication, and calibration using assisting dots on the palette, as well as the result in the lower right corner* (a), and the virtual model (b).

## Conclusion and Future Work

As suggested by its name, Portal acts like a gateway that bridges between two media. Throughout this investigation, we benefited from a diversity of precedents, manifested by different disciplines. This provides an opportunity to speculate on possible application for the study. Inherently, optical illusions are engaging phenomena. Accordingly, we can approach Portal as a medium that effectively communicates with audience. As a future scope of our work, this triggers new studies in terms of social behaviour towards such art-forms.

Moreover, there are several ways in which the algorithm can be improved. More specifically, in the match-finding portion of the algorithm, we can set criteria to consider additional candidate blocks or explore the impact of perceptual color-spaces such as CIE L*a*b*. We can also search over the entire source image rather than discretizing it into blocks.

Another possible approach towards future work of this study is to upgrade Portal as a dynamic set-up where servo motors, or robotic arms are employed to reorient mirrors to generate an infinite number of images. Alternatively, the palette could be an animation on a digital display, and Portal transforms the animation into an entirely different animation.

In addition to the arts, architecture can also benefit from this work in various scales and environments. The scales can range from ornaments of interior spaces to glazed facades of the buildings, that are salient media to employ this application. Through the lens of computer graphics, Portal can serve as a key that establishes connection between two distinct concepts. One prominent example of these concepts would be the three-dimensional projection of Earth and its distorted, yet meaningful, two-dimensional projection.

Last but not least, Portal can take advantage of one historical application of anamorphic projection where hidden messages were embedded within a distorted image. Hypothetically by altering a few blocks of the palette, in a way that the palette remains relatively untouched, we might be able to make drastic changes within the image represented by Portal. This could found significant studies relevant to steganography domain.

## Acknowledgements

We gratefully acknowledge referees for their insightful feedback on this work, and Mr. Guy Gardner for his assistance at the digital fabrication lab of the School of Architecture, University of Calgary.

## Image Credits

- Figure 2 and 3: Credits provided in the captions.
- Figures 6,7,8,12, and 13: Generated effects by the authors. Artforms' credits provided in the captions.
- All other drawings and images by the authors.

## References

[1] Appel, A. (1968). Some techniques for shading machine renderings of solids. In *Proceedings of the April 30–May 2, 1968, spring joint computer conference*, pages 37–45. ACM.

[2] Art+Com Studios (2011). Anamorphic mirror. https://artcom.de/en/project/anamorphic-mirror/.

[3] Art+Com Studios (2015). á la recherche. https://artcom.de/en/project/a-la-recherche-2/.

[4] Baran, I., Keller, P., Bradley, D., Coros, S., Jarosz, W., Nowrouzezahrai, D., and Gross, M. (2012). Manufacturing layered attenuators for multiple prescribed shadow images. *Computer Graphics Forum (Proceedings of Eurographics)*, 31(2):603–610.

[5] Bermano, A., Baran, I., Alexa, M., and Matusik, W. (2012). Shadowpix: Multiple images from self shadowing. *Comput. Graph. Forum*, 31(2):593–602.

[6] Bian, X., Wei, L.-Y., and Lefebvre, S. (2018). Tile-based pattern design with topology control. *Proc. ACM Comput. Graph. Interact. Tech.*, 1(1).

[7] Chen, D., Sitthi-amorn, P., Lan, J. T., and Matusik, W. (2013). Computing and fabricating multiplanar models. *Comput. Graph. Forum*, 32(2):305–315.

[8] Chen, W., Ma, Y., Lefebvre, S., Xin, S., Martínez, J., and wang, w. (2017). Fabricable tile decors. *ACM Trans. Graph.*, 36(6):175:1–175:15.

[9] Colour perception (2019). Colour metric. https://www.https://www.compuphase.com/cmetric.htm. Accessed: 2020-02-18.

[10] Daniel Rozin (2003). Broken red mirror. http://www.smoothware.com/danny/brokenmirror.html.

[11] De Comite, F. and Grisoni, L. (2015). Numerical anamorphosis: an artistic exploration. In *SIGGRAPH ASIA 2015 Art Papers*, page 1. ACM.

[12] Di Paola, F., Pedone, P., Inzerillo, L., and Santagati, C. (2015). Anamorphic projection: analogical/digital algorithms. *Nexus network journal*, 17(1):253–285.

[13] Duncan, N., Yu, L.-F., Yeung, S.-K., and Terzopoulos, D. (2017). Approximate dissections. *ACM Trans. Graph.*, 36(6):182:1–182:13.

[14] Dunn, N. (2012). Digital fabrication principles. In *Digital Fabrication in Architecture*, pages 186–225. Laurence King Ltd.

[15] Esteban Serrano (2015). Floating point. https://esrs.co/tagged/Floating%20Point. Accessed: 2017-11-01.

[16] Hansford, D. and Collins, D. (2007). Anamorphic 3d geometry. *Computing*, 79(2-4):211–223.

[17] Hoskinson, R., Stoeber, B., Heidrich, W., and Fels, S. (2010). Light reallocation for high contrast projection using an analog micromirror array. *ACM Trans. Graph.*, 29(6):165:1–165:10.

[18] Hosseini, S. V., Djavaherpour, H., Alim, U. R., Taron, J. M., and Samavati, F. F. (2019). Data-spatialized pavilion: Introducing a data-driven design method based on principles of catoptric anamorphosis. In *International Society of the Arts, Mathematics, and Architecture, Summer 2019, The Proceedings of the SMI 2019 Fabrication and Sculptung Event*, pages 39–51.

[19] Hosseini, S. V., Taron, J. M., and Alim, U. R. (2017). Optically Illusive Architecture: Producing depthless objects using principles of linear perspective. In *37$^{th}$ Conference of the Association for Computer Aided Design in Architecture (ACADIA) Disciplines & Disruption*, pages 274–283. ACADIA.

[20] Jansen, Y., Dragicevic, P., and Fekete, J.-D. (2013). Evaluating the efficiency of physical visualizations. In *Proceedings of the SIGCHI Conference on Human Factors in Computing Systems*, CHI '13, pages 2593–2602, New York, NY, USA. ACM.

[21] Jovanovic, M., Stojakovic, V., Tepavcevic, B., Mitov, D., and Bajsanski, I. (2016). Generating an anamorphic image on a curved surface utilizing robotic fabrication process. In *34$^{th}$ Conference on education and research in Computer Aided Architectural Design in Europe (eCAADe)_ Complexity & Simplicity*, pages 185–191. eCAADe.

[22] Kalantar, N., Borhani, A., and Akleman, E. (2016). Nip and tuck: A simple approach to fabricate double-curved surfaces with 2d cutting. In *34$^{th}$ Conference on education and research in Computer Aided Architectural Design in Europe (eCAADe)_ Complexity & Simplicity*, pages 335–344. eCAADe.

[23] Kamgar-Parsi, B. and Sander, W. (1989). Quantization error in spatial sampling: comparison between square and hexagonal pixels. In *Proceedings CVPR'89: IEEE Computer Society Conference on Computer Vision and Pattern Recognition*, pages 604–611. IEEE.

[24] Kiser, T., Eigensatz, M., Nguyen, M. M., Bompas, P., and Pauly, M. (2012). *Architectural caustics–controlling light with geometry*. Citeseer.

[25] Kokichi Sugihara (2016). Ambiguous cylinder illusion. http://illusionoftheyear.com/2016/06/ambiguous-cylinder-illusion/.

[26] Kolarevic, B. (2003). Digital production. In *Architecture in the Digital Age: Design and Manufacturing*, pages 49–78. Taylor and Francis.

[27] Levin, A., Glasner, D., Xiong, Y., Durand, F., Freeman, W., Matusik, W., and Zickler, T. (2013). Fabricating brdfs at high spatial resolution using wave optics. *ACM Trans. Graph.*, 32(4):144:1–144:14.

[28] Li, S., Mahdavi-Amiri, A., Hu, R., Liu, H., Zou, C., van Kaick, O., Liu, X., Huang, H., and Zhang, H. (2018). Construction and fabrication of reversible shape transforms. *ACM Trans. Graph.*, 37(6):190:1–190:14.

[29] Malzbender, T., Samadani, R., Scher, S., Crume, A., Dunn, D., and Davis, J. (2012). Printing reflectance functions. *ACM Transactions on Graphics (TOG)*, 31(3):20.

[30] Marcus Raetz (2001). Oui/non. https://www.wikiart.org/en/markus-raetz/oui-non-2001. Accessed: 2014-07-26.

[31] Mitra, N. J. and Pauly, M. (2009). Shadow art. *ACM Trans. Graph.*, 28(5):156:1–156:7.

[32] Papas, M., Houit, T., Nowrouzezahrai, D., Gross, M., and Jarosz, W. (2012). The magic lens: Refractive steganography. *ACM Transactions on Graphics (Proceedings of SIGGRAPH Asia)*, 31(6).

[33] Peng, H., Lu, L., Liu, L., Sharf, A., and Chen, B. (2019). Fabricating QR codes on 3d objects using self-shadows. *Computer-Aided Design*, 114:91 – 100.

[34] Perez-Gomes, A. and Pelletier, L. (2000). Relocating anamorphosis. In *Architectural representation and the perspective hinge*, chapter 1, pages 138–149. MIT Press, Cambridge.

[35] Schüller, C., Panozzo, D., and Sorkine-Hornung, O. (2014). Appearance-mimicking surfaces. *ACM Trans. Graph.*, 33(6):216:1–216:10.

[36] Swaminathan, S., Shi, C., Jansen, Y., Dragicevic, P., Oehlberg, L., and Fekete, J.-D. (2014). Supporting the design and fabrication of physical visualizations. In *Proceedings of the SIGCHI Conference on Human Factors in Computing Systems*, pages 3845–3854. ACM.

[37] Weyrich, T., Peers, P., Matusik, W., and Rusinkiewicz, S. (2009). Fabricating microgeometry for custom surface reflectance. *ACM Trans. Graph.*, 28(3):32:1–32:6.

[38] Whitted, T. (1980). An improved illumination model for shaded display. *Communications*.

[39] Wright, L. (1983a). Grand illusions. In *Perspective in perspective*, pages 139–156. Routledge.

[40] Wright, L. (1983b). The object, the eye and the picture. In *Perspective in perspective*, pages 1–33. Routledge.

[41] Zhao, H., Lu, L., Wei, Y., Lischinski, D., Sharf, A., Cohen-Or, D., and Chen, B. (2016). Printed perforated lampshades for continuous projective images. *ACM Trans. Graph.*, 35(5):154:1–154:11.

# A Feast for The Eyes: Visualising Flavour-to-Vision Synesthesia


Meijia Wu and Oliver Gingrich

The National Centre for Computer Animation, Bournemouth University, UK;
s4919402@bournemouth.ac.uk, gingricho@bournemouth.ac.uk



## Abstract

Flavour-to-vision synesthesia is a rare neurological phenomenon, where a person consistently and involuntarily visualises abstract shapes, colours, or even textures whilst tasting the flavours of food. As this rare condition is currently still largely unknown to and misunderstood by many, this project aims to gain an insight into perceptual experiences of those diagnosed with synesthesia (also known as synesthetes) and to convey these findings to the general public in the form of an artefact. After comparing related projects on the representation of synesthesia, the use of 3D design, and 3D printing in combination with real props was chosen as a suitable medium to produce the final artefact. By conducting first-hand qualitative participant studies with three synesthetes, it was found that every synesthete had consistent visual depictions of flavours. Due to the idiosyncratic nature of flavour-to vision synesthesia, trends could only be found within individual cases, and not across the sampled participants. Consequently, the final artefacts were designed as a set of three sculptures to represent each participant's unique cases of flavour-to-vision synesthesia. The production of 3D-printed sculptures involved both digital and traditional art and design practices. Modifications were required to improve the otherwise less believable surface of the printed sculptures, which were generally unhindered by the chosen medium. This paper discusses the chosen methods, and practical challenges in the production process of the 3D printed research outputs.


## Introduction

Synesthesia is a neurological anomaly where one sensory stimulus triggers another ‘normally’ unrelated sensory experience. Synesthesia is an umbrella term that encompasses all types of jointed experiences [11], some examples include seeing colours when listening to music (also known as chromesthesia), seeing colours projected onto numerals and alphabets (grapheme-colour synesthesia), and even tasting flavours on the tongue when reading words (lexical-gustatory synesthesia).

In this paper, we focus on flavour-to-vision synesthesia, which is when flavours of food evoke visions of abstract visual elements – this rarer subtype of synesthesia has a prevalence of approximately 0.0021% of the population [3]. People who have this type of synesthesia (also known as synesthetes) have a gift for experiencing flavours in an unbiased yet abstract way, allowing many of them to become great chefs [16]. Many synesthetes, however, tend to refrain from sharing their extra-ordinary experiences, often out of fear of being considered psychologically ill by others, since these neurological phenomena are not normally experienced by most people. This ultimately sparked our interest in finding an effective way of representing or conveying the experiences of flavour-to-vision synesthesia to a non-synesthetic audience.

## Background and Related Works

Neurologist Dr Richard E. Cytowic's book [2] provides a comprehensive introduction to synesthesia, in particular, it indicates that synesthetic experience is involuntary and immediate, which means that when a synesthete receives the stimuli of an inducer (e.g the taste of chicken), the concurrent (e.g pointy shape) will occur almost immediately without any effort of imagination. The associations between the inducer and the concurrent are consistent throughout a synesthete's lifetime [14], but these experiences are also idiosyncratic [2] - this means that two synesthetes will never have the same visual experience when tasting the same flavour.

To date, it is still not clear what exactly causes synesthesia [10], nor why certain flavours are synesthetically associated with certain shapes or colours. However, recent studies have also shown the possibility of underlying cross-sensory associations in every culture that influence humans to subconsciously associate certain visual cues with preconceived flavours [15][18]. Synesthetic visions are often compared to the 'Bouba-Kiki Effect' which suggests that humans have innate ability to associate the sharp sound of the word 'Kiki' to a spiky shape, and the deeper sound of 'Bouba' to a more rounded shape. This correlation was also found between flavours and shapes, where sweet and creamy flavours (such as cheese) are often associated with the rounded shape of 'Bouba', while spicy or sour tastes (such as cranberries) are associated with the sharp shape of 'Kiki' [8][12].

One of the most famous references to flavour-related synesthesia in pop culture is perhaps in Pixar's animated movie "*Ratatouille*" [6]. In one scene (see Fig. 1, left), the main character Remi eats a strawberry and a block of cheese, while simultaneously hearing music and 'seeing' movements of shapes and colours in a non-physical black space, similar to the 'mind's eye' that is often described by synesthetes.

An example of the use of Virtual Reality (VR) technology to explain the experience of chromesthesia is "*What's It Like To Hear Colors?*" directed by Mario de la Vega [13]. Here, the use of immersive 360° video allows the viewers to see the visual experience of a chromesthesia synesthete from a first-person perspective (see Fig. 1, right). In both examples mentioned above, the use of an audio-visual medium made it possible to directly communicate the otherwise indescribable personal experiences to its viewers.


**Figure 1:** *Methods of representing synesthesia, left to right: Taste Visualization for Pixar's* ***Ratatouille****,* ***What's It Like To Hear Colors?*** *by Seeker.*

Terri Timely's experimental short animation "*Synesthesia*" [17] uses a mixture of live-action, stop-motion, and practical effects to visualise several types of synesthesia in a surreal manner that is bizarre yet memorable (see Fig. 2, left). While this animation does not accurately represent synesthetic experiences, it does effectively deliver the abstract concept of synesthesia in an entertaining way. The use of real props and live actors in this work emphasises that synesthetic experiences are in fact real.

Another interesting project was the advertising campaign "*Heinz Beanz Flavour Experience*" created by Bompas & Parr in 2013 [1]. The campaign presented five custom-designed physical bowls that were intended  to serve the five flavours of Heinz canned beans in (see Fig.2, right). Each bowl was designed with tactile and visual elements relevant to each of the representative flavours, with the intention that if one was to eat the beans from these bowls, they would be experiencing the visual and tactile stimuli produced by the bowls concurrently to the consumption of the beans – thereby artificially creating a multi-sensory experience similar to synesthesia. The use of 3D printing technology in product design allowed freedom for the architects to sculpt bowls with unusual structural and tactile qualities that would otherwise be more challenging to achieve through traditional means. We decided to make use of 3D printing in combination with real props to produce the artefact that represents flavour-to-vision synesthesia, as the result could be more intimate and believable, which is a quality that otherwise would be difficult to achieve through an audio-visual medium that solely exists on a screen.

**Figure 2:** *Methods of representing synesthesia, left to right:* ***Synesthesia*** *by Terry Timely,* ***Heinz Beanz Flavour Experience*** *by Bompas & Parr.*

## Participant Studies and Artefact Designs

In order to understand the actual flavour experiences of synesthetes, we conducted participant studies to collect more qualitative insights through interviews and visual diaries. The interviews followed a structured list of explorative questions, and the participants were asked to keep a verbal or visual log of their synesthetic visions over the course of one week. Verbal depictions were often limited by the choice of words and required a more personal interpretation, but on the other hand, the sketches from the participants relayed a clearer visualisation of individual participant experiences.  Three qualifying participants were recruited, who were able to synesthetically see flavours in very different ways. This reinforces the theory that synesthesia is idiosyncratic and can be different for everyone. For this reason, multiple designs were created to emphasize the variety of synesthetic experiences, as opposed to attempting to summarise the full spectrum of flavour-to-vision synesthesia within a single design. Below we detail three case studies with the participants.

### *Case Study 1: Participant A's Flavour-to-Shape Synesthesia*

The first participant (who will be referred to as Participant A) possessed the ability to visualise flavours in the form of 2-dimensional shapes as an overlay to his normal vision. These synesthetic visions are always described as a line originating from one point, travelling clock-wise and eventually enclosing to form an abstract shape; the course of the line's travel seems to be influenced in real-time by the participant's reaction to the intensity and flavours of the food, almost like an indicator of his "flavour journey". 25 different flavour depictions were collected from Participant A, and a trend was found within the data that complex flavours produced a less defined shape, and vice versa; sweet and creamy flavours produced rounder and thicker shapes, while sharper flavours such as bitterness and sourness produced pointier and flatter shapes.

Notably, Participant A's depictions of different types of coffee all had a common hat-like shape (see Fig. 3). Here, the bulbous top part of the shape is believed to be linked to the creamy and sweet flavours of the milk, and the flat shape at the bottom would most likely belong to the bitter flavours of the coffee itself. With this in mind, a design was created that surreally combines the appearance of a cup of cappuccino coffee with the literal form of the hat-like shape as perceived through Participant A's synesthetic perception.

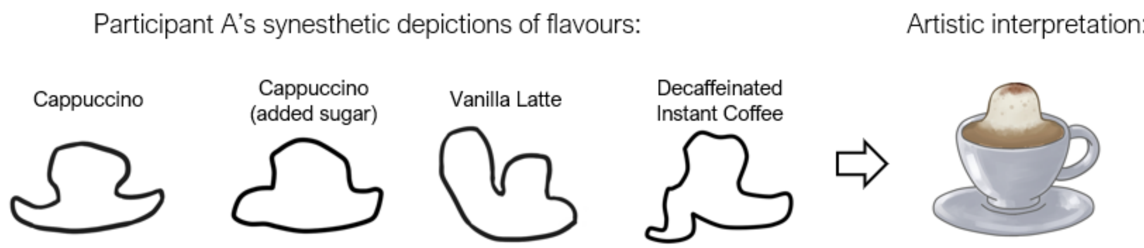


**Figure 3:** *Participant A's synesthetic depictions of various types of coffee and chosen design.*

***Case Study 2: Participant B's Flavour-to-Colour and Flavour-to-Texture Synesthesia***
The second participant's synesthesia allows him to identify flavours in colours and textures. His synesthetic vision not only can have different depth or special qualities in his field of vision, but also can have surface textures of oil, powder, cream etc... Participant B's food diary was verbally recorded and aided by the personal synesthetic colour depictions. From the data collected, it was noticeable that items belonging to the same food groups tend to produce similar colours (and therefore flavours). For example, many of the vegetables produce shades of purple to pink, while seafood was mostly depicted to be orange, and meat and dairy blue.

We focused on this participant's depiction of Chili Mac which illustrated the depth and textural quality of his synesthesia (see Fig. 4). The depictions were interpreted into a three-dimensional design where a pile of grey ash was used to represent the tomato base of the chilli, with blobs of blue produced by beef, and then dusted with a puce powder. During the interview the second participant also mentioned that chilli peppers cause him to see '*a scattering of very tiny, finely cut gemstones (rubies, garnets, emeralds, sapphires)*', which were also added to the final design.


**Figure 4:** *Participant B's synesthetic depictions of Chili Mac and chosen design.*

***Case Study 3: Participant C's Flavour-to-Colour and Flavour-to-Shape Synesthesia***
Varying from the two other participants, Participant C experiences flavours in the form of shapes and colours, including dots, lines, as well as 'open' shapes that fade away (see Fig. 5). Due to the limited timeframe of the project, only a small sample of the participant's synesthetic depictions were able to be obtained, which made it more difficult for interpreting the elements within the drawings later. The only consistency found in the participant's drawings was between the cranberry sauce and cranberry cookie, which both contained elements of the same colour – the colour of red also coincidentally matches the appearance of cranberry itself. Synesthetic visions of flavours rarely conform to the actual colour of the

food themselves - this is called the 'alien colour effect' [4][9]. Because of this, many synesthetes find it rather delightful whenever the colours do coincide with their synesthetic visions. A design was created based on Participant C's synesthetic vision of cranberry sauce. The design is a visual combination of both realistic cranberry sauce and the participant's abstract depiction of its flavour.

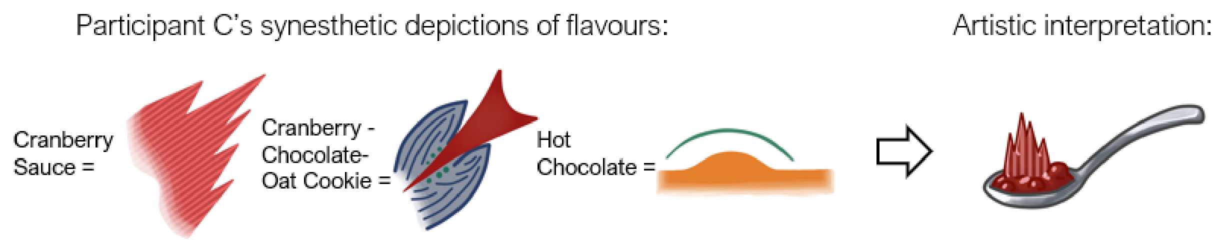


**Figure 5:** *Participant C's synesthetic depictions of various flavours and chosen design.*

## Implementation of the Final Artefact

Initially during the design stage, the artefact was intended to be a series of sculptures that could be displayed in various exhibitions for public accessibility. The sculptures were meant to be life-sized and almost resembling real food – whilst also having an abstract form. By utilizing real tableware and cutlery that could be found at home, 3D printing was only needed to produce the more abstract portions of the designs - this would not only greatly reduce the amount of printing time and material cost. We hoped to close the perceived gap between the concept of synesthesia and reality through an artefact that is surreal yet familiar.

3D-printing allowed the creation of almost any 3-dimensional shapes, but the appearance of the printed and painted sculptures lacked the reflectivity that of real-world food items. In order to improve the photorealism of the final artefact, various types of clear surface varnish were tested to add reflectivity to surfaces while also serving as a surface protection. It was found that acetone spray paint created a surface reflectivity similar to grease (suitable for recreating surfaces of cake, cream etc.), while resin produced glassy reflectivity (suitable for recreating surfaces of jam and liquid).

The 3D model of *Synesthetic Cranberry Sauce* was also blocked out in Maya, then exported into Zbrush where the shapes merged and sculpted into the organic form jam-covered cranberries; a gradient between lighter and deeper red colours was used to paint the sculpture to mimic the subsurface scattering of real cranberry sauce. Finally, resin was used to coat the entire painted sculpture to create a syrup-like reflectivity (see Fig. 6).

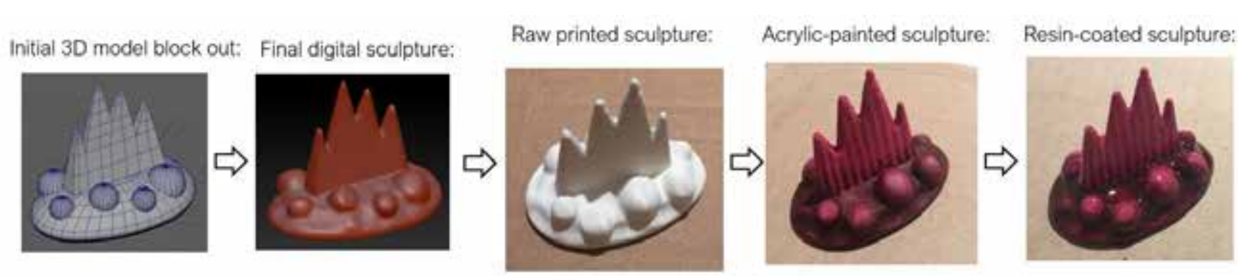


**Figure 6:** *Making of Synesthetic Cranberry Sauce.*

For *Synesthetic Cappuccino*, the model was sculpted in Zbrush to create the organic and airy appearance of the foam; the base of the model is a disc that is scaled to match the diameter of an existing coffee mug. *Synesthetic Chili Mac* on the other hand, involved the creation of a pile of ash, which was difficult to sculpt and 3D print as the grainy texture of ash was below the 3D printer resolution. However, that was avoided by using the hardware's ability to print the surface of a model in a jittering motion, thus giving the printed model a fuzzy surface. The rest of the design were also printed and painted separately, with the blue cube sprayed with a matte varnish to look 'waxy'; the printed diamonds were coated in resin to have more reflectivity like real gemstones - however, they could not achieve the refractive property of real gemstones as the printing material was not transparent. Finally, the smaller shapes were glued onto the model of pile of ash, and then 'dusted' with dots of light puce-coloured paint.

The final artefact is a set of three sculptures (see Fig. 7) that are meant to be appreciated together (also known as a triptych). The artefact is a result of a study of three real cases of synesthesia, as well as a personal exploration of 3D printing and model-making practice.

**Figure 7:** *Final sculptures, left to right: Synesthetic Cappuccino, Synesthetic Cranberry Sauce, Synesthetic Chili Mac.*

The sculpture of *Synesthetic Chili Mac* turned out to be much smaller in comparison to the other two sculptures due to the limited time available for 3D printing - this can however be justified by the fact that *Synesthetic Chili Mac* is not meant to represent the real dish, but an abstract interpretation of Participant B's synesthetic vision. To compensate for the smaller size of the sculpture, it was decided that by arranging the sculptures closer to the viewing point, it would seem bigger through perspective in an exhibition (see Fig. 8).

**Figure 8:** *Final Artefact (A triptych of sculptures) and intended exhibition layout.*

## Conclusions and Discussion

The goal of the project was to conceptualise flavour-to-vision synesthesia and find a way to creatively visualise the abstract phenomenon in a way that would be accessible to the general public. The main challenge was to identify a suitable method to artistically represent synesthesia; after analysing several examples, the conclusion arrived at creating 3D-printed sculptures combined with the use of real props, with consideration for the nature of the type of synesthesia in question. 3D printing proved to be a successful method of creating physical sculptures with a freedom of design. Most obstacles were overcome during the production stage using 3D sculpting techniques, printer settings, and painting techniques. A large contributing factor to the believability of the final artefact was the use of surface varnish which added more realistic reflectivity to the surface of the sculptures. This however does not mean that physical sculptures are the best method of representation for all types of synesthesia, as the choice of medium should be made with regards to the types of sensory modalities involved.

The project examined flavour-to-vision synesthesia through three participants – this is a relatively small sample, but each participant provided very different case studies, which demonstrated the vast spectrum of possible experiences of flavour-to-vision synesthetes. Due to the lack of scientific explanations of synesthesia, interpretations of the participant's depictions may be inaccurate and misleading; it should be emphasised that the artefacts for this project are merely artistic attempts to interpret and visualise specific cases of flavour-to-vision synesthesia, they are not to be taken literally.

With the vast potential of synesthesia's scope, more work should be pursued with regards to creating a more accurate representation of synesthetic experiences – if time nor resources were limited, then a VR experience project should definitely be considered, to provide the public with more immersive and more accurate visual representations of synesthesia; moreover, with the modern '4D cinema' methods (where physical effects are combined with 3D films), more complex types of synesthetic experiences (such as those that involve sensations of temperature, touch, smell etc.) could perhaps also be conveyed to non-synesthetic audiences.

## References


[1] Bompas & Parr. *Heinz Beanz Flavour Experience*. Bompas & Parr, 2013. http://bompasandparr.com/projects/view/heinz-beanz-flavour-experience/

[2] R. E. Cytowic. *The Man Who Tasted Shapes*. 2. Cambridge, Massachusetts: MIT Press, 2003.

[3] S. A. Day, 2007. "Demographic aspects of synesthesia", http://www.daysyn.com/Types-of-Syn.html

[4] S. A. Day, 2011. "The human sensoria and a synaesthetic approach to cooking", Collapse. VII, 378-409.

[5] S. A. Day, 2015. Sean Day: Flavor -> Color; Smell -> Color. http://www.daysyn.com/sean-syn-foods-and-odors.html

[6] M. Gagné, 2007. *Taste Visualization for Pixar's Ratatouille* https://www.gagneint.com/Final%20site/Animation/Pixar/Ratatouille.htm

[7] Sensology by Michel Gagné. https://youtu.be/UVWKtXDvr04

[8] A. Gallace, E. Boschin, and C. Spence. "On the taste of 'bouba' and 'kiki': An exploration of word-food associations in neurologically normal participants". *Cognitive Neuroscience*, 2 (1), 2011, 34–46.

[9] J. Gray, M. Parslow, J. Brammer, S. Chopping, N. Vythelingum, and D. Ffytche. Evidence Against Functionalism from Neuroimaging of the Alien Colour Effect in Synaesthesia. *Cortex*, 42, 2006, 309-318.

[10] J. M. Hupé and M. Dojat. "A critical review of the neuroimaging literature on synesthesia". *Frontiers in human neuroscience*, 9, 103, 2015.

[11] S. Novich, S. Cheng, and D. M. Eagleman. "Is synaesthesia one condition or many? A large-scale analysis reveals subgroups". *Neuropsychology*, 5 (2), 2011, pp 353-371.

[12] V. S. Ramachandran, and E. M. Hubbard. "Synaesthesia: A window into perception, thought and language". *Journal of Consciousness Studies*, 8 (12), 2001, pp 3–34.

[13] What's It Like To Hear Colors? - A VR 360° Synesthesia Experience. https://youtu.be/obrBAysVef0

[14] J. Simner, and E. Bain. "A longitudinal study of grapheme-color synaesthesia in childhood: 6/7 years to 10/11 years". *Frontiers in Human Neuroscience,* vol 7, 2013, pp 603

[15] C. Spence, and O. Deroy. "On the shapes of flavours: A review of four hypotheses". *Theoria et Historia Scientiarum*, 10, 2014, 207-238.

[16] C. Spence, J. Youssef, O. Deroy. Where are all the synaesthetic chefs?. *Flavour*, 4, 29, 2015.

[17] Terri Timely, *Synesthesia.* https://vimeo.com/5297531

[18] R. W. Wang, M. C. Chou, C. H. Sun, and C. C. Hsu. Research into the Differentiation of Package Design: Taste Synesthesia induced by Packaging Shapes. *Japanese Society for the Science of Design*, 57 (5), 2011, pp 117-126.

# Interlocking Vaults by Voronoi Decomposition of 3D Space

Neeraj Yadav[1]

[1]Department of Architecture, Texas A&M University, College Station; nyadavemail@gmail.com

## Abstract

Aided by advancements in computation and fabrication techniques, this paper introduces a novel method to create assemblies by Voronoi decomposition of 3D space. The scope of this paper is limited to the generation of interlocking modules to constitute arches and vaults. Every module is generated in tandem with adjacent modules and is assured to be an exact fit, independent of the intent to have repetitive or non-repetitive modules.

## Introduction

Interlocking patterns are widely found in nature and have been a fascination of architects and engineers throughout history. From early post-and-lintel system of Stonehenge to traditional Japanese woodwork and beyond, there are numerous structures that are testaments to the continuous involvement and body of work that has gone into interlocking structures. While every generation has their own techniques and methods, the current advancements in graphics and visualization along with innovations and affordability in manufacturing are bringing the dawn of a new phase in architecture and construction.

The role of geometry is fundamental to developing sound interlocking structures. Rene Descartes introduced analytical geometry and illustrated a theory in the third part of his *Principia Philosophiae*, published in 1644, to demonstrate the universe as set of (weighted) regions around each star-the "*heavens"* with help of a Vortices diagram [1]. This introduced the notion of dividing space in spheres' of influence. It was much later in 1850 that Peter Gustav Lejeune Dirichlet provided a mathematical formulation on influence of point p on another point q for $R^2$ and $R^3$ vector space [2] while it was in 1908 that Georges Feodosovic Voronoi provided the formulation for $R^n$ vector space [3].

Voronoi tessellation has featured heavily in research and arts over the last few decades. However, the application to interlocking structures and interlocking form-finding have been limited so far. Prior studies have already recognized and assessed that the role of geometry and tessellations is instrumental in understanding and developing topological interlocking systems [4]. Joseph Abellie' and Sébastien Truchet' interlocking flat vaults and their extensions to barrel vaults feature prominently due to the innovative use of repetitive configurations [5]. Now, methods and tools are required to utilize Dirichlet Voronoi tessellation, or Voronoi tessellation as it is widely known as, in relation to interlocking structures. A recent paper discussed the use of 2D Voronoi tessellation after decomposing curves into points and create space-filling structures [6]. This provided an interesting opportunity to explore Voronoi decomposition of 3D space based on curves in order to generate arch and vault assemblies. Meanwhile, another in-press manuscript explores the generation of Abellie Tiles based on fabric symmetries using 3D Voronoi tessellation [7].

The initial research objective was to develop a tool to explore the possibility of generating interlocking arch using curves decomposed to points and their subsequent Voronoi computation. The critical challenge in doing so is determining the bounding geometry for the Voronoi cells while ensuring the absence of any overlap or unintended break in the module and arch form. On receiving positive results, the scope was extended to vault structures. A 7-module arch prototype was fabricated using additive manufacturing to test practicality of a simple interlocking mechanism. This paper presents the method and findings to further explore interlocking geometry in architecture and construction.

## Methodology

The novelty of the presented method is two-fold. Firstly, regarding the boundary determination for the Voronoi decomposition and secondly, regarding the flexible count of unique modules required to complete an arch or vault structure. Figure 1 displays, with the help of a semicircular barrel vault, the coordinates system and terminology followed in this paper.

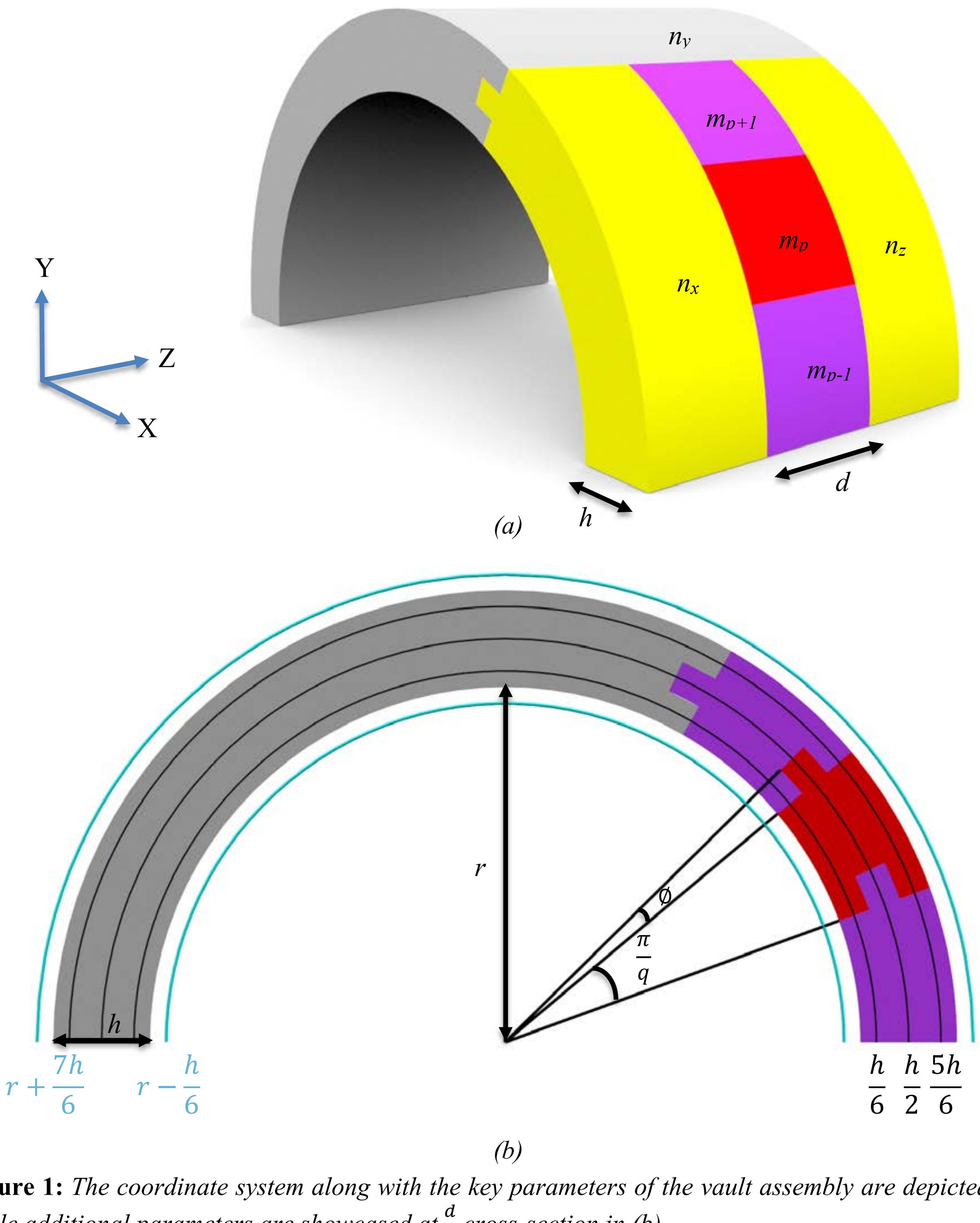


**Figure 1:** *The coordinate system along with the key parameters of the vault assembly are depicted in (a) while additional parameters are showcased at $\frac{d}{2}$ cross-section in (b).*

The overall logic behind the methodology is explained with a 12-step process for a semi-circular barrel vault. Step 1 introduces the fundamentals and terminology while Step 2-6 details the procedure to generate the curves in 3D Space. The decomposition of the curves is detailed in Step 7-12 to determine the seed point collection and neighboring boundary point collection required for 3D Voronoi cell computation.

1. The overall vault structure is considered a linear assembly of *n* arches with *d* depth, *r* rise and *h* cross-section height, where *n* can take any integer value greater than 1, and *d*, *r* and *h* are positive real number as shown in Figure 1a. Length *l* of vault is a scalar function of *n* and *d.*
2. The cross-section of an arch $n_y$ at $\frac{d}{2}$ is divided using three arcs at $\frac{h}{6}$, $\frac{h}{2}$ and $\frac{5h}{6}$ . The innermost and outermost arcs form the guide arcs while the center arc forms the interlock arc providing interlocking in XY plane.
3. Both guide arcs are further divided into $q$ curves representing $m$ modules such that each curve forms an angle of $\frac{\pi}{q}$ at the center. While $q$ can take any integer value greater than 1, only odd integers were assigned to ensures the presence of a keystone and avoid an interlocking plane at the center of the arch. See Figure 1b for representation.
4. The interlock arc is also divided into $q$ curves; however, they are offset by an interlock angle ø, where $\frac{\pi}{q} > ø > 0$, toward the keystone curve and this results in shorting of keystone interlock curve by 2ø $(r + \frac{h}{2})$.
5. All guide curves and the keystone interlock curve are replicated and translated to $\frac{d}{4}$ and $\frac{3d}{4}$ .
6. All interlock curves except the keystone interlock curve are replicated and translated to $\frac{3d}{4}$ and *d* to provide interlocking in Z direction.
7. A total of *q* modules with a set of 9 curves each are identified, and one such set, $m_p$, where $q \geq p > 0$ and $p$ takes integer values, is selected and decomposed into *i* points*.* All endpoints are excluded to avoid any intersection with neighboring modules. Hence, *i* can take any integer value greater than 2. Rest of the points 9*($i$-2) form the seed point collection $s_p$ for the Voronoi computation of module *p*. A curve set $m_p$ is represented with red color in Figure 2.
8. A Module bound is constituted by similar decomposition of $m_{p-1}$ and $m_{p+1}$ curve set to *i* points and excluding the endpoints from the collection. Total points in module bound is 2*9*($i$ – 2).
9. An arch bound is constituted by $n_x$ and $n_z$ arches which can be obtained by translating decomposed $m_{p-1}$, $m_p$ and $m_{p+1}$ of $n_y$ arch by – d and d. Total points in arch bound is 6*9*($i$-2).
10. An inner and outer vault bound is created by decomposition of arch curve with rise $(r - \frac{h}{6})$ and $(r + \frac{7h}{6})$ respectively into *j* points each and offsetting it to $\frac{d}{4}$ and $\frac{3d}{4}$. Total points in vault bound is 2*3*$j$. Here j can take any positive integer value and will accordingly impact the internal and external form of the module.
11. The point collection consisting module bound, arch bound and vault bound serves as the bounding points $b_p$ for the Voronoi computation of module *p*. Upon computation of the Voronoi cells for $s_p$ with $b_p$ as neighboring points, the union of the 3D Voronoi cells will manifest into module *p*. If desired, before taking the union, the generated form can be transformed to a porous module by scaling the cell by a factor *f*, 0.5 for this study, offsetting the scaled faces and extruding them using vector joining the face center and Voronoi cell center. Later, a union of scaled extruded faces can be subtracted from union of original cells to obtain porous modules. Later, Catmull-Clark subdivision [9] can be used for smoothening keeping the corners fixed.
12. The keystone module can be obtained by repeating step 7-11. Rest of the modules can be substituted by translations of module $p$ in a semi-circular vault. Otherwise, every module can be individually generated especially if the design intent is to have non-repetitive and symmetric vault structure or non-repetitive and non-symmetric vault structure.

The bounding point collection referred as $b_p$ is visualized in Figure 2 below. The complete $b_p$ set, for $i = 6$ and $j = 100$, contains 888 points while the $m_p$ set of curves will be sampled to 36 points and form the seed point collection $s_p$.

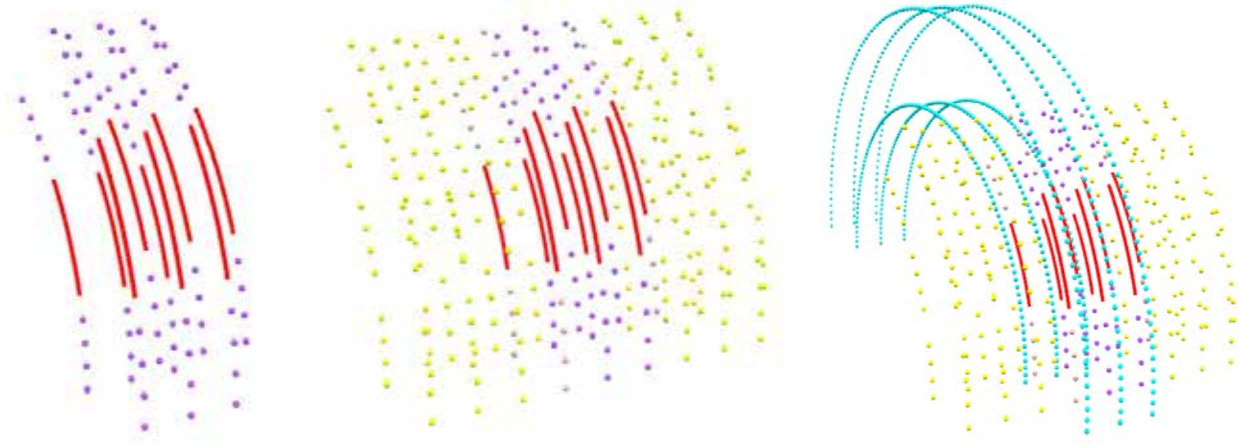

(a) (b) (c)

**Figure 2:** *(a) Red curves are representative of 9 curves, three arcs each at $\frac{h}{6}$, $\frac{h}{2}$ and $\frac{5h}{6}$, that together constitute the $m_p$ set. 72 purple colored points represent the module bound after decomposing the $m_{p-1}$ and $m_{p+1}$ curve set into 6 points each (i = 6) and removing the endpoints. In addition to the module bound and $m_p$ set, (b) shows the arch bound displayed in yellow color. The seed point collection $s_p$ and the module bound is translated to $n_x$ and $n_z$ arches for a total of 216 points (i = 6). Subfigure (c) depicts the vault bound (j = 100) for a total of 600 points in cyan color along with the module bound and arch bound.*

The rendering of the module formed by the $m_p$ set of curves is featured in Figure 3 corresponding to Step 11 in the aforementioned methodology. The conversion of the module obtained by Voronoi decomposition to a porous module is carried out to reduce the weight of the module. If Catmull-Clark subdivision is applied, the corners of the input module should be set to fixed. However, any severe shrinking should be avoided while some minor shrinking can be help offset manufacturing deviations.

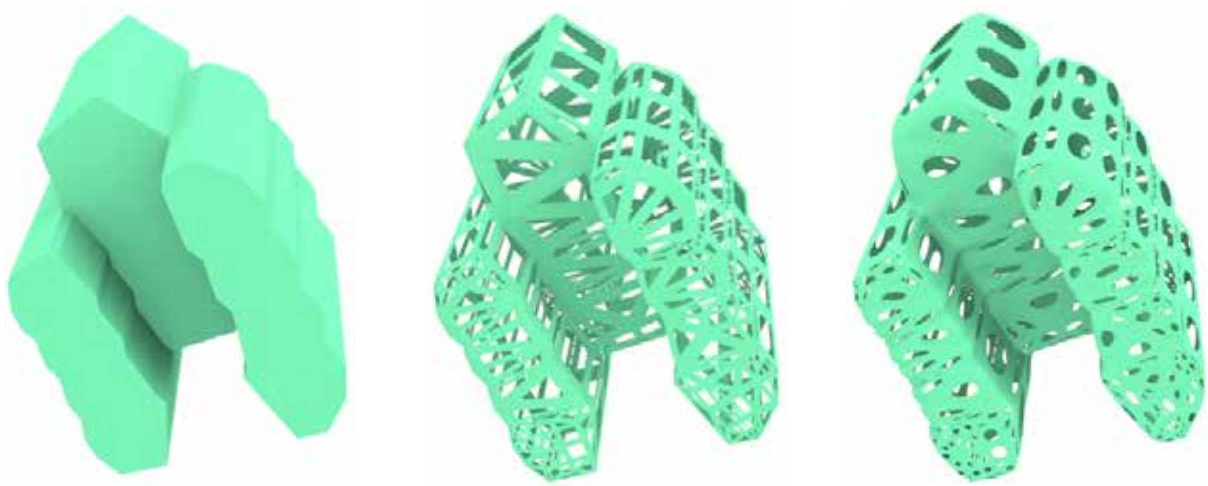

(a) (b) (c)

**Figure 3:** *(a) Module $m_2$ resulting from the curve and bounding point collection $b_p$ shown in Figure 2; (b) Porous version of module $m_2$; (c) Module $m_2$ after Catmull-Clark subdivision while keeping the corners fixed.*

The complete vault assembly from the resulting module in Figure 3c is shown in Figure 4a. The vault assembly consists of two arch ($n$ = 2) and nine modules each ($q$ = 9). The module $m_2$, obtained in Figure 3c, can be translated to replace all other modules except the keystone modules $m_5$. The keystone module is generated following the same process with $m_5$ curve set. The resulting arch is translated by *depth* ($d$ = 3) to obtain a vault comprised of two arches. Figure 4b displays a symmetric vault where all nine modules are generated individually, and seven arches have been assembled together ($n$ = 7). This setup requires 5 unique modules to continue in either direction.

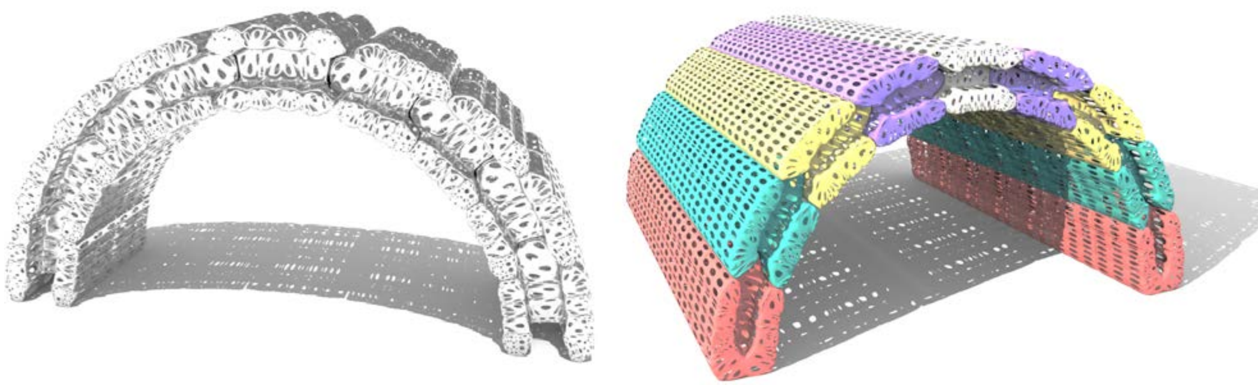

**Figure 4:** *(a) Semicircular barrel vault assembly of two arches after generating the keystone module $m_5$ and translations of side module $m_2$ for a total of 2 unique modules. (b) A semi-circular symmetric interlocking vault involving 5 unique modules that can be repeated to continue the assembly in Z direction. {Parameters: $n = 2$ (a); $n = 7$ (b), $d = 3$, $r = 7$, $h = 2$, $q = 9$, $ø = 5º$, $i = 10$, $j = 100$}*

All the demonstrated designs were generated using the proposed method in Rhinoceros 3D and Grasshopper interface by McNeel and Associates version 6 SR16 [8]. The decomposition of curves and Voronoi computation was carried out using Grasshopper nodes. A screenshot of the algorithm is presented in Figure 5.

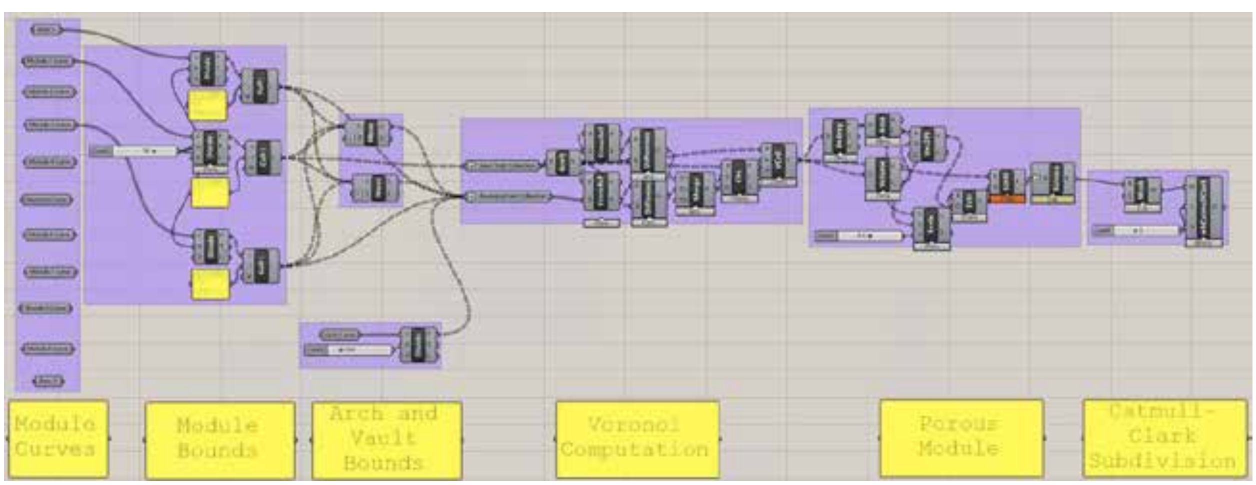


**Figure 5:** *Generic Template for Rhinoceros3D-Grasshopper algorithm.*

While all mentioned parameters are crucial in determining the form of the interlocking modules, the impact of inner and outer vault bound curves and their subsequent sampling to points is of significant prominence in the visual appeal of the arch or vault structure. Figure 6 shows the impact of points contained in the vault bound on the form. The protrusions result from the low $j$ count. Since the vault bound curves are decomposed into fewer points, the seed point collection's influence increases towards the inside as well as the outside vault bound. For this figure, the inner as well as the outer bound curves were decomposed into 17 points. As a result of that, 16 protrusions can be noticed filling the space between the bounding point collection on the inside and outside as determined by Voronoi tessellation.

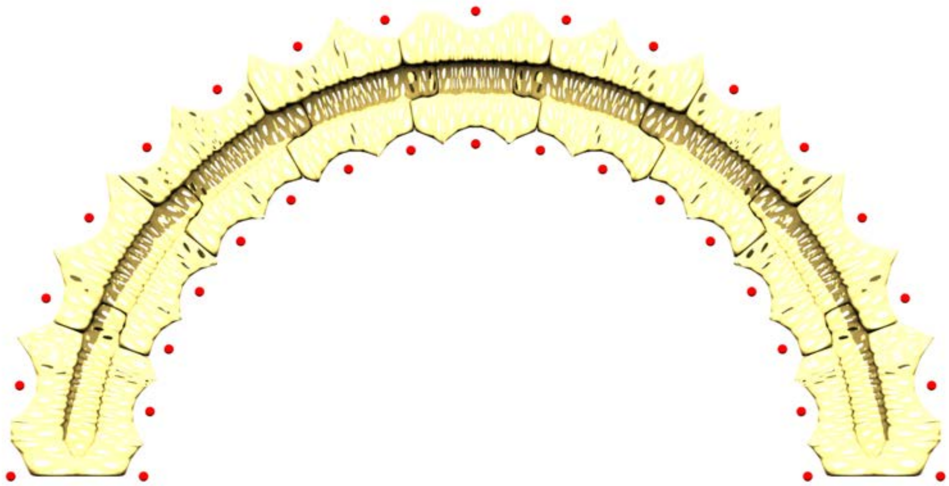

**Figure 6:** *Front view of an arch showing large protrusion resulting from sampling of vault bound curves to relatively less points. {Parameters: n = 1, d = 3, r = 7, h = 2, q = 9, ø = 5º, i = 10, and j = 17}*

Similarly, if *j* count is reduced even further, the protrusion become more pronounced in the internal as well as external form of the arch or vault structure. Figure 7 displays a non-repetitive symmetric vault where the impact of both *i* and *j* is be visualized. The bottom two modules on either side are kept in their non-porous state while the top three modules have been processed to create porous modules and smoothened using Catmull-Clark subdivision.

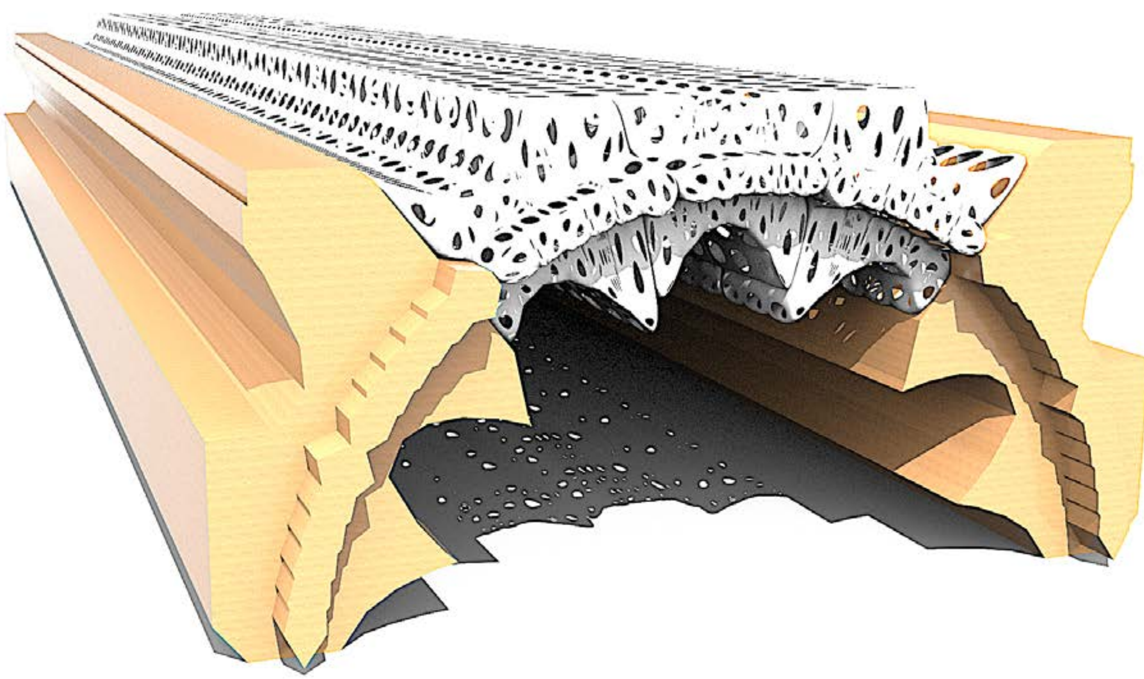

**Figure 7:** *Vault Bound count resulting in protrusions, interior count 7. {Parameters: n = 12, d = 3, r = 7, h = 2, q = 9, ø = 3º, i = 8, and j = 7}*

## Fabrication and Assembly

The modules can be manufactured with traditional injection molding or casting method if the original module is not transformed to a porous module, otherwise, it might be extremely challenging to manufacture them. However, with enhanced feasibility and availability of additive manufacturing, the prototypes can be printed before manufacturing full-scale assemblies. The build plate of available 3D printer should be considered while determining the module size and count of arch or vault structure. Also, in case of additive manufacturing of porous structure, the user needs to recognize if the printing process will require supports. The removal of supports can be extremely challenging if not well throughout beforehand, one alternate is to use water soluble support like polyvinyl alcohol (PVA).

Figure 8 displays one arch prototype that was printed using Fused Deposition Modeling (FDM) with polylactic acid (PLA) on Ender3 3D Printer [10]. The module form was populated with 250 points to generate the internal Voronoi tessellation and was printed without much support structure except for the interlocking extrusions. The PLA supports were broken off before the assembly. The slicing of the computer-aided model was carried out in Ultimaker Cura 4.2.1 [11]. The print settings are as follows: Infill = 20 %, Layer Height = 0.12 mm, Speed 50 mm/s, Bed Temperature = 60 ºC, and Print Temperature = 211 ºC. The model parameters were {n = 1, d = 2, r = 6, h = 2, q = 7, ø = 5º, i = 15, and j = 200}.

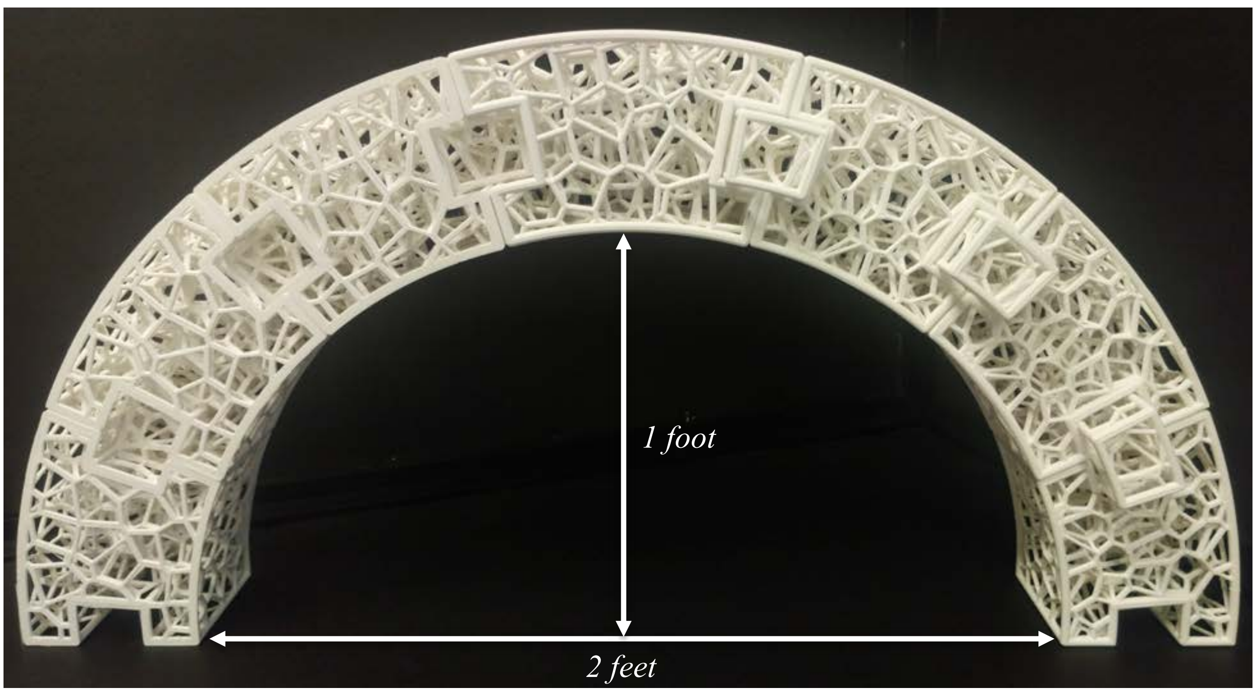


**Figure 8:** An additively manufactured assembly of a 7 module semi-circular arch (1 keystone and 6 repetitive side modules) with 1 foot rise and 2 feet span.

It is worth noting that the interlocking curve is significantly shorter than the guide curves and has a direction associated to it such that arch will interlock horizontally on both sides. The volume generation of the arch in Figure 8 was obtained by thickening of the outer edges of the module and the edges of the internal Voronoi cells to cylindrical pipes. This can be challenging especially for interlocking assemblies since that might result in overlap of modules. Hence, Step 11 was introduced in the methodology to ensure that the volume and thickness of elements in the module can be determined with the scaling factor $f$ (0.5 for this study) to avoid any overlap possibilities while creating porous modules.

The arch is assembled using horizontal translations along the Z axis. This include the keystone module placement which is traditionally placed at the end with a vertical Y direction movement. Shown in Figure 9 is the exploded view of a nine module arch requiring a horizontal movement to interlocking with the adjacent modules as well as the next arch.

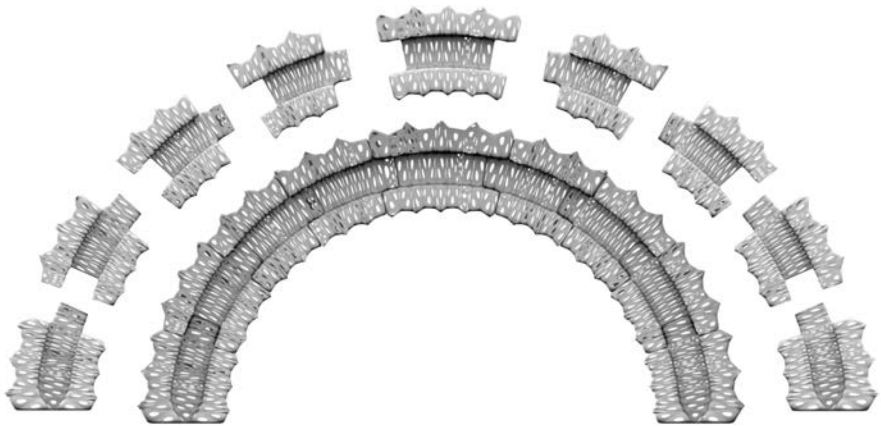

**Figure 9:** *An exploded view of a nine module semi-circular arch with 3 unique modules.*

### Anchoring End Modules

Arches and vaults tend to flatten out under gravity and generally require supports at the ends. If left unsupported, it is unlikely that the vault will stay in place. The stability of the design presented in Figure 8 is mainly due to the light weight of the arch as well as the relatively large depth $d$ and cross-section height $h$ parameters as compared to the scale of the arch itself. However, if the two parameters are reduced without adjusting the scale of the arch, it will likely require anchoring the end modules to maintain the static stability of the structure. One approach is to bind the end modules together using a platform which can compensate for the tensile stresses and the outward movements.

The methodology presented for arches and vaults can be expanded to the design of supports. This can be achieved with a module-based interlocking anchoring foundation. Figure 10 shows a set of curves in red color corresponding to a hyperbolic vault along with the proposed base support generated using non-uniform rational b-spline (NURBS) curves shown in green color.

*(a)* *(b)*

**Figure 10:** *A hyperbolic vault and anchor support assembly generated using the novel method. (a) The nurbs curves for base support are shown in green color while the curves corresponding to the hyperbolic vault are shown in red color. (b) Resulting modules of the vault and anchoring assembly.*

For the design of the anchor support, three nurbs curves were spaced ¼ d distance apart expect in case of end support which has 1 nurbs curve. It is covered by the end module of the vault as displayed in Figure 10a and 11a. Also, during computation of the end modules of the hyperbolic vault, both the guide curves and interlock curves were translated according to Step 5 instead of Step 5 and 6 for simplification of the anchor support and assembly movement. The end support module forms one half of the module bound for the hyperbolic vault end module. Two possible solutions are been discussed in relation to this in Figure 11.

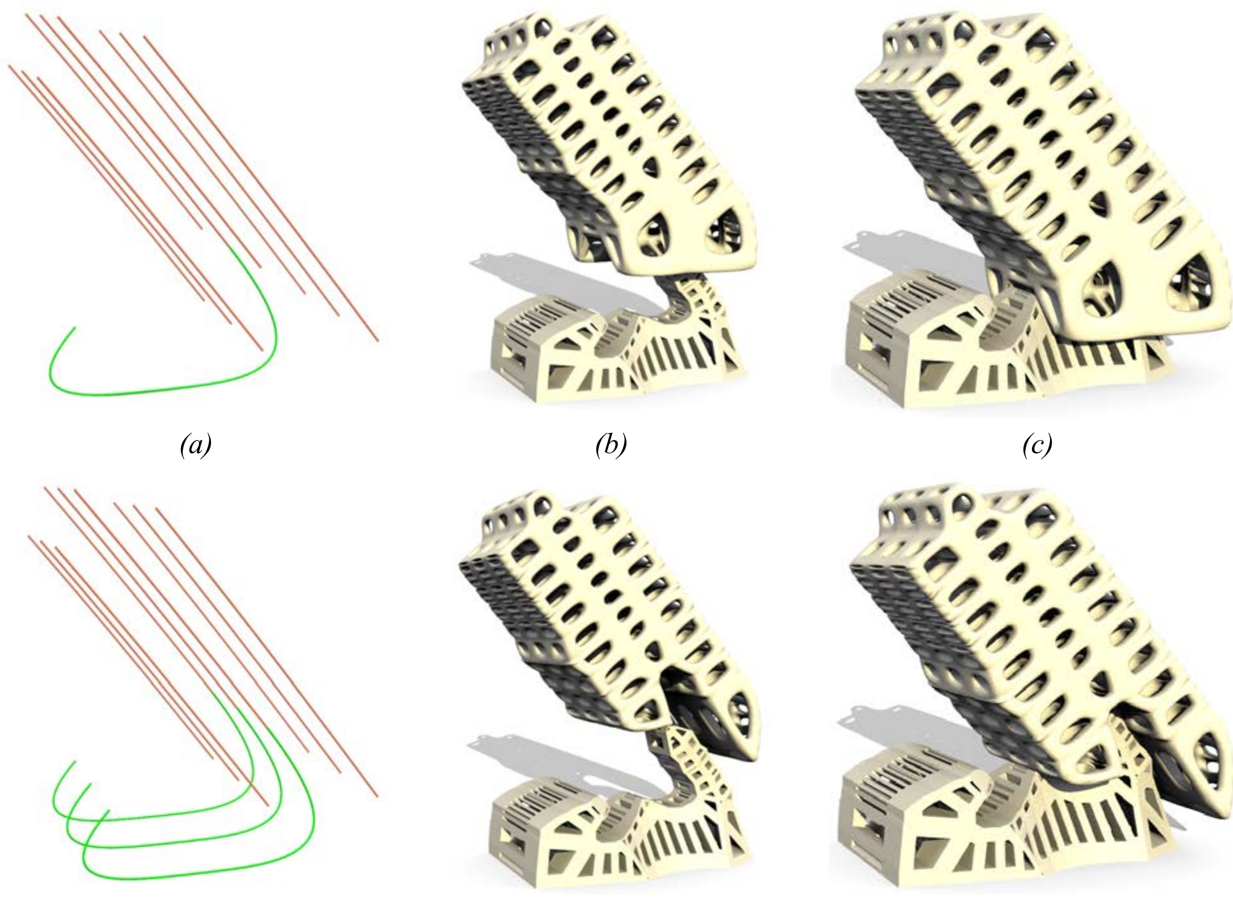

*(a)* *(b)* *(c)*

*(d)* *(e)* *(f)*

**Figure 11:** *End module design for the hyperbolic vault. (a) One green nurbs curve is included in the module bound of the hyperbolic vault end module for which the set of curves is shown in red color. (d) Three green nurbs curves are included in the module bound of the hyperbolic vault end module curve set shown in red color. (b) and (e) are corresponding depiction of the assembly movement. (c) and (f) show the final interlock of the support and vault module.*

The anchoring structure interlocks in XY plane but can slide in Z direction. Once in place, the tensile forces developed in the anchor support due to the vault will likely keep the anchoring modules from slipping out. However, a robust support system should be explored in future studies. The assembly for the anchor supports can be center outwards to end supports, while the assembly for arch or vault could be end modules upwards to the keystone. The interlock angle ø and the weight of the modules will determine if the modules need additional temporary support during construction. A potential assembly sequence is shown in Figure 12.

**Figure 12:** *Potential assembly sequence of an interlocking hyperbolic vault. The end module of vault and end modules of the support will be connected by movement in XY plane while all the rest of the module can be placed with a horizontal movement along the Z axis. Refer to Figure 1 for the coordinate system.*

## Discussions

It is fairly obvious to state that the set of curves in 3D design domain are of crucial importance in determining the form and interlocking mechanism. However, the impact of decomposing the curves into points is also significant. During the decomposition of $m_p$ module curves into $i$ points, the endpoints are excluded because of coincidences with endpoints of adjacent $m_{p-1}$ and $m_{p+1}$ module curve set. As long as the curve decomposition to points is uniformly spaced, the Voronoi computation will ensure that the module cell boundary will overlap with the endpoints.

Decomposition of inner and outer vault bound curves into $j$ points is crucial in determining the internal and external form of the module. For avoiding protrusions, radially project ¼ h arch decomposed points onto the inner bound curve and ¾ h arch points onto outer bound curve. Otherwise, the decomposition can be independent of the module curve decomposition and result in protrusions depending on the $i$ and $j$ parameters. Later will result in a wide range of module shape which can be adjusted according to the design intent. Ideally, increasing the number of $i$ and $j$ points will result in a smoother and uniform surface but also increase the computation expense associated with the solution set. Also, currently the method incorporates all the points of the neighboring modules, and vault bound. This is carried out to account for the possibility of complex free form curves, however, only nearest 400 points from the bounding point collection $b_p$ are considered during the Voronoi computation for each seed point in the collection $s_p$. The form of each seed point's Voronoi cell is affected drastically by the initial 20-50 points and usually minor adjustments are noted after that. 400 nearest points were selected to balance the form and computation expense.

The method presents a generic approach to develop interlocking assemblies of arches and vaults. However, there are additional adjustments that need to be accounted for, especially in case of end modules, as discussed in relation to Figure 11. Also, the flexibility to generate repetitive modules gets limited if the angle made by the module, $\frac{\pi}{q}$ in case of semicircular arches, changes non-uniformly relative to the curve length, for instance in case of parabolic or hyperbolic vault. This is something to be explored in future studies. Another possible variation of the algorithm could be to vary the angle made by the modules in semicircular arches and vaults itself. For instance, Figure 7 and Figure 13 are similar on all the major parameters mentioned in the methodology. However, in Figure 7 all guide curves formed equal angle at the center of the circle ($\frac{\pi}{7} \sim 25.71°$) whereas in Figure 13 the keystone guide curve angle (30º) is different than the rest of the guide curve angles (25º). This in turn changes the eventual form of the arch and should be considered as another parameter and tool in the future studies.

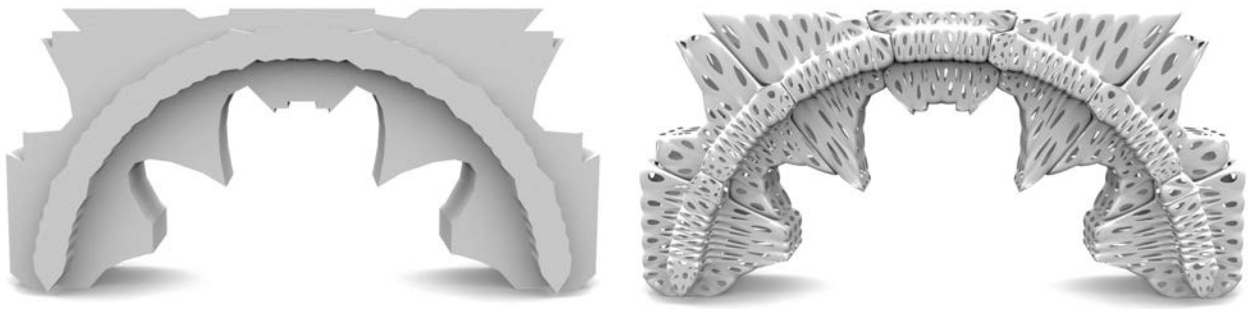

**Figure 13:** *An interlocking arch symmetric about the center keystone with keystone guide curve forming a larger angle at the center (30º) as compared to the rest of the modules (25º) . (Left) Union of all modules; (Right) Arch assembly with porous modules. {Parameters: n = 1, d = 3, r = 7, h = 2, q = 9, ø = 3º, i = 8, and j = 7}*

Meanwhile, interlocking arches similar to Figure 6 can be useful in exploring modified versions of modules. Figure 14 below shows one such modification. The original module in 14a was obtained after a low *j* count of vault bound. The use of Kangaroo Physics, a physics-based plugin for Grasshopper, was utilized to turn the edges into spring-based systems [12]. The interlocking edges were fixed along with some additional desired edges while the rest of the surface was allowed to reach an equilibrium state. This effectively provide one solution to retain the interlocking properties and getting rid of any unwanted protrusions as seen in 14b. The complete assembly with the modified module and original keystone module is shown in 14c.

(a) (b) (c)

**Figure 14:** *(a) Original porous module obtained by the proposed methodology {Parameters: n = 1, d = 3, r = 7, h = 2, q = 7, ø = 5º, i = 5, j = 18}. (b) Modified porous modules after the use of spring-based system to get rid of unwanted protrusions while preserving the interlocking edges. (c) Interlocking semicircular arch assembly with six modified porous modules and one original keystone modules*

While this paper has presented evidence that the method can be used to generate a wide range of interlocking arch and vault assemblies, there is tremendous scope for future applications. Interlocking domes should be explored in the next phases along with evaluations of the structural performances of the geometric forms. Meanwhile, additional studies on various interlocking patterns and weaving techniques, especially those utilizing Voronoi tessellation-based form generation, should be utilized to enhance stability of the interlocking structures in the future [13]. Examining the role of the interlock angle ø in supporting the arch during construction sequence can be another objective for future studies.

## Conclusion

This paper presented a novel method to generate interlocking arches and vaults by Voronoi decomposition of 3D space using curves. It was demonstrated to work with semi-circular arcs, hyperbolic segments and nurbs curves. Additive manufacturing was utilized for fabricating interlocking arch modules, and conceptual extension to anchor support structure was also explored. The method is likely to provide architects and designers a powerful tool to generate interlocking structures while presenting adequate scope for future research and practical applications.


## Acknowledgements

I would like to acknowledge that this work is a result of many stimulating discussions and collaborations over the past few years. Special thanks to Ergun Akleman, Julian Kang, and Wei Yan. I would also like to thank the reviewers for their constructive feedback towards improving the manuscript.


## References


[1] R. Decastes. *Principia Philosophiae*. 1644

[2] G. L. Dirichlet. "Über die Reduktion der positiven quadratischen Formen mit drei unbestimmten ganzen Zahlen." *J. reine angew. Math.* vol. 40, 1850, pp. 209-227.

[3] G. Voronoi. "Nouvelles applications des paramètres continus à la théorie des formes quadratiques." *J. reine angew. Math.* vol. 133, 1907, pp. 97-178.

[4] A. Borhani and N. Kalantar. "APART but TOGETHER - The Interplay of Geometric Relationships in Aggregated Interlocking Systems." Proceedings of the 35th eCAADe Conference, vol. 1, 2017, pp.639-648.

[5] G. Fallacara (2006). "Digital stereotomy and topological transformations: reasoning about shape building." Proceedings of the second international congress on construction history, vol. 1, 2006, pp. 1075-1092.

[6] S.G. Subramanian et al. "Delaunay Lofts: A biologically inspired approach for modeling space filling modular structures." *Computers & Graphics*, vol 82, 2019, pp. 73-83.

[7] E. Akleman et al. "Generalized Abeille Tiles: Topologically Interlocked Space-Filling Shapes Generated Based on Fabric Symmerties. *Computers & Graphics*, 2020.

[8] McNeel and Associates. "Rhinoceros3D". https://www.rhino3d.com

[9] E. Catmull and J. Clark. "Recursively generated B-spline surfaces on arbitrary topological meshes." *Computer-Aided Design,* vol. 10, 1978, pp 350-355.

[10] Shenzhen Creality 3D Technology Company, Limited. "Ender 3 3D Printer". https://www.creality3dofficial.com/products/official-creality-ender-3-3d-printer

[11] Ultimaker. "Ultimaker Cura 4.2.1". https://ultimaker.com/software/ultimaker-cura

[12] D. Piker. "Kangaroo Physics". https://www.food4rhino.com/app/kangaroo-physics

[13] V.R. Krishnamurthy et al. "Bi-Axial Woven Tiles: Interlocking Space-Filling Shapes Based on Symmetries of Bi-Axial Weaving Patterns." 46th Annual Graphics Interface Conference, 2020.

# EXTENDED ABSTRACTS

# Analogue Randomiser researches graphic chaos.

**Dr Jack Tait Sole author**
**Fine Artist practicing in Abergavenny Wales UK taitographs.co.uk**

## Abstract

The paper studies graphic chaos from an art perspective. The 'Analogue Randomiser Programmer' helps drawing machines investigate a greater element of chaos in graphic systems. In previous research into Programmable Analogue Drawing Machines a balance was struck between determinism and quasi-random inputs, creating expressive images displaying coherence. Contrary to expectation, determinism persisted even when a quasi-randomness input predominated. Recent encouraging research into 'Near Chaos' was limited by programmers using fixed sequential sequences. Some machines had inbuilt quasi-randomness enhancing the non-linearity of the whole system. The current 'Randomiser' increases the potential for chaos and is analogous to a 'throw of a dice' producing six outputs. Mechanical details and images show how the Randomiser moves my research into more chaotic territory than was the case in earlier 'near chaos' work with sequential programmers.


**Figure 1.** *The Randomiser showing the two flywheels and the three main outputs. These may be combined in pairs to make 6 choices.*

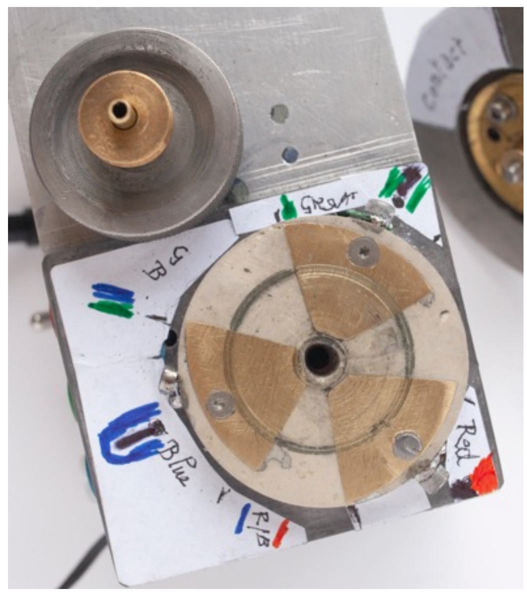


**Figure 2.** *Randomiser brass contact wheel.*

**Figure 3.** *Randomiser, timer, spin motor and large flywheel.*

**Figure 4.** *Wide contact covers two outlets.*

## Introduction

Previous work on different drawing machines [1], [2] & [3] either relied on integral programming or were governed by sequential timers. Simple instructions led to complex drawings created by a balance of quasi-randomness and determinism. Coherent images selected, lending themselves to further enhancement. Many machines made encouraging images but the rigid determinism of fixed sequential timers proved a limiting factor. Interest in chaotic graphic drawings [4] & [5] eventually called for a fully random input. The Randomiser machine is the solution. Results from two machines are shown but the machines are not described in detail. They are a New Drum plotter machine **Fig 5.** and a flat-bed X:Y plotter with added pen rotator **Fig 6**. The later drawings emphasise the graphic chaos created by the Randomiser.

## The Analogue Randomiser

From now on the Randomiser outcomes **Figure 1**. are described as 'random' not 'quasi-random' as there is a significant difference between results. The device has a timer and a spin motor. The latter moves the contact which can settle on six possible outlets. There are three single outlets and three others where the contact straddles two of them, making six in total. When the timer has pulsed the spin motor, one of the six possibilities is chosen when the spin comes to rest. The spin motor is geared down, via a belt drive to the contact rotor, where two flywheels help it to be random. A small to the spin motor and large to the contact rotor. **Figures 1 & 4.** The spin time is precisely controlled, long enough to produce a random result but not to continue motion once the power is directed to the selected outlet. This fine adjustment prevents the contact rotor 'flipping on ' each outlet before settling on its final place. The Randomiser, albeit at prototype stage, is sufficiently non-linear to function satisfactorily.

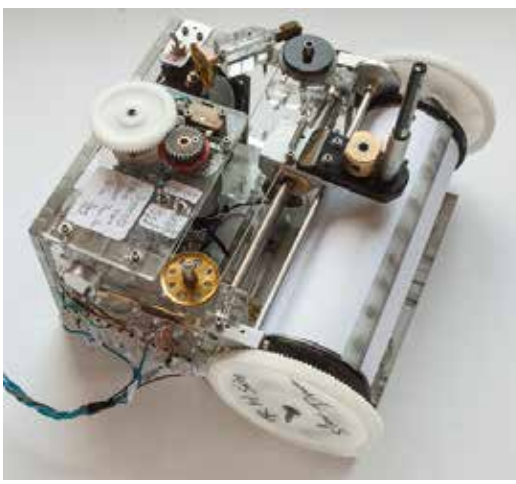

**Figure 5.** *New Drum plotter machine.*

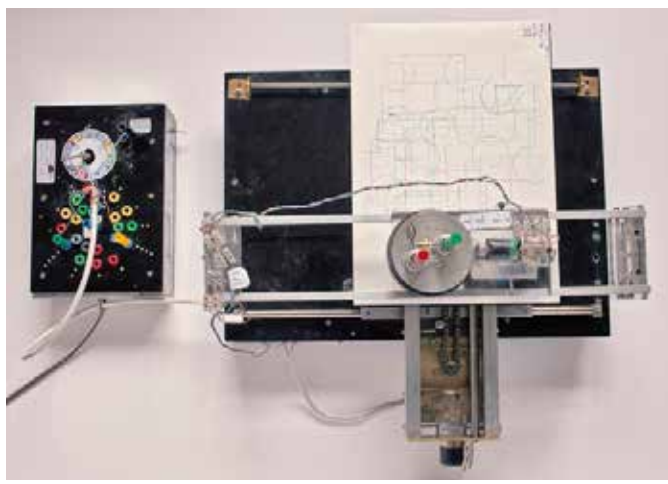

**Figure 6.** *X:Y rig with pen rotator, pen lift and timer/ programme.*

***New Drum plotter machine. A partial solution.***

The redesign of a 1970 drum plotter machine **Figure 5**, was a step towards investigating chaos. Increased quasi-randomness was created by multiple D.C. motors. The X axis motor has constant speed variation via a rotating resistor and an auto-reverse relay. Two Y axis inputs, via a differential and a pen lift, are driven by a further motors. Combining its inherent quasi-randomness with the Randomiser's six outputs worked.

***X:Y Plotter research.*** The X:Y plotter with pen-lift is a simpler machine, designed to create drawings enhanced in Adobe Photoshop. Comparisons may be made with sequential timer/programmer results with those from the Randomiser. The significant feature exploited with this machine is the facility to switch on two motions at the same time giving straight and diagonal lines, curves and circles.

***Strands of work***
Two have been undertaken, one using the Randomiser with the New Drum Machine and the second with the X:Y plotter, which includes a pen-rotator and pen-lift device. **Figures 7 & 8** below show the extent of chaotic images within the limitations of either an integral programme or an external timer /programmer controlling the drawing machines. They can be compared to **Figures 9 - 12.**

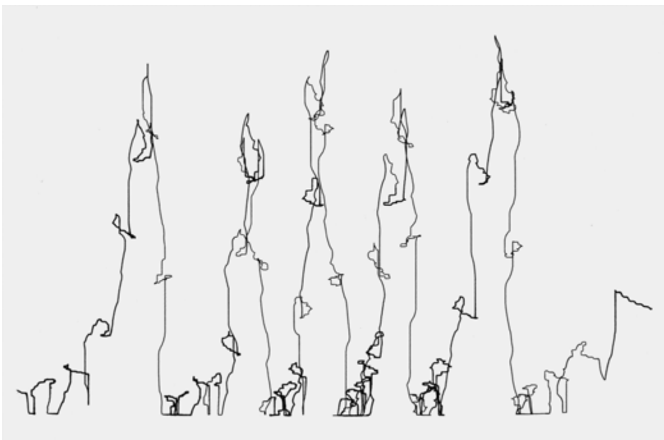

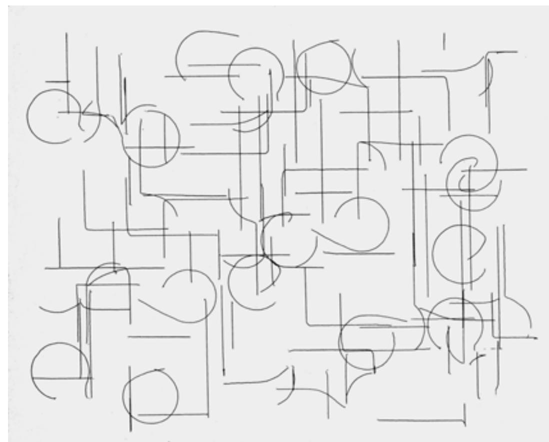

**Figure 7.** *Chaotic line from New Drum machine.* **Figure 8.** *Drawing on Flat bed X:Y plotter with pen lift.*

## Randomiser drawings

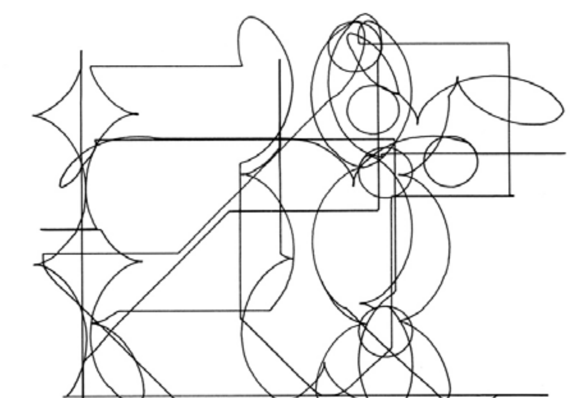

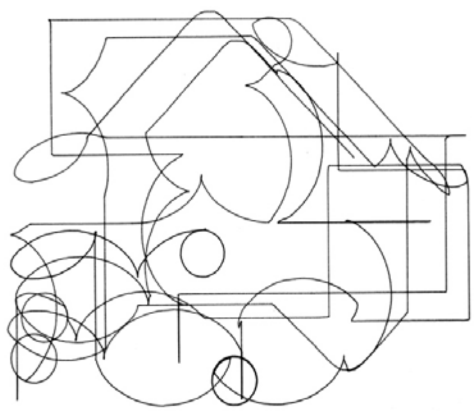

**Figures 9 & 10** *Flat-bed X:Y plotter drawings; presence of circles and diagonal lines show difference to New Drum images.*

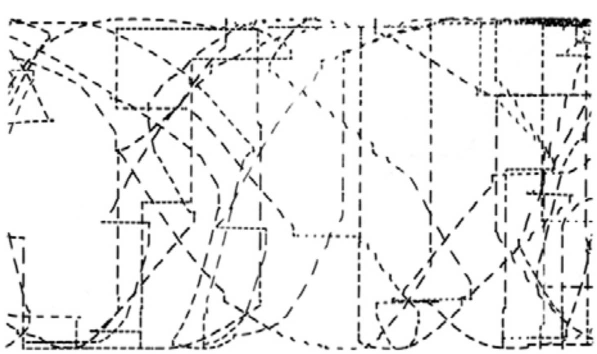

**Figures 11 & 12** *New Drum drawings, first with constant pen lift, second continuous line, both showing graphic chaos.*

***'Goldilocks' ratio***

This ratio applies when using the New Drum machine. If the Y1 to Y2 ratio is too close it cancels out part of the Randomisers 'randomness'. A large ratio over-emphasises horizontal lines, a small one cramps the drawing. Y1:Y2 =1:2 is the best ratio and when the full X motor speed is close to the Y1 speed.

## Evaluation

The final drawings in **Figures 9 - 12** justify the building of the Randomiser, demonstrating its contribution to a chaotic distribution of line. Defining what is a chaotic image is difficult and I can only share my intuitive judgement of it. Past drawings have displayed elements of chaos without a random input **Figures 7 & 8** , but given the non-linear nature of programmer and machine combinations, some overlap is inevitable. The drawings, **Figures 9 & 10,** may be compared with the programmer's drawing **Figure 8.** The persistence of determinism is caused by the inherent design of the X:Y plotter rig; it can only draw straight lines or circles with the pen rotator. With the X:Y plotter, the Randomiser is able combine straight lines and circles producing curves and diagonal lines by combining X,Y and pen rotator. *(Pen lift is not available; four outlets are needed for this on the plotter.)* These results are close to chaos but still show some element of coherence. Drawings from the New Drum machine allow extended variations, due to its greater range of actions, such as the auto reverse and voltage variation of the X axis motor with the double Y axes.

Evaluation of any art work is subjective. James Gleick **[6]** points out that non-linear systems are unpredictable even if the exact starting point of each image were to be set. Gombrich **[7]** holds that the response to an art work is wholly governed by what the 'beholder' brings to the viewing. Two further points may be considered. Some time ago my response to a random result, programmed into a drawing was "I would not have 'thought' of that". This still obtains today. The last word should go to my hero Paul Klee **[8]** who coined the expression "Taking a line for a walk". A happy mean exists where the walk with chaos should lead to interesting places but avoid going round aimlessly in circles.

## Conclusion

A series of images are shown for the reader to assess and arrive at their own view. The Randomiser research is current. The questions which absorbs me is seeking persistence of determinism in an art work. Deciding whether or not a particular image is wholly chaotic is speculative. Does some hint of coherence manifests itself? Is the persistence of determinism a problem? The recognition of coherence combined with curiosity is the mainspring of my motivation. No definitive answers to these questions are offered but it can be stated that the recent pursuit of looking into 'near chaos' and entering a chaotic graphic domain has lent a additional dimension to an extended body of work. It might also be felt that questions are more important than answers. Questions are never ending and answers are always temporary and subject to change.

## References


[1] Tait, Jack (2011) *"Programmable Analogue Drawing Machines*". PhD thesis MIRIAD, Manchester Metropolitan University.

[2] Tait Jack ( 2013) "*Art by Machine*". Bronydd Press Clyro Wales.

[3] Tait, Jack (2017). http://taitographs.co.uk (retrieved 12 March 2019).

[4] Tait, Jack (2019) *"Secondary Near Chaotic Patterns from Analogue Drawing Machines"*. Special Issue Topological Modelling Mathematics, Volume 7, Issue 1 (January 2019).

[5] Tait Jack (2019) "*Near chaos graphic images*". Biomedical Journal of Scientific & Technical Research.

[6] Gleick, James (1987) "*Chaos, The amazing science of the unpredictable"*, Vintage, London.

[7] Gombrich, E H (1960) "*Art and Illusion: a study in the psychology of pictorial representation"*, Phaidon, London.

[8] Klee, Paul (1997) *Painting Music*, Prestel Verlag, Munich

# Toward Fabricating Surfaces as Patchworks of Pantographic Lattices

James Mallos, Sculptor, Washington DC, USA

### Abstract

An elegant way to fabricate a patch of curved surface is to constrain the perimeter of a patch of wire mesh. The technique is familiar to sculptors; it is known by the term *gridshell* among architects, and *pantographic lattice* among metamaterial technologists. This paper presents results of the author's preliminary research on fabricating 3D-printed surfaces out of rudimentary pantographic lattice patches that can be quickly printed flat, and then seamed together (constraining the perimeters of the patches at the same time) by a simple chain stitching technique.

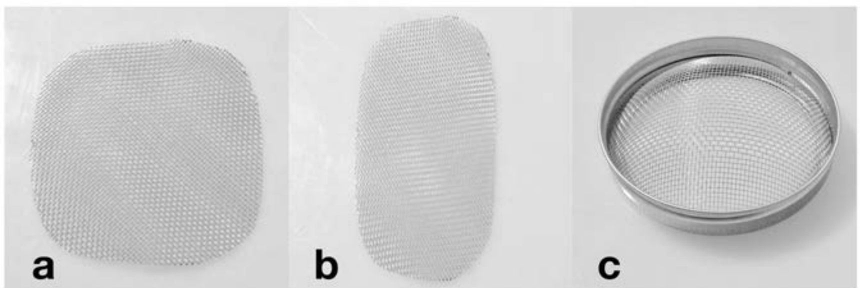


**Figure 1:** *Shape changer: a) a patch of wire mesh; b) the same patch conformed to a new perimeter; c) the same patch conformed to a perimeter incompatible with planarity.*

### Introduction

It is a common observation that woven fabric drapes differently from, say, plastic film, because it offers little resistance to shear—and the draping is sensitive to the orientation of the grain of the fabric. When a stiff fabric is used, say, the wire mesh used in a kitchen strainer [1], the effect is so pronounced that merely constraining the perimeter of a patch of fabric to a shape incompatible with planarity causes it belly out into a three-dimensionally curved surface (Figure 1.) In recent decades this shape-changing behavior has caught the interest of both architects at the large scale (gridshells) and metamaterial technologists at the small scale (pantographic lattices). Computer scientists interested in modeling the dynamics of hair and fur have at the same time contributed fast algorithms that aid the computational modeling of grids. This paper presents some preliminary results in the author's attempt to harness this now well-understood phenomenon to make large models quickly in small 3D printers—a commonly felt need in educational and shared-use environments.

### Background

In 1878 Tchebyshev [16, 13, 6] described how a woven fabric—which he modeled as a pin-jointed, equilateral rhombic grid ('fishnet' in fabric parlance)—can be made to conform to a portion of a curved surface. Starting from two crossing curves on the surface, the discrete version of his geometrical construction can be accomplished with just a compass. Tchebyshev also derived a fundamental limit on the amount of curvature such a construction can span: for example, it is not possible to wrap a sphere with fishnet without producing a singularity. His purely geometric model still gives useful first approximations for gridshells and pantographic lattices.

In 1970, the erection of Frei Otto's Mannheim Gridshell [8] sparked the architectural interest in gridshells that has continued to this day. Many gridshells utilize the shape change effect, being assembled flat and erected by compressing the perimeter, usually with lifting assistance from cranes above or an inflated membrane below. As a practical matter, architectural gridshells are usually limited to structural members that are straight when on the ground; and the erected gridshell needs to be rigidified against asymmetric loads and rendered water-tight in some way. (In 3D printing we are not limited to members that are straight when printed; the present research does not address how to to rigidify the assembled model or make it water-tight.)

Mathematical modeling of gridshells is now quite advanced. Bending and torsion of structural members that are not round or square in cross-section [3], or are curved when on the ground [11], can now be modeled. Algorithms originally developed in computer graphics to realistically model hair in motion have made gridshell modeling faster [2, 1]. Algorithms have also been developed that can cover a curved surface with a patchwork of grids [9] (thereby escaping Tchebyshev's curvature limit,) design wire meshes with interactive user input and a degree of freedom in approximation to the guiding form [5], automatically place singularities (i.e., vertices that are not 4-valent) to extend a Tchebyshev net to cover an entire surface [14], and design freeform gridshells using the theoretical minimum of material [12].

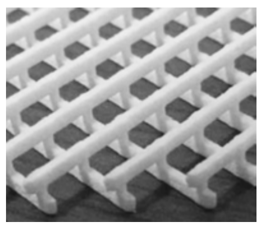

**Figure 2:** *A pantographic lattice 3D-printed for metamaterial research [4].*

More recently, metamaterial engineers have been interested in pantographic lattices [4] (miniature gridshells in the flattened state) that can be realized by 3D printing (Figure 2). There has also been metamaterial research into the shape change effect in pantographic lattices with curved members [7].

## The Goal

FDM 3D printing is slow. Build volume is expensive. These limitations are acutely felt where the user has limited machine time, as in a classroom or maker space. It would be nice to be able to quickly make models larger than the build volume in these situations—even if some post-printing assembly were required. The shape changing effect in pantographic lattices seems to offer some hope to get around this problem since flat objects can be quickly printed on the build plate. Metamaterial research [4] has shown that pantographic lattices can be successfully 3D printed (Figure 2.) Taking a hint from 'zippable' shape representations [15] it would seem possible to join 3D lattice patches by chain stitching loops printed along their perimeter. Chain stitching is a very easy hand technique that has traditionally been used to 'zip' and 'unzip' saddle bags [10] (Figure 3.)

## Main Challenges

### *Fast-to-Print Pantographic Lattices*

The pantographic lattice of Figure 2 is too refined to print quickly. A faster alternative would be to extrude the upper layer of rods at a speed and temperature that produces small cylinder-to-cylinder welds to the lower

**Figure 3:** *A traditional chain stitch closure on a saddlebag [10].*

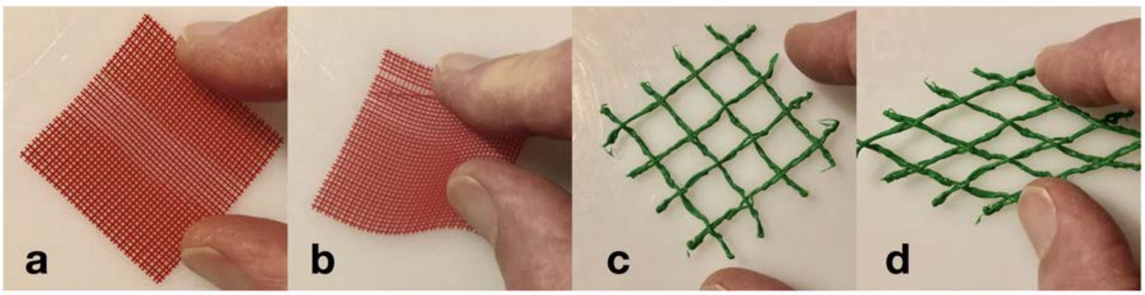


**Figure 4:** *Fast Lattices: a-b) two-pass; c-d) four-pass.*

rods (Figure 4a). Unfortunately, my trials found no happy medium where scissor action was loose enough to shear without curving, yet welds were strong enough to bind the fabric securely together (Figure 4b.)

A four-pass lattice seems more promising, though I have only sketched it with a 3D pen (Figure 4c-d.) In a four-pass lattice the extruder retraces each path, making z-hops (vertical jumps) over rods it is crossing (thereby avoiding a weld,) and presses down along any rod it is retracing (thereby producing a linear weld.) The result is like a net of twined braiding, but with linear welds rather than twists joining the paired strands. The welds are not severely loaded by the scissoring action, so they do not need to be especially secure.

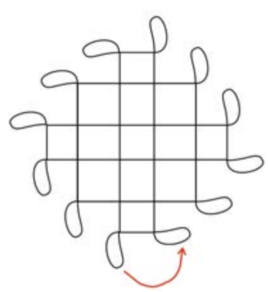

**Figure 5:** *Using a chain stitch to constrain the perimeter of a 3D-printed pantographic lattice: each terminal loop encloses, in this case, its counterclockwise neighbor. The last stitch must be locked in another way.*

### *Chain Stitching the Seams*

I envision constraining the perimeter of the patches, and seaming them together, by chain stitching loops that are printed integral to the lattices (Figure 5.) The loops are sized to properly constrain the lattice only after the loops of the adjoining patch are intertwined in the manner of a chain stitched seam in crochet. Thus each seam is in effect chain-stitched twice. This is actually an advantage. It is always possible to find a spanning tree in any graph on the sphere (by breaking certain edges at their midpoint), and thus to tour all its edges (seams) in a closed loop that goes along each seam twice. Given such a plan of seaming, only the last stitch needs to be locked.

## Summary and Conclusions

I have sketched a novel way to fabricate larger shapes more rapidly using the 3D printing resources available to schools and maker spaces. Much needs to be done to bring this to fruition.

## References


[1] Changyeob Baek, Andrew O Sageman-Furnas, Mohammad K Jawed, and Pedro M Reis. Form finding in elastic gridshells. *Proceedings of the National Academy of Sciences*, 115(1):75–80, 2018.

[2] Miklós Bergou, Max Wardetzky, Stephen Robinson, Basile Audoly, and Eitan Grinspun. Discrete elastic rods. In *ACM SIGGRAPH 2008 papers*, pages 1–12. 2008.

[3] Bernardino D'Amico. *Timber Grid-shell Structures: form-finding, analysis and optimisation*. PhD thesis, Edinburgh Napier University, 2015.

[4] Francesco dell'Isola, Ivan Giorgio, Marek Pawlikowski, and Nicola Luigi Rizzi. Large deformations of planar extensible beams and pantographic lattices: heuristic homogenization, experimental and numerical examples of equilibrium. *Proceedings of the Royal Society A: Mathematical, Physical and Engineering Sciences*, 472(2185):20150790, 2016.

[5] Akash Garg, Andrew O Sageman-Furnas, Bailin Deng, Yonghao Yue, Eitan Grinspun, Mark Pauly, and Max Wardetzky. Wire mesh design. *ACM Transactions on Graphics*, 33(4), 2014.

[6] Étienne Ghys. Sur la coupe des vêtements. Variation autour d'un thème de Tchebychev. *L'Enseignement Mathématique*, 57(1):165–208, 2011.

[7] Ivan Giorgio, Alessandro Della Corte, Francesco Dell'Isola, and David J Steigmann. Buckling modes in pantographic lattices. *Comptes rendus Mecanique*, 344(7):487–501, 2016.

[8] Ian Liddell. Frei Otto and the development of gridshells. *Case Studies in Structural Engineering*, 4:39–49, 2015.

[9] Yannick Masson. *Existence and construction of Chebyshev nets and application to gridshells*. PhD thesis, 2017.

[10] Edith Eliza Ames Norton. *Rugs in their native land*, page 135. Dodd, Mead, 1910.

[11] Julian Panetta, MINA Konaković-Luković, Florin Isvoranu, Etienne Bouleau, and Mark Pauly. X-shells: A new class of deployable beam structures. *ACM Transactions on Graphics (TOG)*, 38(4):1–15, 2019.

[12] Davide Pellis and Helmut Pottmann. Geometry and statics of optimal freeform gridshells. 2020.

[13] Eugene Vladimirovich Popov. Geometric approach to Chebyshev net generation along an arbitrary surface represented by nurbs. In *International Conference Graphicon*, 2002.

[14] Andrew O Sageman-Furnas, Albert Chern, Mirela Ben-Chen, and Amir Vaxman. Chebyshev nets from commuting polyvector fields. *ACM Transactions on Graphics (TOG)*, 38(6):1–16, 2019.

[15] Christian Schüller, Roi Poranne, and Olga Sorkine-Hornung. Shape representation by zippables. *ACM Transactions on Graphics (TOG)*, 37(4):1–13, 2018.

[16] Pafnuty L Tchebychev. Sur la coupe des vêtements. In *Association française pour l'avancement des sciences, Congres de Paris*, pages 154–155, 1878.

# 3D Modeling Stylized Characters

Ben Heymann[1] and Felice House[2]

[1]Texas A&M University, College Station; benheymann@tamu.edu
[2]Texas A&M University, College Station; flh93@tamu.edu

## Abstract

In this work, we present a workflow for 3D modeling stylized characters. The analysis provides methodology and information to develop appeal. The process begins with choosing developed concept art that displays accurate anatomy. A blocking stage follows to achieve desired physical form of the character. Further refinements are then applied to obtain anatomical accuracy to enhance character believability. The study also breaks down facial and body features to emphasize key modeling techniques. There is also a focus on construction, or topology of the character. Character models will physically deform along with textures, so topology is critical. Quad-based topology is optimal and ensures the character is ready to move into the next stage of production. These stages work to build an appealing stylized character that is production ready.

## Motivation & Introduction

### Introduction

In this work, we present a stage-by-stage process for building 3D stylized characters. Using this process, we have developed three different stylized characters based on concept art. This methodology allows for an iterative and non-destructive workflow. The stages of 3D character modeling within this methodology are incremental. This allows for an artist to navigate back to any state of the character's development. In animation or gaming pipelines, this is important because creative direction may shift. In the development of this methodology, we have worked with Ryan Tottle, a modeling supervisor from Walt Disney Animation Studios.

## The Workflow

Our workflow consists of the five stages. We first analyse the concept art. Then, we construct base models using quad-meshes to use Catmull-Clark subdivision. We then add details for face and body features. In the last stage, we print the resulted shapes. In the following, we explain each stage in detail.

**Stage 1: Analysing Concept Art and Block-In.** Three different characters were chosen. "Chibi Sailor Moon," based on the concept art of Helen Chen, was the first character. Her dynamic mid-jump-pose inspired me to create this character in 3D. The second character is "Mother Earth," based on the concept art of David Lojaya. The line of action in her pose along with the elegance behind this concept art were our inspiration. The last character was "Chief Bulldog," based on the concept art by Justin Runfola. The grumpy and comedic expression inspired me to create this bulldog character. Character modeling begins with blocking out shapes that make-up the character's profile. They are flexible and meant to achieve general anatomical shapes. These shapes represent forms of the body. This is important because as the character is being developed, the design may change. Using these free-form shapes will allow flexibility for iterative adjustments. The blocking stage marks an efficient time to classify proportions.


Figure 1: *Concept art used for character modeling.*

**Stage 2: Quad-Based Mesh Creation.** Creating mesh topology follows blocking out the character. The blocking process is effective because it is iterative. It allows the shape to develop so edge flow placement in the character's topology can be the strongest. The edge flow in topology is an interlocking series of continuous mesh edges. They control the smoothed form of an animated subdivision surface [4]. With each subdivision, the model becomes smoother. The faces are being multiplied and spaces between each vertex is averaging out. Cycling between different subdivision levels is an effective working strategy [6]. More detail is possible the more divided the model is. The highest subdivision level controls the lowest subdivision level. Any work done in the high-subdivided model results in vertices falling into place.

***Stage 3:*** **Modeling Facial Features.** Across human and animal-based characters, the jawline defines communication and expressions. Underlying musculature is also important to define in facial areas to enhance expression. For example, muscles are responsible for controlling the movement of the eyebrows. When the eyebrows rise, the underlying frontalis muscle pulls the outer lying skin This creates horizontal wrinkles in the forehead, translating to emotional output from the character. From a stylized perspective these wrinkles are important. For appeal, the definition of the wrinkles should be soft and not too prominent. Before focusing on individual hair strands, it is important to block in a whole shape to define the mass of hair. Areas where hair strands are more apparent, define the active zones. These zones are typically defined with the concept art and can resemble movement. Since hair is lightweight, it will lean or fall in a certain direction due to gravity. It is also important to imply a transition between the forehead and front most hairs for anatomical accuracy. The blocking stage is an excellent time to create the cavity that represents the eye socket. From a stylization perspective, the eyelids need a certain amount of thickness to be present. Defining the tear ducts in the corner of the eye will enhance believability. Adding a slight cross-eye can also make the character more appealing [6]. While animal ear shapes tend to vary, human ears generally all have the same shape. From a stylized perspective, the space within the ear is a defined planar space. Controlling the complexity of shapes within the ear keeps a cleaner aesthetic. However, there are small but important anatomical features to define like the relationship between the tragus and antitragus (Figure 2). Also, tapering in the thickness from the top of the ear down to the earlobe enhances believability. These are some key points to define in the structure of the ear to keep the detail minimal. The minimal detail will direct the eye of the viewer to more important parts of the face. This is essential for appeal so viewers do not get fixated on details. It is more important to clearly read the character's appeal.

Muscles are generally smaller in the head compared to the rest of the body. Yet, they are some of the most important. Facial muscles are communicative tools that work to establish expression and emotion. Showing signs of these underlying muscles on the surface of the model can go a long way. It is defining in selling character emotion and believability. For example, when we smile, the risorius, zygomaticus, and other muscles work to pull back the lips. This creates a fold between the cheek and corner of the mouth. This simple, yet complex action is important. Especially when a character is showing emotion that requires movement of the mouth. The upper lip sits in front and tends to be thinner than the lower lip. It has a more prominent peak as it curls back towards the mouth [1]. When modeling the mouth, it is effective for the shape to be in a neutral pose to keep symmetry. This can be modified when the expression is set forth. For an appealing stylized look, the lips should have a crease that defines the outline. This should not be sharp. When looking at the face from the profile view certain lines are present. From the nose down to the chin there is a vertical line pointing back towards the body. Even though the face is a whole, each facial feature sits differently on the surface. The top of the nose slopes into our face and requires a smooth transition as it merges into the forehead. The nostril wings are perpendicular to the face, creating crease. Like the lips, defining the crease is important. Keeping the crease softer and less prominent creates more appeal. Adding a visible flat surface across the bridge of the nose adds appeal and structure. That surface runs along the front of the nose as it blends into the face. This subtle definition is not distracting and resembles underlying anatomy.

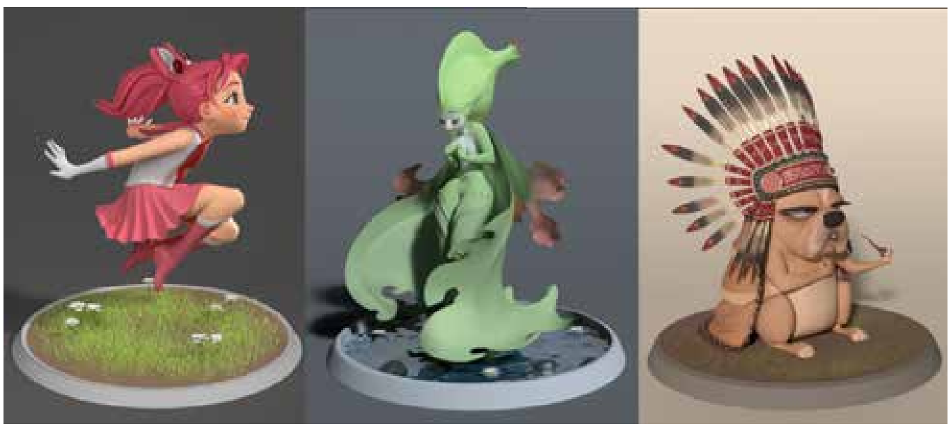

Figure 5: *Final renders of character models.*

**Stage 4: Modeling Body Features.** The human body and most animals have close to symmetrical anatomy. Retaining symmetry will mirror over modeling work from either side, which saves time. It is important to offset features to break away from perfect symmetry towards the end. Bone structure appears at the point of the shoulder, elbow, hands, and part of the wrist. This is important to define in stylized characters. Since stylized animal-based characters have human proportions, the same concepts will apply. Males tend to have more defined musculature on the arm region. It is good practice to show off undulations under the skin for both genders. It is important to keep the hands as simple as possible while defining joints and knuckles. This will keep the aesthetic clean and appealing. Females tend to have softer-looking fingers with more taper down to the fingertip. Males have more prominent knuckles and generally more square fingers. There is a lot of anatomy and complexity within our hands. Finding the balance between simplicity and underlying structure will create character appeal. When analyzing the concept art of a character, there are gender differences in the torso. For example, females tend to have a thicker layer of fatty tissue compared to males. This can affect how much muscle should be showing. From the shoulders to the hips, females tend to have a broader pelvic bone and males tend to have broader shoulders. Females also have more of an hourglass figure because they tend to have a narrower waist. This creates a general contrast. The female usually has a curvier appearance while the male tends to be straighter. Though character designs vary, sticking to base proportions will help sell the model. The legs and feet are another important and intricate part of the body because they support the entire weight. The kneecap, or patella, is an important area to define on a stylized character. The tibia which runs along the front of the lower leg also is important since they do show through the skin. Working with simple geometric forms while refining the shapes will help keep a uniform design. Thinking of the kneecap region as the shape of a triangle, is an example of this. It is close to the actual shape of the patella and is a good start, following refinements to match the concept art. Since the kneecap represents the area of a joint, it appears more angular. While muscles tend to be more rounded like with the calf on the back part of the lower leg. Simplicity is always a key element for creating appeal in character models.

**Stage 5: Printing Models.** We chose to 3D print the mother earth character model. This presented challenges and a learning experience. Analyzing the form of a character is important when 3D printing. You must incorporate balance in the 3D model, so it is able to stand on its own especially if it is a character. Using pieces as support to help your model balance on its own will work as well. In this case, We used the rocks as base for the cape to rest on and support the entire model. Separating the character into pieces can improve your chances of a successful print. It is important also that your model has no holes in the mesh so the print will be intact. If the model is not watertight, the print will collapse in on itself. Once the pieces were successfully printed and coated in primer, they were glued together (Figure 4). We used super glue to bond the main model to the rocks. The cape was also bonded to the surrounding rocks providing balance for the whole model. The super glue proved to be effective in supporting the pieces together. The pieces of filament in the back side of her hair were extremely small. This made it difficult to bond them to her hair. The physical results were satisfying in representing the 3D form; however, the cost was high.

**Figure 4** : *Final PVA-based material used for 3D print.*

## References


[1] Barber, Barrington. Anatomy for Artist. Arcturus Holdings, 2018.

[2] Chen, Helen. “Chibi Sailor Moon” Instagram. Figure 1, Sept. 2, 2019, https://www.instagram.com/p/BvPHOmvAQ0n/

[3] Lojaya, David. “Mother Earth” Instagram. Figure 1, Oct. 17, 2019, https://www.instagram.com/p/B0tYcLKH3CL/

[4] Niko, Terry. “Modeling for Animation – Body.” CGmascot, May 14, 2013, www.cgmascot.com/design/modeling-for-animation-body/.

[5] Runfola, Justin. “Chief Bulldog” Instagram. Figure 1, Nov. 20, 2019, https://www.instagram.com/p/BvHT9gjltOp/

[6] Tottle, Ryan. Personal Interview. 25 September 2019.

# A new grid-based midsurface generation algorithm

Christoph Schinko[1] and Torsten Ullrich[2]

Fraunhofer Austria Research GmbH & Graz University of Technology, Austria
[1]christoph.schinko@fraunhofer.at, [2]torsten.ullrich@fraunhofer.at

## Abstract

A midsurface consists of surface elements (2D) representing three-dimensional, thin solids whose local thickness is small compared to its other dimensions. These simplified representations allow a significant acceleration of almost all physical simulations – a prerequisite for rapid prototyping in the context of 3D additive manufacturing. In this article we present a new algorithm that can extract a midsurface of a thin solid using a grid-based approach: The first step builds a binary 3D grid and marks each voxel that contains some part of the input surface geometry. The second step interprets the binary grid as a density field and applies a kernel to it. In the third step, the vertices of the original input data are moved within the density field towards the climax. Finally, vertices which approach each other are clustered and merged. Having merged all clusters of vertices, the resulting two-sided, incident surfaces are merged to one-sided surfaces. The result is a midsurface. The algorithm has been designed to run fully automatic and the presented proof of concept delivers convincing results.

## Introduction

Dimension reduction transformation is widely used in Computer-Aided Engineering (CAE) analysis as it substantially reduces the compexity of physical simulations. Computer-Aided Design (CAD) models are therefore transformed into a representative surface known as "Midsurface" [1]. It is a simplified, idealized 2D-surface lying (mostly) midway of a thin-walled CAD model and mimicking its shape. Midsurfaces are part of the family of medial objects representing simplified versions of thin-walled, solid input objects. The goal of a midsurface is to reduce the complexity of simulations by switching from 3D volume representations to 2D surface representations. As a consequence the midsurface definition depends (i) on the input and (ii) on the output of a subsequent analysis:

**Definition:** The *midsurface* of a closed, thin-walled object is a set of surfaces which reveal in an CAE analysis the same results (within a $\delta$-tolerance) as the closed, thin-walled input model.

Therefore, the correctness of any midsurface transformation can only be examined within a given context. Nevertheless, the simplified representation of a midsurface reduces the number of features of an object – according to its definition without significant differences in the simulation results. Due to less degrees of freedom (DOF) the simplified model allows a considerable acceleration of almost all physical simulations; thus, it saves time and resources. Consequently, the automatic extraction of reasonable midsurfaces is an important field of research. This article presents a new grid-based approach to solve this problem.

## Related Work

The creation of midsurface geometry is an area of extensive research. Still, a lot of manual labor is required to create reduced dimensional models from solid geometries, both in terms of computational geometry and surface reconstruction. Naturally, related work can be found in these two categories.

### *Top-Down*

Many approaches of midsurface construction work on boundary representations [12] in a top-down manner; i.e. a complex part is split into small parts, which can be transformed into a midsurface representation more easily. The first step of these approaches is usually a decomposition step according to semantic interrelationships [14]. Due to the inherent difficulty of finding a general solution to the midsurface generation problem, Y. H. Woo and C. U. Choo propose a divide and conquer approach [15]. The work of Nolan et al. presents an approach to automatically create mixed dimensional meshes [9]. It uses feature detection to cluster a surface into three categories: long-slender regions, thin-sheet regions, and complex regions. The state-of-the-art approach based on decomposition [4], on identification of corresponding faces [2], and on a Divide-and-Conquer strategy [3] has been developed by Y. H. Kulkarni: "Development of Algorithms for Generating Connected Midsurfaces using Feature Information in Thin-Walled Parts" [1].

***Bottom-Up***

Due to the nature of our approach being grid-based, this Section focuses on a subgroup of so-called thinning approaches. The idea behind these approaches is to iteratively shrink an object locally by offsetting its boundary towards its interior. This process is stopped, when the interior vanishes and just a (potentially non-manifold) surface structure remains. Work on thinning approaches dates back to the late seventies: P. Kwok and V. Ranjan give a good overview of the most important thinning algorithms up to 1991 [5]. All presented algorithms work on voxel data and eventually result in a skeleton rather than a surface. S. Prohaska and H.-C. Hege propose a robust, noise resistant criterion for the characterization of plane-like skeletons [11]. Their algorithm is based on a distance map and the geodesic distance along the object's boundary. After obtaining a skeleton of lines and surfaces, the focus is on obtaining a surface representation for expressive rendering of complex structures. In contrast to the already mentioned algorithms that return skeletons, the work by T.-C. Lee and R. L. Kashyap on thinning algorithms is concerned with parallel thinning for extracting medial surfaces and medial axes of binary voxel data [6]. Another thinning algorithm for extracting medial surfaces is presented by C.-M. Ma and S.-Y. Wan [7]. It defines two sets of voxels on the gridthat are iteratively reduced. It is proven to preserve connectivity. Another thinning approach for medial surface extraction is presented by K. Palágyi and G. Németh [10]. The proposed algorithms rely on sufficient conditions for parallel, topology-preserving reduction operators. A novel thinning scheme using iteration-level endpoint checking is proposed in follow-up work [8].

## Midsurface Generation

The new grid-based approach consists of four steps, which are illustrated in Figure 1.

***Rasterization Step***

The new algorithm can be applied to triangle meshes only. This prerequisite is not a limitation as most CAD systems offer the possibility to export the tessellated geometry (e.g. in STL format). Besides the tessellated geometry the algorithm needs two additional values: $\varepsilon$ and $\delta$, which are the smallest distance and the greatest distance between two opposite surfaces that should be merged to one midsurface. All other subsequent parameters are set automatically and do not need to be modified.The first step builds a binary 3D grid and marks each voxel that has a non-empty intersection with the input surface geometry. If the grid size $\alpha$, i.e. the edge length of each cube in the voxel grid, is not specified, the algorithm uses the default value $\alpha = \frac{1}{2}\varepsilon$.

***Voxel Kernel***

The second step interprets the binary grid as a density field with the values 0.0, if a voxel does not contain any geometry, and 1.0 otherwise. The main idea of the second step is to spread the density values using a kernel. The overlaps of the kernels at the position of the midsurface result in significantly higher values compared to their neighborhood. The algorithm uses a uniform distribution over a 3D sphere with radius $\kappa$. The implementation simply sums for each voxel $(i, j, k)$ the values of all surrounding voxels $(r, s, t)$ with an Euclidean distance less than $\kappa$ between the voxels' centers. The default value is $\kappa = \frac{1}{2}\delta$.

**Figure 1:** *The new midsurface generation algorithm samples the input geometry (top row, left) to a binary 3D grid (top row, middle). Then the binary grid is interpreted as a density field and applies a kernel to it (top row, right; cut for visibility). Afterwards, the vertices of the original input data are moved within the density field towards the climax (bottom row, left). Finally, vertices which approach each other are clustered and merged. The result is a midsurface. Input and output geometry are shown in the bottom-right rendering (cut for visibility).*

***Vertex Climax***

In the third step, the vertices of the original input tessellation data are moved within the density field generated in the previous steps. The start position of a moving vertex is the center of its corresponding voxel. Then each vertex moves to the center of a neighboring voxel with the highest density until no improvement concerning density values is possible or the length of the movement path exceeds the greatest distance $\delta$ between two opposite surfaces that should be merged to one midsurface.

***Vertex Clustering & Topological Cleaning***

Having moved all vertices, the resulting set of vertices is clustered using a mean-shift clustering algorithm with a window size $\omega$ with default value $\delta$. The result is already a two-sided midsurface. If a one-sided midsurface representation is needed, a dense resampling of the two-sided midsurface and a reconstruction according to Shawn and Watson [13] returns the desired representation.

## Conclusion

A midsurface allows a significant acceleration of almost all physical simulations. With a few exceptions, these midsurfaces cannot be generated fully automatically. The acceleration of the subsequent simulation currently justifies even the manual creation of midsurfaces, so that manual re-engineering is still the first choice in many engineering offices.

This article directly targets the interplay of theory and practice: we present a new algorithm to extract a midsurface of a thin solid automatically using a grid-based approach. The first concept already delivers convincing results. The algorithm has been designed to run fully automatic. This is an important property for automated tests and simulations in a rapid prototyping scenario.

## Acknowledgments

The authors would like to thank Ulrich Krispel and Andreas Riffnaller-Schiefer for fruitful discussions; Peer Bertram and Martin Schwarz for their expert knowledge in construction and simulation. Furthermore, the authors gratefully acknowledge the support of the Austrian Research Promotion Agency, (Forschungsförderungsgesellschaft) for the research project (K-Projekt) "Advanced Engineering Design Automation (AEDA)".

## References

[1] Kulkarni, Y. H. *Development of algorithms for generating connected midsurfaces using feature information in thin walled parts*. PhD Thesis at Savitribai Phule Pune University, 2016.

[2] Kulkarni, Y. H., and Kale, M. Formulating midsurface using shape transformations of form features. *Proceedings of All India Manufacturing Technology, Design and Research 5* (2014), 981–985.

[3] Kulkarni, Y. H., Sahasrabudhe, A., and Kale, M. Dimension-reduction technique for polygons. *International Journal of Computer-Aided Engineering and Technology 9* (2017), 1–17.

[4] Kulkarni, Y. H., Sahasrabudhe, A., and Kale, M. Leveraging feature generalization and decomposition to compute a well-connected midsurface. *Engineering with Computers 33* (2017), 159–170.

[5] Kwok, P. C. K., and Ranjan, V. A survey of 3-d thinning algorithms. *Vision Interface 6* (1991), 13–20.

[6] Lee, T.-C., and Kashyap, R. L. Building skeleton models via 3-d medial surface/axis thinning algorithms. *Graphical Models and Image Processing (CVGIP) 56* (1994), 462–478.

[7] Ma, C.-M., and Wan, S.-Y. A medial-surface oriented 3-d two-subfield thinning algorithm. *Pattern Recognition Letters 22* (2001), 1439–1446.

[8] Németh, G., Kardos, P., and Palágyi, K. Topology preserving 3d thinning algorithms using four and eight subfields. *Image Analysis and Recognition 6111* (2010), 316–325.

[9] Nolan, D. C., Tierney, C. M., Armstrong, C. G., Robinson, T. T., and Makem, J. E. Automatic dimensional reduction and meshing of stiffened thin-wall structures. *Engineering with Computers 30* (2014), 689–701.

[10] Palágyi, K., and Németh, G. Fully parallel 3d thinning algorithms based on sufficient conditions for topology preservation. *Discrete Geometry for Computer Imagery (DGCI) 5810 (LNCS)* (2009), 481–492.

[11] Prohaska, S., and Hege, H.-C. Fast visualization of plane-like structures in voxel data. *IEEE Visualization 13* (2002), 29–36.

[12] Schinko, C., Riffnaller-Schiefer, A., Krispel, U., Eggeling, E., and Ullrich, T. State-of-the-art overview on 3d model representations and transformations in the context of computer-aided design. *International Journal on Advances in Software 3 & 4* (2017), 446–458.

[13] Shawn, M., and Watson, J.-P. Non-manifold surface reconstruction from high-dimensional point cloud data. *Computational Geometry 44* (2011), 427–441.

[14] Sun, L., Tierney, C. M., Armstrong, C. G., and Robinson, T. T. Automatic decomposition of complex thin walled cad models for hexahedral dominant meshing. *Procedia Engineering 163* (2016), 225–237.

[15] Woo, Y.-H., and Choo, C.-U. Automatic generation of mid-surfaces of solid models by maximal volume decomposition. *Transactions of the Society of CAD/CAM Engineers 14* (2009), 297–305.

# CONTENTS

## Proceedings of Fabrication and Sculpting Event

# *The Proceedings of the SMI 2020 Fabrication & Sculpting Event (FASE)*

*In Cooperation with ISAMA*

ISBN 978-0-359-71699-9
90000
9 780359 716999

**FASE Paper Chairs:**

**Oleg Fryazinov**
**Melina Skouras**
**Shinjiro Sueda**

**Proceedings Editor:**

**Ergun Akleman**

**Front Page Sculpture:**

**Steve Reinmuth**
**Carlo H. Séquin**

**Back Page Sculpture:**

**Carlo H. Séquin**

**Cover Design:**

**Ergun Akleman**